DISSECTING THE ROLE OF LINKER HISTONE H1 VARIANTS IN EMBRYONIC STEM CELLS

A Dissertation
Presented to
The Academic Faculty

By

Po-Yi Ho

In Partial Fulfillment
Of the Requirements for the Degree
Doctor of Philosophy in the
School of Biological Sciences

Georgia Institute of Technology

December 2017

DISSECTING THE ROLE OF LINKER HISTONE H1 VARIANTS IN EMBRYONIC STEM CELLS

Approved by:

Dr. Yuhong Fan, Advisor
School of Biological Sciences
Georgia Institute of Technology

Dr. Alfred H. Merrill
School of Biological Sciences
Georgia Institute of Technology

Dr. Ingeborg Schmidt-Krey
School of Biological Sciences
Georgia Institute of Technology

Dr. Chong H. Shin
School of Biological Sciences
Georgia Institute of Technology

Dr. Athanassios Sambanis
School of Chemical & Biomolecular Engineering
Georgia Institute of Technology

Date Approved: August 7, 2017

To Brandon,

for feeding me everyday, always being there for me on those days I almost gave up,

lighting on the dark site in my heart.

To Aker,

for your smiling face waiting for me every night, those nights we cuddled on the couch

while I was writing.

To Ho family,

for your endless support and love.

ACKNOWLEDGEMENTS

Firstly, I would like to express my sincere gratitude to my advisor Dr.Yuhong Fan. She has been a great teacher and mentor who has guided me and enabled me to rise and explore the limits of my potential. She has taught me to develop solutions in a novel manner and laid the groundwork for me to develop my problem-solving skills. I will forever cherish all the scientific discussions and great moments we have shared during my Ph.D. adventure. Without her, I would have never been able to accomplish this task.

I would like to thank all my committee members; Dr. Alfred H. Merrill, Dr. Ingeborg Schmidt-Krey, Dr. Chong H. Shin, and Dr. Athanassios Sambanis for all their valuable suggestions and advice during our committee meetings. I would like to particularly thank Dr. Alfred H. Merrill, for being a great support and a mentor par excellence throughout this journey. He has been very instrumental in guiding me through every hurdle and dealing with unforeseen and often complicated issues. When I felt lost, I knew he is always there to point out a bright path for me.

I would also like to thank the School of Biological Sciences and Georgia Institute of Technology for giving me this opportunity and supporting my continuing research journey in an environment of learning and innovation. I am very fortunate to have worked with the former and current members of the Fan lab; Dr. Magdalena Medrzycki, Dr. Yunzhe Zhang, Dr. Kaixiang Cao, Dr. Chenyi Pan, Samantha Leigh Lasater, Dr. Paul Guy Cooper, Hiba Hamdan, Dr. Jin Xu, Ting Wu, Norah Mckissic, David Giles, Orezime Uyeh, Yael Jordan Toporek, Leyla Larsson, Yusra Asif, Alexis

Jacob, Rebecca Robbins and Bhakti Sangani. I am grateful to them for all the useful ideas, discussions, and fun times that we have shared. My life in Atlanta wouldn't have been so great without all the amazing friends I have made along the way. Thanks to Dr. Samantha Katz and Dr. Lee Katz, for being my second family in the USA and making me feel welcome at the beginning of my Ph.D. life! I am thankful to have Gary Newnam as our best lab neighbor. Without him, I can't imagine how I could survive tantrums of our instruments. And thanks to all my friends back home, especially Chengyi Chen, Laing Yin, and Chia-ling Chang. Even though we are half an Earth apart, I felt they were always with me throughout good times and tough times.

Most importantly, I would like to thank my family and my family-in-law for their continued love and support in all my endeavors. My parents and my brother have been a big source of strength and it is their unconditional love that has brought me this far. My family-in-law made me feel like at home again in this new nation. With their kindness and support, I never felt alone here. I am also blessed to have my doggy Aker and kitty Indrik with me throughout this journey. They both give me unbridled joy and happiness everyday, and their smiling faces always cheer me up even after a rough day. Finally, my best friend and husband, Brandon, has undoubtedly been the biggest inspiration and stood by me during my most trying times. All my achievements during my Ph.D. wouldn't have been possible without his eternal belief and encouragement. Thank you for walking through the dark with me!

TABLE OF CONTENTS

LIST OF FIGURES

LIST OF ABBREVIATIONS

3D	three-dimensional
A214	absorbance at 214 nm
bFGF	basic fibroblast growth factor
bp	base pair
C-terminal	carboxyl-terminal
CDKs	cyclin-dependent kinases
CDS	coding DNA sequence
DNA	deoxyribonucleic acid
DNMT1	DNA (cytosine-5)-methyltransferase 1
DNMT3B	DNA (cytosine-5)-methyltransferase 3B
E11.5	mouse embryonic day 11.5
E9.5	mouse embryonic day 9.5
EB	embryoid body
EDTA	ethylenediaminetetraacetic acid
EMANIC	electron-microscopy assisted nucleosome interaction capture
ESCs	embryonic stem cells
FBS	fetal bovine serum
FLAG-H1d	FLAG-tagged H1d
FRAP	fluorescence recovery after photobleaching
GAPDH	glyceraldehyde 3-phosphate dehydrogenase

GCN5	general control nonderepressible-5
GD	globular domain
GFAP	glial fibrillary acidic protein
GFP	green fluorescent protein
GH5	the globular domain of H5
H1 QKO ESCs	H1c/H1d/H1e/H10 quadruple knockout embryonic stem cells
H1 QKO/H1d ESCs	H1d overexpression in embryonic stem cells with H1c/H1d/H1e/H10 knockout
H1 QKO/H1d-CTD ESCs	CTD of H1d overexpression in embryonic stem cells with H1c/H1d/H1e/H10 knockout
H1 QKO/H1d-GD ESCs	GD of H1d overexpression in embryonic stem cells with H1c/H1d/H1e/H10 knockout
H1 QKO/H1d-NTD-GD ESCs	NTD and GD of H1d overexpression in embryonic stem cells with H1c/H1d/H1e/H10 knockout
H1 TKO ESCs	H1c/H1d/H1e triple knockout embryonic stem cells
H1 TKO/GFP-H1d ESCs	GFP tagged H1d overexpression in embryonic stem cells with H1c/H1d/H1e knockout
H1 TKO/GFP-H1dK46R ESCs	GFP tagged H1d-K46R overexpression in embryonic stem cells with H1c/H1d/H1e knockout
H1 TKO/H1d ESCs	FLAG tagged H1d overexpression in embryonic stem cells with H1c/H1d/H1e knockout

H1 TKO/H1dK46R ESCs	FLAG tagged H1d-K46R overexpression in embryonic stem cells with H1c/H1d/H1e knockout
H1.2S173p	phosphorylation at Ser173 on H1.2
H1.4K26me	methylation at Lys34 on histone H1.4
H1.4K34ac	acetylation at Lys34 on histone H1.4
H1.4S187p	phosphorylation at Ser187 on H1.4
H1.4S35p	phosphorylation at Ser35 on H1.4
H1/nuc	H1 to nucleosome
HATs	histone acetyl-transferases
HILS1	Histone Linker H1 Domain, Spermatid-Specific 1 (Pseudogene)
HP1	Heterochromatin protein 1
HPLC	high-performance liquid chromatography
HRE	hormone responsive element
ICR	imprinting control regions
K26	lysine at positin 26
K34	lysine at positin 34
K46R	lysine to arginine mutation at amino acid 46
Kb	kilo base pairs
LIF	leukemia inhibitory factor
mAU	milli-absorbency units
MEF	mouse embryonic fibroblast
MMTV	hormone-inducible mouse mammary tumor virus

MS	mass spectrometry
N-terminal	amine-terminal
NEAA	nonessential amino acids
nm	nanometers
NSC	neural stem cell
NTD-GD	N-terminal domain and globular domain
NURF	Nucleosome Remodeling Factor
Oct4	octamer-binding transcription factor 4, as known as POU domain, class 5, transcription factor 1 (Pou5f1)
PARylation	poly(ADP-ribosyl)ation
PBS	phosphate buffered saline
PCR	polymerase chain reaction
PLO	poly-L-ornithine
PR	progesterone receptor
PRC	Polycomb repressive complexes
PRC2	Polycomb repressive complex 2
PRC4	Polycomb repressive complex 4
PTM	Posttranslational modifications
RA	retinoic acid
rFRI	relative fluorescence recovery intensity
RNA	ribonucleic acid
ROI	region of interest

ROIbg	background ROI
ROIe	experimental ROI
ROIref	refernce ROI
RP-HPLC	reversed phase HPLC
S.D.	standard deviation
S.E.M.	standard error of the mean
SLBP	stem loop binding protein
t(1/2)	the half time of recovery
TAF1	Transcription initiation factor TFIID subunit 1
TFDII	Transcription factor II D
TNF-α	tumor necrosis factor alpha
TUBB3	β-tubulin isotype III
WT	wildtype

SUMMARY

H1 Linker histones are key chromatin structural proteins that facilitate the folding of higher order chromatin structure. Besides its structural function, H1 has been shown to act as a general transcriptional repressor *in vitro* but has a more specific role in regulating gene expression *in vivo*. Linker histone H1 is essential for mammalian development and H1 depletion impairs ESC differentiation. To further dissect the role of linker histone H1 in embryonic stem cells (ESCs), here, we have utilized a functional reconstitution approach to identify the regions of H1 proteins that are important to mediate neurite outgrowth during neural differentiation of ESCs.

We have previously established ESCs deficient of multiple H1 variants and found that H1 depleted ESCs are impaired in neural differentiation, with markedly reduced neurite outgrowth from their respective embryoid bodies (EBs) in a neural differentiation scheme. Here, we first generated H1 reconstituted ESC lines by overexpressing exogenous H1d proteins in H1 depleted ESCs. We find that overexpression of H1d in H1 depleted ESCs significantly restored the neurite outgrowth capacity of embryoid bodies (EBs) formed from ESCs.

Next, to dissect the role of individual domains of H1d in ESC differentiation, we constructed a series of vectors to express H1 deletion mutants in H1 depleted ESCs. We generated H1 reconstituted H1 ESC lines expressing different domains of H1d, including H1d-CTD, H1d-NTD-GD, and H1d-GD. These reconstituted ESCs exhibited normal characteristic ESC colony morphology and cell growth rate. Embryoid bodies (EBs) formed from these ESCs were induced to differentiate toward

neural lineages. Our results show that reconstitution with H1d-GD and H1d-NTD-GD increases neurite outgrowth of EBs, suggesting a partial rescue of the differentiation deficiency phenotype of H1 depleted ESCs. In contrast, reconstitution of H1 depleted ESCs with H1d-CTD did not rescue the neurite outgrowth defects of H1 depleted ESCs during neural differentiation. Together, these results suggest that the globular domain of H1d is critical in mediating the neurite outgrowth during neural differentiation of ESCs.

Lastly, we investigated the potential role of H1 modifications in ESC differentiation. We have focused our study on a conserved H1 modification hotspot, K46, which is located within the globular domain of H1d. Toward this end, we constructed an expression vector encoding the H1d mutant ($H1d^{K46R}$) containing a lysine-to-arginine mutation at site K46, and expressed $H1d^{K46R}$ in H1c/H1d/H1e triple knockout (H1 TKO) ESCs by stable transfection. HPLC analysis demonstrates that $H1d^{K46R}$ binds to chromatin and maintains the same biochemical properties as H1d. While H1 TKO/$H1d^{K46R}$ ESCs exhibited normal ESC morphology and cell growth rate, they were impaired in neural differentiation, having comparable neurite outgrowth rate as H1 TKO EBs. These results suggest that K46R mutation of H1d disrupts the function of H1d in mediating the neurite outgrowth of EBs, suggesting a critical role of post-translational modification(s) on H1d K46 in ESC differentiation.

Hyperdynamic plasticity of chromatin proteins has been suggested to be important for proper ESC differentiation. To further dissect the potential mechanisms underlying the defects of $H1d^{K46R}$ mutant, we set out to characterize and compare the mobility of $H1d^{K46R}$ and H1d in ESCs *in vivo* using fluorescent recovery after

photobleaching (FRAP) assay. To do that, we constructed expression vectors encoding GFP fused to the N-terminus of H1d and of H1d^{K46R}. GFP-H1d and GFP-H1d^{K46R} vectors were separately transfected into H1 TKO ESCs, and stable ESC clones expressing similar levels of GFP-H1d and GFP- H1d^{K46R} were selected and cultured for FRAP assay. Compared with H1d, H1d^{K46R} displayed a moderately reduced recovery rate after photobleaching. These results suggest that K46R mutation decreases dynamic mobility of H1d in ESCs, which may partially contribute to the defects of H1d^{K46R} in mediating proper ESC differentiation.

In summary, through a series of studies aimed at dissection of different regions and sites of H1d, we pinpoint GD as a key domain of H1 in mediating neurite outgrowth during neural differentiation of ESCs. Furthermore, our results suggest that the modification(s) on K46 of H1d are critical for proper ESC differentiation and are likely to increase the dynamic plasticity of H1d.

CHAPTER 1

INTRODUCTION

In eukaryotic cells, genomic DNA is packaged into chromatin by association with histones. Histone proteins can be classified into two groups, core histones (H2A, H2B, H3, and H4) and linker histones (H1). The basic repeating unit of chromatin is the nucleosome, which is formed by wrapping 147 bp of DNA in 1.7 super helical turns around a histone octamer consisting of two copies of each of the four core histones proteins (Van Holde, 1989; Wassarman and Wolffe, 1999; Wolffe, 1997). This structure establishes the extended, "beads on a string" chromatin conformation observed under electron microscope. Linker histone H1 sits outside of the nucleosome core particle, binding to the nucleosome at the entry and exit sites of the nucleosomal DNA, seals additional 20bp DNA flanking the entry and exit site of nucleosome. By binding to nucleosomes as well as the linker DNA between nucleosomes, H1 facilitates the folding of chromatin into a more compact fiber with a diameter of ~30 nm (Van Holde, 1989; Wassarman and Wolffe, 1999; Wolffe, 1997).

1.1. Linker Histone H1 Variants

Among the histone family, linker histone H1 is the most divergent and heterogeneous class of histone proteins. Multiple allelic H1 variants exist in multi-cellular organisms. Despite the greater divergence among H1 variants, each variant is conserved evolutionarily, suggesting that individual H1 variants might have unique properties (Brown, 2001).

In mammals, there are 11 different H1 variants identified, including seven somatic H1s (H1a, H1b, H1c, H1d, H1e, $H1^0$ and H1x) and four germ- cell-specific H1s (H1oo, H1t, H1t2, and HILS1) (Happel and Doenecke, 2009). H1a to H1e (H1a (H1.1), H1b (H1.5), H1c (H1.2), H1d (H1.3), and H1e (H1.4)) are the major somatic H1s, which are ubiquitously expressed in nearly all cells with their synthesis coupled to S-phase of the cell cycle in a DNA replication-dependent manner. $H1^0$ (H1.0) and H1x are replacement H1s, which are regulated based on cellular status and synthesized in a DNA replication-independent manner. $H1^0$ is accumulated in terminally differentiated cell types that have stopped dividing (Zlatanova and Doenecke, 1994). H1x is the most divergent H1 variant with only ~30% sequence homology with other H1 variants. While H1x is expressed throughout the cell cycle or after induction of differentiation (Happel and Doenecke, 2009; Happel et al., 2005; Yamamoto and Horikoshi, 1996), it is not present in a comparable level as the major somatic H1s and $H1^0$ in ESCs and multiple tissues. H1oo, H1t, H1t2, and HILS1 are tissue specific H1s. H1oo and H1t are expressed in oocytes and testis, respectively, whereas H1t2 and HILS1 are H1t-related H1s expressed in spermatids (Happel and Doenecke, 2009; Harshman et al., 2013b; Kowalski and Palyga, 2012; Meergans et al., 1997).

Most histone H1 genes, including H1a-H1e and H1t genes, are located in a large cluster on chromosome 6 in humans and chromosome 13 in mice (Marzluff et al., 2002). Genes encoding other H1 variants are solitarily located on distinct chromosomes. $H1^0$ resides on human chromosome 22 and mouse chromosome 15, whereas H1x is located on human chromosome 3 and mouse chromosome 6. All H1

genes are transcribed by RNA polymerase II. The mRNA transcripts of the replication-dependent H1 genes, including major somatic H1 variants (H1a, H1b, H1c, H1d and H1e) and H1t, contain no introns, and do not have a long poly-A tail. Instead, their pre-mRNAs have a distinct stem-loop structure at the 3' end for efficient pre-mRNA processing. The histone RNA hairpin-binding protein or stem loop binding protein (SLBP) recognizes and binds to the 3' stem-loop structure to enhance translation (Allard et al., 2005; Gorgoni et al., 2005; Ling et al., 2002; Marzluff et al., 2002; Whitfield et al., 2000). The transcription of these H1 genes occur in the S phase of the cell cycle, is regulated in transcription initiation, 3′ end processing and mRNA stability. In contrast, the mRNAs of the replication-independent H1s, $H1^0$, H1x, H1oo, H1t2 and Hils1, are polyadenylated and most of those genes contain introns (Happel and Doenecke, 2009).

1.2. H1 Domains

All mammalian H1s have a tripartite structure containing three distinct domains (Figure 1): a short N-terminal domain (NTD) (composed of 20- 40 amino acids), a highly conserved central globular domain (GD) (composed of ~ 80 amino acids) and a long C- terminal domain (CTD) (composed of 100 ~ 120 amino acids) (Happel and Doenecke, 2009; Pan and Fan, 2016).

The N-terminal domain of H1 is normally unstructured in aqueous solution but it may be able to form an alpha helix structure in the presence of trifluoroethanol or DNA molecules (Vila et al., 2001). Based on its sequence, the N-terminal domain

can be divided into two regions, a proline- and alanine-rich hydrophobic extreme N-terminal region and a shorter highly basic region close to the globular domain (Bohm and Mitchell, 1985; Vila et al., 2001). The first half of the N-terminal domain lacks basic residues thus it is not expected to have a strong binding interaction with DNA. In contrast, the second half of the N-terminal domain is highly basic, with one Arginine and multiple (five or more) Lysine residues, and adopts alpha helical conformation in trifluoroethanol or in the presence of DNA. The proximity of this region to the globular domain and the highly positive charges of this region may facilitate the stability of the interaction between DNA and the globular domain of the linker histone (Vila et al., 2001). Although the N-terminal domain is not essential to H1-binding to Chromatin, deletion of the N-terminal domain modestly reduces the binding affinity of H1 to chromatin both *in vivo* and *in vitro* (Allan et al., 1986; Hendzel et al., 2004; Oberg and Belikov, 2012; Vyas and Brown, 2012). These studies suggest that the N-terminal domain may server as an anchor for proper positioning of H1 to the nucleosome.

The central globular domain is the most conserved and most hydrophobic domain among the three domains of H1. It is highly conserved across different H1 variants and different species (Baxevanis and Landsman, 1998; Cutter and Hayes, 2017; Kowalski and Palyga, 2016; Lyubitelev et al., 2016). X-ray crystallography of the globular domain of H5, the predominant H1 variant in avian erythrocytes, has revealed that the globular domain contains a characteristic winged-helix motif comprising three alpha helixes with three beta hairpin structures, similar to a number

of sequence-specific non-histone DNA-binding proteins (Fan and Roberts, 2006; Ramakrishnan et al., 1993; Zhou et al., 2013).

The H1 globular domain protects 20 additional base pairs of linker DNA flanking from micrococcal nuclease digestion, to similar extent of H1 (Allan et al., 1980; Syed et al., 2010; Zhou et al., 1998). *In vitro* studies suggest that the globular domain binds to the nucleosomal DNA at the dyad axis, and likely is the main region regulating the binding of H1 to the nucleosome. The crystal structure of GH5 suggests that two clusters of residues, forming two DNA binding sites, for its binding to two adjacent duplixes of DNA (Ramakrishnan et al., 1993). In addition, systematic mutagenesis and analysis of H1 mobility by fluorescence recovery after photobleaching (FRAP) have identified several residues crucial in GD for its nucleosome binding. These studies help to explain the binding mode of the globular domain to the nucleosomal DNA (Brown et al., 2006; Cui and Zhurkin, 2009; Fan and Roberts, 2006; Ramakrishnan et al., 1993). Additionally, different residues of the globular domains in different H1 variants contacting the nucleosome could explain the different binding affinities of H1 variants in dynamic interaction during chromatin condensation (George et al., 2010).

The C-terminal domain typically encompasses around 50% of the entire H1 protein. As the largest domain of H1, the C-terminal domain is the least conserved region among different histone variants (Happel and Doenecke, 2009). Similar to the N-terminal domain, the C-terminal domain has as an intrinsically disordered structure in solution and forms a stochastic random coil. Upon DNA binding, the C-terminal domain could adopt a much more condensed secondary structure (Roque et al., 2005).

The C-terminal domain is highly positively charged, with 40% composed of lysine, 20–35% alanine and 15% proline residues (Hansen et al., 2006), and this amino acid residue composition could facilitate chromatin condensation through neutralizing DNA backbone charges (Lu and Hansen, 2004). This feature also assists the low-affinity H1 binding to form the secondary structure in the C-terminal domain to promotes high-affinity binding and stabilizes the higher–order structure formation of chromatin condensation (Allan et al., 1980; Allan et al., 1986; Lever et al., 2000; Misteli et al., 2000; Syed et al., 2010). Mutagenesis studies coupled with FRAP assay reveal that distinct DNA-binding regions in the C-terminal domain are required for high-affinity of chromatin binding (Allan et al., 1986; Hendzel et al., 2004; Lu et al., 2009; Lu and Hansen, 2004). The CTD secondary structure formed upon binding to linker DNA is also responsible for the formation of nucleosome stem structure (Fang et al., 2012).

In addition to the highly positive charge property of C-terminal domain contributing to the stabilizing H1-chromatin binding, the conserved DNA binding S/TPXK motifs in CTD are critical for the high affinity binding of H1 to chromatin *in vivo*. *In vitro* studies have demonstrated that the T/SPXK motifs interact with the linker DNA to promote DNA condensation. Deletion of a thirty-four amino acids region within CTD including three S/TPKK repeats resulted in a 90% decrease in DNA condensation (Bharath et al., 2002). Detailed FRAP analysis of H1.1 mutants identified two residues, Thr^{152} and Ser^{183}, as novel regulatory switches of modulating H1.1 binding affinity *in vivo*. Mutants or phosphorylation of crucial residues in the S/TPXK motifs in CTD may disrupt their ability to form secondary structure without

changing the overall net charges of this domain (Hendzel et al., 2004).

Additionally, the C-terminal domain is involved in protein-protein interactions. Proteomics approach has successfully identified that the C-terminal domain contributes to the $H1^0$ interaction with several groups of proteins, which function in RNA metabolism in the nucleolus, including core splicing factors, ribosomal proteins, rRNA processing factors and proteins involved in cellular transport (Kalashnikova et al., 2013). Recent study has shown that H1 regulates DNA methylation specifically at the H19 and Gtl2 imprinting control regions (ICR) through the recruitment of DNA methyltransferases, DNMT1 and DNMT3B, and the H1 C-terminal domain directly mediates these interactions (Yang et al., 2013).

Collectively, based on previous *in vitro* and *in vivo* studies, a model of dynamic binding of H1 to chromatin is proposed: when linker histones approach chromatin, the C-terminal domain of H1 binds weakly and nonspecifically to the linker DNA, followed by the globular domain specifically binds at the nucleosomal dyad axis, and lastly, the reposition of both the C- and N-terminal domains leads to stabilize the nucleosome and further compact of chromatin fiber into higher-order structures (Bednar et al., 2017; Brown et al., 2006; Catez et al., 2006).

1.3. Posttranslational modifications (PTMs) of Linker Histone H1

Posttranslational modifications (PTMs) of linker histone H1 have been observed since early 1970s (Balhorn et al., 1972). Due to the lack of site- and modification-specific antibodies against H1 variants, studies on histone H1

modifications have long faced challenges. However, recent studies, taking advantage of mass spectrometry proteomics, development of new antibodies, as well as functional studies, have made significant progresses in identification and characterization of various histone H1 modifications in both tail regions and the center globular domain. These studies shed new lights on the functional implications of H1 modifications. Some modifications are commonly present in different mouse tissues and conserved among species, whereas others are more specific, only present in certain H1 variants or tissues. In-depth characterization, by mass spectrometry of H1 histones isolated from the cultured cells and mouse tissues, have identified dozens of different H1 modifications, including acetylation, methylation, phosphorylation, ubiquitination, formylation and poly(ADP-ribosyl)ation (PARylation) (Wisniewski et al., 2007). Recent studies have begun to characterize the importance of histone modifications in chromatin structure and gene regulation as well as cellular functions (Harshman et al., 2013b; Hergeth and Schneider, 2015; Kamieniarz et al., 2012; Kowalski and Palyga, 2016; Weiss et al., 2010). A number of common and conserved modifications of H1 that have been characterized will be discussed here (Figure 2).

Phosphorylation and acetylation of H1 would affect the protein biochemical property by reducing the positive net charges. As a consequence, both modifications could weaken the interaction of H1-DNA complexes and thus reduce chromatin compaction. Phosphorylation and acetylation of histones have been generally linked to increased chromatin accessibility and transcriptional activation (Jenuwein and Allis, 2001; Strahl and Allis, 2000). Phosphorylated H1 is enriched in transcriptionally active chromatin as detected by antibodies against phosphorylated

H1 (Chadee et al., 1995; Lu et al., 1995), and H1 phosphorylation modulates mouse mammary tumor virus (MMTV) transcription and hormone (Bhattacharjee et al., 2001; Koop et al., 2003; Vicent et al., 2002). H1 phosphorylation has been shown favor H1 removal from active promoter regions. However, the level of H1 phosphorylation during mitosis are correlated with chromatin compaction in contrast to the correlation between H1 phosphorylation with chromatin relaxation in the interphase (Bradbury et al., 1974; Bradbury et al., 1973; Halmer and Gruss, 1996; Krishnan et al., 2017; Roque et al., 2016). During the progression of the cell cycle, the level of phosphorylation is at the lowest during the G1 phase, rising during S phase, reaching its maximal levels in mitosis, and decreasing sharply at the end of mitosis in telophase (Boggs et al., 2000; Gurley et al., 1995; Halmer and Gruss, 1996; Harshman et al., 2013a; Krishnan et al., 2017; Langan et al., 1989). It is suggested that the chromatin condensation in metaphase, accompanied by H1 hyper-phosphorylation, might be structurally and mechanistically distinct from other chromatin states associated with partial phosphorylation or un-phosphorylated H1.

Previous studies as well as the comprehensive mass spectrometry analyses of H1 histones mentioned above have identified multiple sites for phosphorylation and acetylation (Figure 2) (Talasz et al., 2009; Wisniewski et al., 2007). Phosphorylation of linker histones occurs primarily in the tail regions, especially the C-terminal tail, where several sites located in (S/T)-P-X-(K/R) motifs recognized by cyclin-dependent kinases (CDKs), and one site in a non-consensus motif in the N-terminal domain. Several Serine residues (S17, S172 and S188) are phosphorylated during G1 and S phase, and the phosphorylation of Threonine (T10, T137 and T154) occurs

during mitosis (Talasz et al., 2009).

The acetylation of H1 occurs on specific lysine residues (Figure 2) and is catalyzed by histone acetyl-transferases (HATs). Acetylation on the lysine residues at position 16, 34 in N-terminal domain, and at positions 46, 52, 64, 75, 80, 85, 90, 97 of globular domain, and position 168, 191 in the C-terminal domain of H1 has been detected in mammals (Wisniewski et al., 2007). The specific HATs responsible for various forms of H1 acetylation are poorly characterized. Recent studies show that the lysine 34 (K34) of H1.4 is acetylated by GCN5 (general control nonderepressible-5)-containing SAGA and ATAC complexes (Kamieniarz et al., 2012).

The other abundant H1 modification, methylation, does not involve changes in charges in H1 proteins. Several forms of methylation of H1 have been found with different numbers of methyl residues at specific sites: mono-, di-, or tri-methyl for lysines and mono- or di-methyl for arginines. Mono- or di-methylation have been detected on the lysine residues at position 26, 34 in N-terminal domain, and at positions 46, 63, 75, 107 of globular domain of H1.1-H1.4 (Wisniewski et al., 2007). Based on the site and the degree of methylation, histone methylation mediates either the transcriptional activation or silencing (Kouzarides, 2007). Among methylation sites of H1s (Figure 2), the Lysine at position 26 (K26) in the N-terminal domain is the most well characterized H1 methylation. In mammalian cells, the K26 of H1.4 and H1.2 is methylated the polycomb repressive complexes (PRC), PRC4 and PRC2, respectively (Kuzmichev et al., 2004; Kuzmichev et al., 2005). It is a highly conserved modification in all of the somatic H1 variants, which can be found in vertebrates and also in Drosophila melanogaster (as K27me2), indicating a conserved

function of this modification (Bonet-Costa et al., 2012).

Ubiquitination and formylation of H1 have been recently identified. Both modifications occur on lysine residues. They are newly characterized and appear to serve important functions. Ubiquitination at K46 of H1.2, H1.3 and H1.4, and K116 of H1.1 are the only ubiquitination detected in the proteomics study (Wisniewski et al., 2007), whereas ubiquitination at K63 was investigated in recent study (Thorslund et al., 2015). The results suggest that K63 ubiquitylated H1 is a receptor for E3 ubiquitin ligase, RNF168, at double-strand break (DSB) modified chromatin, and may mediate RNF168 recruitment, facilitating chromatin remodeling to allow efficient DSB repair (Thorslund et al., 2015). On the other hand, formylation has been found in all-major somatic H1s, H1.1- H1.5 in MCF cells by mass spectrometry (Wisniewski et al., 2007). Formylation at K90 (in H1.1-H1.4) was detected in human cells, while the most frequently occurring formylation site occurs on K63 in both in human cells and mouse tissues. Using radiolabeling and sensitive bio-analytical methods, it has been shown that the N(6)-formyl-lysine residue as a secondary modification arising from 5'-oxidation of deoxyribose in DNA after the treatment of a nucleosome linker-selective DNA-cleaving agent, neocarzinostatin. The results suggest that the histone H1 formylation might be considered as a signal of DNA upon oxidative stress (Jiang et al., 2007).

Other than general features of various forms of H1 modifications, specific sites have distinct functional implications. For example, using antibodies specific for phosphorylated Ser^{17}, Ser^{172}, and Thr^{10} of H1.5, immunofluorescence labeling of synchronized HeLa cells showed distinct localization patterns for these

phosphorylated forms of H1s as well as co-localization of Ser^{172} phosphorylation of H1.5 and H1.2 with DNA replication and transcription sites, suggesting various forms of H1 phosphorylation associating with different functions during cell cycle (Talasz et al., 2009). Site-specific interphase H1 phosphorylation has also been implicated to facilitate both RNA polymerases I- and II- transcription and may be involved in ribosome biogenesis and control of cell growth (Zheng et al., 2010).

Importantly, a few H1 modifications have been shown to be involved in cross-talks among different modifications. Both methylation and acetylation have been found on K34 of H1, and such H1 PTMs appeared to be conserved in mammals and avian species (Sarg et al., 2015). However, acetylation and methylation of H1 K34 are linked to distinct functional aspects. Acetylation at lysine 34 of histone H1.4 (H1.4K34ac) is enriched at the promoters of active genes and specifically interacts with TAF1, a subunit of the general transcription initiation factor TFIID. Thus, H1.4K34ac could either increase dynamic mobility of H1 *in vivo* or recruit the transcriptional machinery to stimulate transcription (Kamieniarz et al., 2012). In contrast, methylation at H1.4K26 is shown to serve as a binding platform for HP1 (Heterochromatin protein 1) in the area lacking of methylated H3K9 and thus is likely to participate in transcriptional repression (Daujat et al., 2005). Moreover, being part of an "ARKS" motif in the N-terminal domain, adjacent Ser27, when phosphorylated, inhibits HP1 binding. The potential combinatorial modifications in H1 provide an example for crosstalk between modifications which creates a methylation/ phosphorylation switch identical to the one for histone H3 (Fischle et al., 2008) to control heterochromatin formation (Daujat et al., 2005).

Taken together, the post-translational modifications of linker histone H1 not only implicate in chromatin architecture but also mediate gene regulation as well as other cellular processes.

1.4. Objectives

Linker histone H1 plays key roles in the stabilization and folding of chromatin structure. H1 is also crucial in mammalian development and ESC differentiation (Fan et al., 2003; Zhang et al., 2012). However, the underlying mechanisms of H1 mediating these processes remain to be explored. Multiple H1 variants exist in mammals. Mice with single or double H1 variants knockouts reproduce normally, but compound depletion of H1c/H1d/H1e causes embryonic lethality at midgestation (Fan et al., 2003; Fan et al., 2001; Rabini et al., 2000; Sirotkin et al., 1995). H1c/H1d/H1e triple knockout in ESCs leads to a broad range of chromatin structure changes but specific changes in gene expression (Fan et al., 2005). The H1c/H1d/H1e triple knockout ESC cells are impaired in ESC differentiation (Zhang et al., 2012).

In order to further dissect the mechanism of function of H1, this study focuses on testing the role of different domains of linker histone H1 variants as well as the key H1 modification in ESC differentiation. We take a functional reconstitution approach by complementing H1 depleted ESCs with various H1 domains and mutants to address this issue. We use a 3D neural differentiation scheme to investigate the effects and function of H1 domains and H1 mutant with specific point mutation in

ESC differentiation. The results will provide insights into the potential roles and mechanisms of histone H1 ESC differentiation.

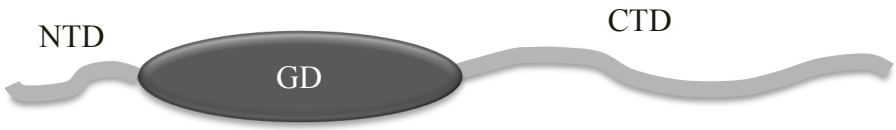

Figure 1. A schematic diagram of metazoan H1 domains.
All metazoan H1s have a three-domain structure: a short N-terminal domain (NTD) (composed of 20- 40 amino acids), a highly conserved central globular domain (GD) (composed of ~ 80 amino acids) and a long C- terminal domain (CTD) (composed of 100 ~ 120 amino acids).

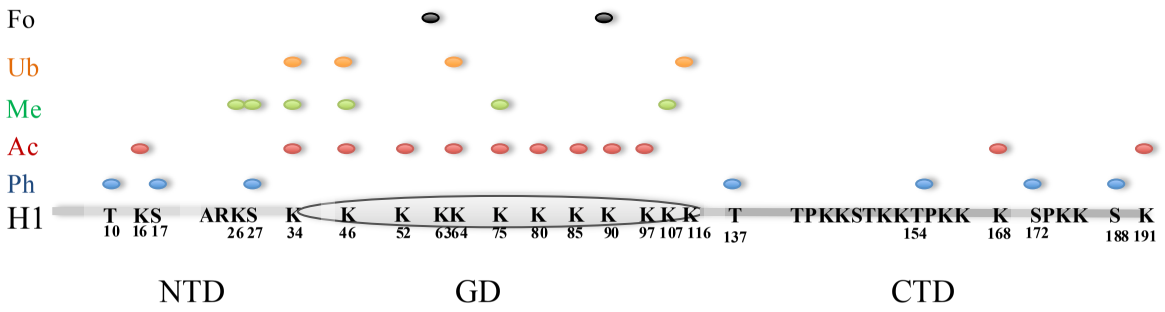

Figure 2. A schematic view of H1 PTMs.
PTMs of mammalian H1s are depicted as dots color-coded as follows: phosphorylation (blue), acetylation (red), methylation (green); ubiquitination (orange); formylation (black).

CHAPTER 2

MATERIALS AND METHODS

2.1. ESC cell culture

H1 depleted ESCs were derived previously from the outgrowth of inner cell mass of the blastocysts of their respective genotypes. ESCs were cultured in ESC culture media on mitotically inactivated mouse embryonic fibroblast (MEF) feeder cells in tissue culture dishes (Corning, Cat #: 3506) pretreated with 0.1% gelatin (Sigma-Aldrich, Cat. #: G1890) at 37°C with 5% CO_2 in a CO_2 incubator. The MEF cells were mitotically inactivated using mitomycin C to prepare the MEF feeder cells. Briefly, MEF cells were cultured in the media containing Dulbecco's modified Eagle's medium (DMEM, Life Technologies, Cat #: 12100-061), 10% fetal bovine serum (FBS) (Sigma, Cat #: 16A165), 100 U/mL penicillin and 100 µg/mL streptomycin (GEMINI, Cat #: 400-109) at 37°C with 5% CO_2. When MEF cells were grown to 70~80% confluence, mitomycin C (GEMINI, Cat #: 400-134P), dissolved in DMEM media, was added to the culture media at 10 µg/mL and the MEF cells were cultured in the presence of mitomycin C for 3 hours in the incubator. This was followed with three washes with DMEM to completely remove mitomycin C, after which the mitotically inactivated mitomycin C-treated cells were dissociated by 0.25% Trypsin-EDTA solution (Life Technologies, Cat #: 25200-056) and, plated on 0.1% gelatin (Sigma-Aldrich, Cat #: G1890) pre-treated cell culture dishes to form the feeder layer of cells for ESC culture. The feeder layers were prepared at least six hours prior to

ESC plating.

ESC culture media is consisted of DMEM supplemented with 15% FBS (Gemini, ESC grade, Cat #: 100-106), 1X MEM nonessential amino acids (NEAA, Life Technologies, Cat #: 11140050), 100 U/mL penicillin and 100 μg/mL streptomycin (GEMINI, Cat #: 400-109), 0.1 mM β-mercaptoethanol (Life Technologies, Cat #: 21985-023), and 100 U/mL of leukemia inhibitory factor (LIF; ESGRO, Chemicon, Cat #: ESG1106). ES cultures were re-fed with fresh ESC culture media daily, and passaged every two to three days accordingly. Feeder cells were removed and ESCs were grown on feeder-free culture dishes for differentiation experiments.

2.2. Generation of ESC clones with stably transfected FLAG-H1d or FLAG-H1d-domains

Vectors for expressing FLAG-H1d domains were constructed by inserting DNA fragments corresponding to the FLAG tagged H1d domains were prepared via PCR amplification followed by *Nhe*I digestion and DNA fragment purification. A FLAG-tag sequence (DYKDDDK) was fused to the N-terminus of H1d domains in frame to create FLAG-H1d domains. Each DNA fragment containing the respective FLAG tagged H1d domain was cloned into an expression vector containing H1d 5' and 3' homology regions and a Blasticidin resistant gene. The vector for expressing FLAG-H1d was generated previously in the Fan Lab by Dr. Kaixiang Cao (Cao et al., 2013).

FLAG-H1d or FLAG-H1d-domain expression vectors were transfected into mouse ESCs depleted of H1 using electroporation (BioRad, GenePulser Xcell). Twenty-four hours post transfection, Blasticidin (Corning, Cat #: 3513-03-9) selection at 20 mg/mL was applied for 10-13 days with ESC culture media containing Blasticidin. ESC colony formation was observed with an AxioVision microscope (Carl Zeiss) and cell images were taken on selected clones and processed by AxioVision software. Stable Blasticidin-resistant ESC clones were picked, trypsinized, and passaged to 24-well plate coated with mitotically inactivated feeder layer MEFs, and cultured.

2.3. Western blotting

ESCs were harvested and lysed in the RIPA lysis buffer (10 mM Tris-Cl (pH 8.0), 1 mM EDTA, 1% Triton X-100, 0.1% sodium deoxycholate, 0.1% SDS, 140 mM NaCl, and 1 mM PMSF). ESC lysates were subsequently centrifuged at 14,000rpm at 4^0C for 10 minutes, and the supernatant was transferred to a new tube mixed with SDS loading dye (100 mM Tris-Cl (pH 6.8), 4% (w/v) sodium dodecyl sulfate; electrophoresis grade, 0.2% (w/v) bromophenol blue, 200 mM dithiothreitol), followed by heating at 100^0C for 5 minutes to denature the proteins. Samples of individual ESC clones were analyzed for the expression of exogenous FLAG-H1d, or FLAG-H1d-domains or FLAG-H1d^{K46R} by Western Blotting using an anti-FLAG antibody (Sigma-Aldrich, F3165). Western blotting of ESC lysates with an anti-β-Actin (Sigma-Aldrich, A5316) antibody was included as an internal control for the

normalization of relative expression level of FLAG-H1d (FLAG-H1d-domains or FLAG-H1d^{K46R}). Cell lysates samples prepared in SDS loading dye as described above along with a protein molecular weight marker (Precision Plus ProteinTM Standards, Bio-Rad, Cat# 161-0375) were loaded onto 10% or 15% Acrylamide Gels for SDS Polyacrylamide Gel Electrophoresis (SDS-PAGE), followed by transfer of the proteins to nitrocellulose membranes (Bio-Rad, Cat# 162-0115) using a BioRad Trans-Blot® Electrophoretic Transfer Cell according to the manufacturer's manual. The membranes were subsequently incubated for one hour with blocking buffer (Odyssey® Blocking Buffer (PBS), Cat# 927-40000), followed by addition of the primary antibodies, such as the anti-FLAG antibody (Sigma-Aldrich, F3165) or anti-β-Actin antibody (Sigma-Aldrich, A5316) and incubated for one hour at room temperature or overnight at 4^0C. The membranes were washed for five times using 1X PBST0.1% (1X PBS buffer containing 0.1% of Tween-20). The membranes were incubated for one hour in room temperature in blocking buffer with addition of corresponding species-specific Alexa Fluor conjugated secondary antibodies, such as goat anti-mouse Alexa Fluor 680 (Invitrogen, Cat #A28183) or goat anti-mouse Alexa Fluor 800 (Invitrogen, Cat #A32730), followed by wash for five times with 1X PBST0.1% (1X PBS buffer containing 0.1% of Tween-20). The membranes were subsequently placed in 1X PBS buffer and protected from light prior to image scanning. The images of the Western blotting were scanned by LI-COR's Odyssey® (LI-COR) and the intensities of FLAG and β-Actin signals of each sample were quantified using Image Studio™ software (LI-COR). The normalized expression levels were calculated and plotted using Microsoft Excel program (Microsoft).

2.4. *In vitro* neural differentiation of ESCs

Neural differentiation of ESCs was performed following a protocol established previously with modifications (Zhang et al., 2012). Prior to neural differentiation, ESCs were cultured under the conditions as described above, trypsinized with 0.25% trypsin-EDTA solution (Life Technologies, Cat #: 25200-056) , and resuspended as single cell suspension at 5 x 10^4 cells/mL in the EB media (DMEM supplemented with 15% FBS (Sigma, Cat #: 16A165), 1X MEM nonessential amino acids (NEAA, Life Technologies, Cat #: 11140050), 100 U/mL penicillin and 100 μg/mL streptomycin (GEMINI, Cat #: 400-109), 0.1 mM β-mercaptoethanol (Life Technologies, Cat #: 21985-023). EBs were generated by hanging drop method. Briefly, 96 droplets with 1000 ESCs in each 20 μL volume droplet of EB media were plated on a cover of 15-cm petri dish, which were inverted. The hanging drops were incubated for five days at 37°C with 5% CO_2 in a CO_2 incubator for form EBs. EBs (at day 5) were gently collected in EB media and transferred to ultra-low attachment dishes (Corning, Cat #: CLS3262) and treated with 1 μM all-trans retinoic acid (Sigma-Aldrich, Cat #: R2500) for an additional three days (day 5+3). The day 8 EBs were collected and transferred to tissue culture dishes (Corning, Cat #: 3506) coated with 5 μg/mL poly-L-ornithine (Sigma-Aldrich, Cat #: P3655) and 5 μg/mL laminin (Life Technologies, Cat #: 23017015) and cultured in NeuroCult NSC proliferation medium (StemCell Technologies, Cat #: 05700) supplemented with bFGF 100 ng/mL GenScript, Cat #: Z03116) for up to

fifteen days (day8+15). Differentiating EBs at day 8+5, day 8+10, and 8+15 were analyzed for phenotypes. Neurite outgrowth from differentiating EBs on day 8+5 was observed with an AxioVision microscope (Carl Zeiss). Neurites extended from differentiating EBs were counted. Images were taken and processed by AxioVision software. The numbers of neurite-forming EBs were counted and recorded on day 8+5. Statistical analysis of neurite numbers was performed using GraphPad Prism 6 software (GraphPad Software) and the results were analyzed by the student-unpaired t-test.

2.5. Construction of K46R mutation in H1d

The mouse H1d-K46R mutation, corresponding to A135G mutation in the DNA sequence of H1d gene, was introduced into the expression vector GFP-H1d. The GFP-H1d expression vector (generated previously by Dr. Chenyi Pan in the Fan Lab) has the same design as the expression vectors of FLAG-H1d or FLAG-H1d-domains as described above in section 2.2. The following primers were used to amplify two DNA fragments from the GFP-H1d vector, which contain GFP and $H1d^{K46R}$ sequences; the first pair: 5'-ctagtaaagcttagaacgctagccaccatggtgagcaaggg-3' and 5'-ccgagctcatcacca<u>G</u>ggctgtggccg-3'; the second pair 5'-ctgtacaagtccgagaccgctcccgcg -3' and 5'-cggccacagcc<u>C</u>tggtgatgagctcgg-3'. Capital and underline letters indicate the A135G conversion. Restriction enzyme, *Nhe*I, was used for cloning GFP-$H1d^{K46R}$ PCR fragments into the expressional vector via Gibson Assembly.

Next, in order to create the FLAG-tagged H1d^{K46R} expression vector, the GFP portion of the GFP-H1d^{K46R} expression vector was replaced by a FLAG tag. The FLAG-H1d^{K46R} fragment was prepared by PCR with the following primers: 5'-tagtaaagcttagaacgctagccaccatgGACTACAAAGACGATGACGATAAAtccgagaccgct cccgcggcgcctg-3' and 5'- caggacgcaccactgctagcctacttcttgcgaggggcagcc-3'. Capital letters indicate the FLAG tag sequence. Restriction enzymes, *Nhe*I and *Xho*I, were used for cloning the FLAG-H1d^{K46R} PCR fragment into the expressional vector.

Sequencing was performed on the plasmid DNA of the GFP-H1d^{K46R} and FLAG-H1d^{K46R} expression vectors to validate the full length of H1d, including the K46R mutation.

2.6. Generation of H1 TKO/GFP-H1d, H1 TKO/GFP-H1d^{K46R}, and H1 TKO/FLAG-H1d^{K46R} ESC lines

GFP-H1d, GFP-H1d^{K46R}, and FLAG-H1d^{K46R} expression vectors were transfected into mouse H1c/H1d/H1e tripled knockout ESCs (H1 TKO ESCs) as described previously (Fan et al., 2001). Briefly, 2x10^7 cells were transfected with 20 ug DNA using electroporation following the manufacturer's instruction (BioRad). Twenty-four hours post transfection, Blasticidin (Corning, Cat #: 3513-03-9) selection at 20 mg/mL was applied for 10-12 days with ESC culture media containing Blasticidin. ESC colony formation was observed with an AxioVision microscope (Carl Zeiss) and cell images were taken and processed by AxioVision software. Stable Blasticidin-resistant ESC clones were picked, trypsinized, and passaged to 24-

well plate coated with mitotically inactivated feeder layer MEFs, and cultured for subsequent analysis. H1 TKO/FLAGH1d ESCs were generated previously in the Fan Lab by Dr. Yunzhe Zhang (Zhang et al., 2012).

2.7. Extraction of histones

Total histones of ESCs were extracted from chromatin with 0.2 N of sulfuric acid and analyzed followed by protocols as described (Fan and Skoultchi, 2004; Medrzycki et al., 2012). Briefly, cultured ESCs, depleted of feeder cells, were washed with PBS and harvested by trypsinization, and centrifuged. ESC cell pellet was resuspended in PBS and centrifuged, and the pellet was resuspended in sucrose buffer (0.3 M of sucrose, 15 mM NaCl, 10 mM HEPES at pH 7.9, 2 mM EDTA, 0.5 mM PMSF) containing 0.5% NP-40, and transferred to a B-pestle dounce and dounced for 10 times at intervals for 10 minutes. The lysed cells were centrifuged to collect the nuclei pellet, which was resuspended in high salt buffer (0.35 M KCl, 10 mM Tris-HCl at pH 7.2, 5 mM $MgCl_2$, with 0.5 mM PMSF and proteinase inhibitor added freshly), and dounced in a small dounce and incubation on ice for 20 minutes. The solution was centrifuged and the pellet was resuspended in 0.2 N of sulfuric acid and the pellet was grinded using an eppendorf tube pestle dounce, and incubated at 4°C with rotation overnight. The following day, the supernatant was collected after centrifugation and the total histone proteins were precipitated by the ethanol precipitation procedure. After washing three times with 75% ethanol, the histone pellet was air-dried and stored at -80°C for HPLC analysis or other experiments.

2.8. High performance liquid chromatography (HPLC) analysis of histones

RP-HPLC was used to fractionate and quantify individual H1 variants as described previously (Fan and Skoultchi, 2004; Medrzycki et al., 2012). Briefly, approximately 50 μg of total histone extracts in 100 uL ddH2O were injected into a C18 reverse phase column (Vydac) on an ÄKTAPURIFIER UPC10 system (GE Healthcare). H1 variants and core histones were fractionated with an increasing acetonitrile gradient previous documented (Fan and Skoultchi, 2004; Medrzycki et al., 2012). The elutes were monitored at 214 nm (A_{214}), and the HPLC profiles were recorded and analyzed with ÄKTA UNICORN 5.11 software (GE Healthcare). The signals for individual peaks of H1 variants as well as that for core histone H2B were calculated to determine the H1/nucleosome ratio. The values of all peaks were adjusted by the number of peptide bonds in each H1 variant and H2B. The total H1/nucleosome ratio was determined by dividing the normalized A_{214} of all H1 peaks by half of the normalized A_{214} of the H2B peak.

2.9. Fluorescence recovery after photobleaching (FRAP) analysis

The FRAP analysis was performed on H1 TKO/GFP-H1d and H1 TKO/GFP-H1d^{K46R} ESCs according to previously described protocols (Lippincott-Schwartz et al., 2001; Reits and Neefjes, 2001; Sprague and McNally, 2005). ESCs were passaged onto a gelatin-treated glass bottom dish (WillCo-Dish Glass Bottom Dish, Cat #:

CLS1810-02) a day before live-cell imaging. Imaging and photobleaching were conducted on a Zeiss LSM 710 NLO Confocal Microscope (Carl Zeiss Micro Imaging Inc.) using an argon laser (488 nm). Cells were chosen randomly with respect to GFP protein expression level, nuclear shape, and cell size. The data from the FRAP analysis were collected from 5 independent experiments for both H1 TKO/GFP-H1d and H1 TKO/GFP-H1d^{K46R} ESC lines with 30 cells analyzed per experiment. The fluorescence signals from GFP-H1D and GFP-H1D^{K46R} proteins during FRAP analysis were analyzed by Zen Microscope Imaging Software Black Edition (Carl Zeiss Micro Imaging Inc.). After defining a region of interest (ROI) of an individual cell where FRAP analysis was to be performed, pre-bleach and post-bleach images of the GFP-H1D proteins were visualized using a 63Å~ Plan Apochromat oil objective (NA 1.4) and recorded for up to 240 seconds with 2 second interval after the bleach. To bleach all fluorescent GFP proteins in the nucleus within the experimental ROI (ROIe), maximal laser power (100% of full power) was applied to the defined ROIe.

To analyze the signals from the FRAP analysis, a background ROI and a reference ROI were determined within the same field for each experimental ROI in each scan. A background ROI (ROIbg) with minimum GFP intensity as well as a reference ROI (ROIref) representing average level of GFP fluorescence intensity were selected and utilized for calculations. Raw fluorescence intensity values from bleached (ROIe), background (ROIbg), and reference ROIs (ROIref) were exported to Microsoft Excel to be normalized to obtain the relative fluorescence recovery intensity (rFRI) according to formula ((ROIe)- (ROIbg))/((ROIref)- (ROIe)) as

previously described (Phair et al., 2004). The percentage of fluorescence recovery for each time point was calculated by dividing the rFRI of each time point by the average rFRI before photobleaching. The photobleached time point was used as a baseline for further calculation of half-time recovery rate as well as plotting of the fluorescence recovery curves. Statistical analysis was carried out using Prism 6 software (GraphPad Software, Inc.). The non-linear regression and the exponential one-phase association model was used to calculate the halftime recovery rate and statistics significance of the fluorescence recovery curves. The student-unpaired t-test was used to compare the statistics significance of the halftime recovery rate between two samples.

CHAPTER 3

RESULTS

3.1. An experimental approach to generate and characterize H1 reconstituted ESC lines.

In order to dissect the potential role of individual H1 domains as well as the specific site of H1 post-translational modifications, we took advantage of H1 depleted ESCs that are impaired in ESC differentiation and utilize an approach of functional reconstitution by overexpression of exogenous H1 or H1 mutants in the H1 depleted ESCs. Characterization of these H1 reconstituted ESCs will allow us to test the key H1 variant, H1 domains and sites in mediating ESC differentiation.

The overview of the generation and characterization of H1 reconstituted ESC lines with exogenous H1 or H1 mutants is shown in Figure 3. Vectors to effectively express exogenous H1s or H1 mutants in ESCs were constructed to insert a FLAG tag at the N-terminus of H1d (and H1d mutants) (Figure 3). The FLAG tag allows analysis of the expression levels of the exogenous H1s and H1 mutants in ESC clones by Western blotting using highly specific anti-FLAG antibody. We have previously demonstrated that the FLAG tag at the N-terminus of H1d does not interfere with biochemical or chromatin binding properties of H1d and that FLAGH1d is functionally equivalent to H1d during mouse development (Cao et al., 2013). The vectors also contain a Blasticidin resistant gene, which allows the screening of stably transfected ESC clones using Blasticidin (Figure 3). The expression vectors were

transfected into H1 depleted ESC cells. The stably transfected ESC colonies resistant to Blasticidin selection were picked and cultured. For each experiment, twenty-four to ninety six colonies were individually analyzed to gauge the expression levels of transfected H1s or H1 mutants by Western blotting using anti-FLAG antibody. Western blotting using antibody again β-ACTIN, a house keeping protein, was performed in parallel as internal control for protein loading for the ESC lysate of each ESC clone in SDS PAGE. A high ratio of the FLAG signal to the β-ACTIN signal indicates high expression of the respective exogenous H1 or H1 mutant proteins. Two to four ESC clones with high expression levels of transfected H1 or H1 mutants were selected from each experiment for further characterization of ESC phenotypes, ESC morphology, H1 variants profile of ESCs by high-performance liquid chromatography (HPLC) analysis of histones, as well as neurite outgrowth of differentiating EBs.

A distinct phenotype displayed by H1 TKO and H1 QKO ESCs in ESC differentiation is their severely compromised neurite outgrowth detected in a 3D *in vitro* neural differentiation assay that we previously established and optimized in the lab (Figure 4) (Zhang et al., 2012; Pan et al., manuscript in preparation). The *in vitro* neural differentiation of ESC is a well-established system for studying regulatory mechanisms during ESC differentiation processes. The protocol we adopted and optimized involves the preparation of embryoid bodies (EBs), which are formed from three-dimensional (3D) aggregates of ESCs (Figure 4). ESCs, passaged without feeder cells, were harvested, counted, and 1000 ESCs (day 0) were used for

preparation of each embryoid body following the hanging drop method as described in Material and Methods section 2.4. Embryoid bodies formed using the hanging drop method were incubated in the hanging drops for five days. These (day 5) EBs were subsequently harvested and transferred to low-attachment dishes, and treated with all-trans retinoic acid (RA) for an additional three days (day 8) to promote the differentiation toward neural lineages. These day 8 EBs were subsequently transferred to poly-L-ornithine (PLO)- and laminin-coated culture dishes and cultured in neural differentiation media for further neural differentiation. Five days post the transfer of EBs to PLO/laminin treated plates (referred as day 8+5), numerous neurites sprout from majority of the day 8+5 EBs as shown in WT EBs (Figure 5). These EBs were cultured to allow further differentiation for up to fifteen days post transfer (day 8+15). For this thesis, the quantitative assessment of neurite outgrowth was performed on day 8+5 EBs in this differentiation scheme (Figure 4). On average, over 70% of WT EBs had neurites outgrowth. Previous studies indicate that neurite outgrowth from EBs is correlated with neural differentiation and the expression of neuronal markers (Zhang et al., 2012). We quantify neurite outgrowth as a measure for neural differentiation. Over 100 EBs were examined and the percentage of neurite-forming EBs was calculated as the number of EBs that showed neurite outgrowth of the total number of EBs.

Two H1 depleted ESC lines, H1c/H1d/H1e/$H1^0$ quadruple knockout (H1 QKO) ESCs and H1c/H1d/H1e triple knockout (H1 TKO) ESCs, were used in this thesis study. Zhang et al. have demonstrated that H1 TKO ESCs are impaired in ESC differentiation and that H1 TKO EBs have marked reduced neurite outgrowth

compared with WT EBs (Zhang et al., 2012). More recently, Pan et al. have shown that H1 QKO ESCs had even more severe defects in neurite outgrowth compared with H1 TKO ESCs (Pan et al, manuscript in preparation). Thus, the H1 QKO ESCs, lacking endogenous H1c, H1d, H1e, and $H1^0$, provide a clean cellular system for us to use functional reconstitution approach to test the individual H1 variant and its domains in restoration of the neural differentiation defects of H1 QKO ESCs.

H1 TKO ESCs and H1 QKO ESCs were derived previously from the outgrowth of inner cell mass of the blastocysts of their respective genotypes. Compared with WT ESCs, H1 TKO and H1 QKO ESCs had approximately 50% reduction of the total H1 levels, but displayed normal ESC morphology and expression of the pluripotency gene Oct4 (Fan et al., 2005; Zhang et al., 2012; Pan et al., manuscript in preparation). The H1 TKO and H1 QKO ESCs also maintain normal ESC characteristic colony morphology, and comparable cell proliferation rate in ESC self-renew as WT ESCs (Figure 5) (Fan et al., 2005; Zhang et al., 2012; Pan et al., manuscript in preparation). However, following the neural differentiation protocol described above, by day 8+5, wild type (WT) EBs developed numerous robust and extended neurite and were surrounded by a radial monolayer of migrated neural cells, whereas most H1 TKO EBs and H1 QKO EBs exhibited impaired migration of neural cells failed to have neurite outgrowth. For the minority of H1 TKO EBs and H1 QKO EBs, which had neurite outgrowth, they formed fewer and shorter neurites (Figure 5). Quantitative measurements showed that on average 35% of H1 TKO EBs and 21.8% of H1 QKO EBs had neurite outgrowth, whereas 74.1% of WT EBs had robust neurite outgrowth (Figure 6). Thus, these cells and

experimental system offer an opportunity to quantitatively measure the restoration of phenotype defects in neural differentiation of ESCs.

3.2. Partial rescue of the neurite outgrowth defects of H1 QKO ESC by H1d

Before we began to dissect the role of H1 domains in ESC differentiation, we first set to test the rescue of neurite outgrowth defects of H1 QKO ESCs by overexpression of a full-length H1 variant. We chose to test H1d variant among the four H1 variants, $H1^0$, H1c, H1d, and H1e, depleted in H1 QKO ESCs, because H1d is one of the most abundant H1 variants in ESCs, EBs, and in mouse somatic tissues and that overexpression of H1d in H1 TKO ESCs mitigates the impairment of differentiation in H1 TKO (Fan et al., 2003; Fan et al., 2005; Zhang et al., 2012). Expression vector containing the FLAG-tagged full length H1d (Figure 7A) was constructed and transfected into H1 QKO ESCs. Forty-eight stably transfected ESC clones were picked, cultured and established into ESC lines. These 48 H1QKO/H1d ESC lines were analyzed for the expression levels of exogenous FLAGH1d by semi-quantitative Western blotting assays using an anti-FLAG antibody. Western blotting with anti-β-Actin was performed to serve as normalization control. Representative Western blotting results are shown in Figure 7B. The clone marked with asterisks showing high expression levels of exogenous H1d, was used in subsequent analysis (Figure 7B).

Two H1 QKO/H1d ESC lines which had high expression of reconstituted H1d protein levels were further analyzed for ESC morphology and self-renew properties.

These H1 QKO/H1d ESCs exhibited normal ESC colony morphology (Figure 8) and had comparable growth rate as WT and H1 QKO ESCs. However, when these H1 QKO/H1d ESCs were induced to differentiate along neural lineage using the 3D *in vitro* neural differentiation scheme as described above, H1 QKO/H1d EBs had improved neurite outgrowth with more EBs forming neurites and more neurites from neurite forming EBs as compared with H1 QKO EBs, suggesting that H1d overexpression mitigate the defects in neurite outgrowth observed in H1QKO ESCs (Figure 9). Quantitative analysis of neurite outgrowth from day 8+5 EBs of more than 200 EBs revealed that over 50% of H1 QKO/H1d EBs had neurite growth, which was significantly higher than H1 QKO EBs, which had 21.8% of neurite-forming EBs (Figure 10). These results suggest that H1d reconstitution was able to restore the deficiency in the ESC differentiation of H1 QKO ESCs. However, H1 QKO/H1d EBs had fewer neurite forming EBs compared with WT EBs, which had 74.1% of EBs forming neurite formation, suggesting that H1d reconstitution partially rescues H1 QKO ESCs neurite outgrowth defects.

3.3. Overexpressing H1d-CTD in H1 QKO ESCs does not restore neurite outgrowth in H1 QKO ESCs.

All linker histone H1 proteins contain three domains; a small N-terminal domain (NTD), the highly conserved globular domain (GD), and a long C-terminal domain (CTD). Several studies have suggested that individual H1 domains may have different functions due to their distinctive amino acid residue compositions and

secondary structures (Cutter and Hayes, 2017; Happel and Doenecke, 2009; Kowalski and Palyga, 2016; Lyubitelev et al., 2016). Among the three H1 domains, the C-terminal domain accounts for more than half of the linker histone sequences and is important for high affinity binding of H1 to chromatin. Both the globular domain and the C-terminal domain have been shown to be important for chromatin binding. N-terminal domain of H1d is smallest domain, only consisting ~38 a.a., and is unstructured. To dissect the effects of H1 domains in ESC differentiation, we set out to test CTD and NTD-GD (covering both NTD and GD) domains of H1 in ESCs by overexpressing them in H1 QKO ESCs.

We first investigated the effects of overexpressing H1d-CTD in the H1 QKO ESCs by following the experimental approach described above in section 3.1 (Figure 3). A vector expressing FLAG tagged H1d-CTD (Figure 11A) was constructed and transfected into H1 QKO cells, followed by Blasticidin selection. Forty-eight stably transfected ESC clones were picked, cultured, and analyzed for their expression levels of exogenous FLAG-H1d-CTD by semi-quantitative Western blotting assays using anti-FLAG and anti-β-Actin antibodies. Representative Western blotting results are shown in Figure 11B. The clone marked with asterisks had high expression of H1d-CTD and was used for further analysis (Figure 11B).

Two H1 QKO/H1d-CTD ESC lines were expanded in culture and characterized for ESC properties as well as EB differentiation. These ESCs exhibit normal ESC colony morphology and self-renew properties as compared with WT and H1 QKO ESCs (Figure 12). *In vitro* neural differentiation of H1 QKO/H1d-CTD ESCs was carried out to assess whether overexpression of H1d-CTD in H1 QKO

ESCs restores neurite outgrowth in H1 QKO EBs. Among the total H1 QKO/H1d-CTD EBs analyzed at day 8+5, the neurite-forming EBs accounts for 24.3%, similar to the 21.8% of neurite-forming EBs among H1 QKO EBs (Figure 13, Figure 14). In addition, the neurites from neurite forming EBs in H1 QKO/H1d-CTD EBs on average are fewer than WT but are similar to those present in H1 QKO EBs. These results indicate that overexpressing H1d-CTD does not restore neurite outgrowth defects of H1 QKO EBs and that H1d-CTD is not the key domain for H1d in mediating ESC differentiation.

3.4. Overexpressing H1d-NTD-GD in H1 QKO ESCs partially rescues neurite outgrowth defects of H1 QKO EBs

Next, we tested the role of H1d-NTD-GD in ESC differentiation by overexpressing this portion of H1d in the H1 QKO ESCs. Using a similar approach as studies described above, FLAGH1d-NTD-GD (Figure 15A) was introduced into the H1 QKO ESC cells and stably transfected ESC clones with highly expressed H1-NTD-GD were selected for the subsequent neural differentiation study (Figure 15B). H1 QKO/H1d-NTD-GD ESCs displayed normal ESC colony morphology as WT and H1 QKO ESCs (Figure 16).

We induced the neural differentiation of H1 QKO/H1d-NTD-GD ESCs to analyze the influence on neurite outgrowth by reconstitution of H1d-NTD-GD into H1 QKO ESCs. In contrast to H1 QKO and H1 QKO/H1d-CTD ESCs, H1 QKO/H1d-NTD-GD EBs displayed robust neurite outgrowth with long and thick

neurites sprouting from day 8+5 EBs (Figure 17), similar to those observed in WT and H1 QKO/H1d EBs. Quantitative measurements supported the observations and revealed that an average of 38.2% of H1 QKO/H1d-NTD-GD EBs were neurite forming EBs, which was significantly higher than 21.8% ($p<0.05$), the percentage of neurite-forming EBs among H1 QKO EBs but remained lower than 50.1%, the percentage of neurite-forming EBs among H1 QKO/H1d EBs (Figure 18). These results suggest that overexpressing H1d-NTD-GD was able to mitigate the neurite outgrowth defects of H1 QKO EBs even though H1d-NTD-GD is not as effective as full length H1d in restoring the neurite outgrowth defects of H1 QKO EBs.

3.5. H1d-GD Overexpression partially rescues the neurite outgrowth defects of H1 QKO EBs

The fact that H1 QKO/H1d-NTD-GD EBs exhibited improved neurite outgrowth compared with H1 QKO EBs suggest that the key domain(s) for H1d in mediating ESC neural differentiation could be one or both of NTD and GD. As the GD is highly conserved among H1 variants and the NTD is rather small and unstructured (Happel and Doenecke, 2009; Pan and Fan, 2016), we decided to further narrow down the region of H1d for testing to GD alone. To achieve this goal, we constructed an expressional vector, which expresses FLAG tagged H1d-GD (Figure 19A), and expressed the H1d-GD in H1 QKO ESCs following the experimental approach described above in section 3.1. Western blotting screening of forty-eight stably transfected ESC clones identified a few H1 QKO/H1d-GD ESC lines with high

expression levels of H1d-GD (Figure 19B). These ESC lines were further analyzed for ESC colony morphology and growth rate. These cells had similar colony morphology and growth as WT and H1 QKO ESCs (Figure 20). The results demonstrated that overexpressing H1d-GD did not cause abnormalities in ESC morphology or self-renew.

When induced to differentiate along neural lineage, day 8+5 EBs of H1 QKO/H1d-GD had robust neurite formation, comparable to those observed from WT and QKO/H1d EBs (Figure 21). Quantitative analysis of neurite outgrowth from H1 QKO/H1d-GD EBs at day 8+5 revealed that ~ 38% of H1 QKO/H1d-GD EBs analyzed were neurite-forming EBs, which is significantly higher than H1 QKO EBs (Figure 22).

3.6. GD is the key domain of H1d for mediating neurite outgrowth of differentiating EBs

Among all functional reconstitutions of H1 depleted ESC lines analyzed above, H1 QKO/H1d, H1 QKO/H1d-NTD-GD and QKO/H1d-GD had improved neurite outgrowth compared with H1 QKO ESCs (Figure 23). Collectively, comparisons of the regions corresponding to the full-length H1d, H1d-CTD, H1d-NTD-GD, and H1d-GD as well as the neurite outgrowth capacity of the respective H1 QKO/H1d, H1 QKO/H1d-CTD, H1 QKO/H1d-NTD-GD and QKO/H1d-GD ESCs, revealed that H1 QKO/H1d-GD ESCs had comparable neurite forming capacity as H1 QKO/H1d-NTD-GD and H1 QKO/H1d EBs (Figure 24, Figure 25). This is in

contrast to the lack of rescue by H1 CTD in restoration of neurite outgrowth of H1 QKO ESCs. These results indicate that GD is the domain of H1d responsible for mediating the restoration of neurite formation in H1 QKO EBs.

In summary, these results suggest that GD is the key domain of H1d for mediating neurite outgrowth of differentiating EBs and that the rescue effect of H1d in neurite outgrowth restoration is largely mediated through its globular domain.

3.7. Post-translational modifications (PTMs) on H1d at lysine 46 (K46) are critical for mediating the role of H1d in ESC differentiation

H1 plays an important role in chromatin condensation and regulation of specific gene expressions. Aforementioned studies from this thesis suggest that GD is the most important domain in mediating the role of H1d in neurite outgrowth from EBs. Previous studies show that histone H1s are subject to a variety of post-translational modifications, including phosphorylation, acetylation, methylation, ubiquitination and formylation (Kamieniarz et al., 2012; Wisniewski et al., 2007). To further dissect the role of H1d GD in ESC differentiation, we turned to individual sites within the GD of H1. Post-translational modifications of histones are key to mediate the function of histones in chromatin structure and function. While a few post-translational modifications of H1 have been investigated, the functions of most H1 PTMs remain unexplored (see introduction section 1.3).

To identify the potential key sites in H1, we compiled and compared the reported PTMs detected in mammalian H1 variants from previous studies

(introduction section 1.3 and Figure 26). Among all the sites with PTMs in the globular domain of mouse H1d, K46 is unique in that it is highly conserved among H1b, H1c, H1d and H1e in both mouse and human (Baxevanis and Landsman, 1998; Cutter and Hayes, 2017; Kowalski and Palyga, 2016; Lyubitelev et al., 2016; Pan and Fan, 2016) and that it is also a hot spot for multiple H1 modifications, including acetylation, ubiquitination and tissue-specific methylation (Kowalski and Palyga, 2016; Wisniewski et al., 2007) (Figure 26). Therefore, we have focused on the site lysine 46 within the globular domain of mouse H1d.

To test if the PTMs on Lys 46 are required for mediating the role of H1d in ESC differentiation, we set out to disrupt the modifications on this site by making point mutation at this site. We decided to mutate the lysine to arginine at the site 46 so not to change the charge of the site because both lysine and arginine are positively charged amino acids. We first constructed FLAG-tagged H1d^{K46R} expressional vector in which K46R mutation was introduced into the H1d expressional vectors (Figure 27). Sequencing of the entire FLAG-tagged H1d^{K46R} portion of the expression vector verified that the K46R is the only mutation introduced into the FLAG-H1d sequence (Figure 28). The FLAG-tagged H1d^{K46R} expression vector was transfected into H1 TKO ESCs and twenty-four stably transfected ESC clones resistant to Blasticidin selection were picked. The expression levels of exogenous FLAG-H1d^{K46R} in these H1 TKO/ H1d^{K46R} ESC clones were analyzed by Western blotting analysis using anti-FLAG and anti-β-Actin antibodies as described in Material and Methods section 2.6. We identified H1 TKO/H1d^{K46R} ESC lines with high expression levels of FLAG H1d^{K46R} proteins (Figure 29). These selected H1 TKO/FLAG H1d^{K46R} ESCs

displayed the normal ESC colony morphology and cell growth as WT and H1 TKO ESCs (Figure 30).

We next induced neural differentiation of the H1 TKO/H1d^{K46R} ESCs and compared their neurite formation with that of WT and H1 TKO ESCs using the *in vitro* neural differentiation scheme. Interestingly, there was no noticeable improvement in neurite outgrowth of day 8+5 EBs when comparing H1 TKO/H1d^{K46R} with H1 TKO ESCs (Figure 31 and Figure 32). The differences in the percentage of neurite forming EBs in respective H1 TKO EBs (35%) and H1 TKO/FLAG H1d^{K46R} (26.2%) are not statistically significant ($p>0.05$), whereas both H1 TKO EBs (35%) and H1 TKO/FLAG H1d^{K46R} ESC lines had significantly lower percentage compared to the 74.1% of neurite-forming EBs among WT EBs (Figure 32). These results demonstrated that K46R mutation of H1d disrupts the rescue effect of H1d in H1 TKO ESCs and suggested that the PTMs on K46 of H1d are required for mediating the role of H1d in ESC differentiation.

Figure 33 summarizes the results and the comparisons from quantitative analysis of H1 depleted ESCs reconstituted with H1d, H1d domains and H1d^{K46R} mutant. These results suggest that GD is the key domain of H1 in mediating the role of H1 in ESC differentiation and that the PTMs on K46 of GD are necessary for H1 functions in ESC differentiation.

3.8. H1d^{K46R} binds chromatin and has the same biochemical properties as H1d

As discussed above, because both lysine and arginine are positively charged amino acids, H1d^{K46R} is expected to maintain the same levels of positive charges and hydrophobicity as H1d. Nevertheless, it remains a formal possibility that K46R mutation disrupts the protein structure and properties of H1d, which could potentially account for its failure in rescuing the neurite outgrowth defects in H1 TKO/H1d^{K46R} EBs. To further understand the underlying mechanisms contributing to the functional differences caused by K46R mutation, we set out to characterize the biochemical properties of H1d^{K46R}.

Toward this end, we analyzed and compared chromatin bound H1 histones from H1 TKO/H1d^{K46R} ESCs and H1 TKO/H1d ESCs by high performance liquid chromatography (HPLC). H1 TKO/H1d ESCs were previously established (Zhang et al., 2012). Both H1 TKO/H1d and H1 TKO/H1d^{K46R} ESC lines express high levels of respective exogenous FLAG-H1d and FLAG-H1d^{K46R} as shown in Western blotting using an anti-FLAG antibody (Figure 34). Chromatin was extracted from WT, H1 TKO, H1 TKO/H1d and H1 TKO/H1d^{K46R} ESCs. Total histones were subsequently extracted from isolated chromatin using 0.2N H_2SO_4 and subjected to HPLC analysis following previously established protocols as described in Material and Methods section 2.7 and section 2.7. H1 variants and core histones were eluted with an increasing gradient of acetonitrile. WT ESCs exhibited distinct peaks for H1^0, and H1a to H1e, where mouse H1d and H1e were eluted in the same peak as previously described (Fan 2001 MCB). As expected, the HPLC profile of histones extracted

from H1 TKO ESCs lacks the peaks corresponding to H1c, H1d, and H1e, demonstrating the deletion of these three H1 variants (Figure 35).

FLAG-H1d proteins have the same biochemical properties and hydrophobicity as H1d and are functionally equivalent to H1d *in vivo* (Cao et al., 2013). As previously demonstrated, FLAG-H1d were eluted in the same peak as H1d in HPLC analysis of histone extracts (Figure 35). HPLC analysis of histones extracted from the H1 TKO/H1d^{K46R} ESCs also showed a peak was eluted at the same position as H1d and FLAGH1d, suggesting the peak being H1d^{K46R} (Figure 35). The peaks at of the position of H1d from HPLC analysis of histone extracts H1 TKO/H1d and H1 TKO/H1d^{K46R} ESCs were eluted and analyzed by Western blotting using an anti-FLAG antibody (Figure 36). The Western blotting results verified the respective eluted proteins being FLAG tagged exogenous proteins. The fact that the histones were extracted from purified chromatin and that H1d^{K46R} proteins were eluted in the same peak position as endogenous H1d suggest that H1d^{K46R} binds chromatin, maintains the biochemical properties of H1d and has similar hydrophobicity as H1d.

3.9. K46R mutation in H1d decreases H1d dynamics

To further dissect the effects of K46R mutation on the proteins of H1d, we turned to study the mobility of H1d^{K46R} and compared with that of H1d by Fluorescence recovery after photobleaching (FRAP) analysis. FRAP assay is a powerful method for studying protein mobility and dynamics *in vivo* (Lippincott-Schwartz et al., 2001; Reits and Neefjes, 2001; Sprague and McNally, 2005). In order

to determine the kinetics of diffusion H1d^{WT} and H1d^{K46R} mutant, we first constructed vectors expressing GFP-H1d and GFP-H1d^{K46R} proteins in which Green Fluorescent Protein (GFP) was fused to the N-terminus of full length H1d and H1d^{K46R} (Figure 37). GFP-H1d and GFP-H1d^{K46R} expression vectors were stably transfected into H1 TKO ESCs as described in Material and Methods section 2.6.

Stable ESC clones of H1 TKO/GFP-H1d and H1 TKO/GFP-H1d^{K46R} were picked and analyzed using an anti-GFP antibody (Figure 38). Immunoblots with anti-β-actin antibody are included as loading controls (Figure 38). Clones of H1 TKO/GFP-H1d and H1 TKO/GFP-H1d^{K46R} that selected for FRAP analysis expressed comparable amounts of GFP fused proteins (Figure 39).

We next performed FRAP analysis on H1 TKO/GFP-H1d and H1 TKO/GFP-H1d^{K46R} ESCs to determine the mobility of H1d and H1d^{K46R} *in vivo* as described in Material and Methods section 2.9. In FRAP analysis, the protein "mobility" is determined by the rates of diffusion and transport of the fluorescent molecule through the cellular environment (Lippincott-Schwartz et al., 2001; Reits and Neefjes, 2001; Sprague and McNally, 2005). The visualized images of a single nucleus and the changes/recovery of fluorescence intensity were collected from the pre-bleach period to 240 seconds post-bleaching and a recovery curve was plotted (Figure 40).

The recovery rate of each post-bleaching time point was normalized with the baseline intensity at photobleaching and used for calculation of the half-time of recovery as detailed in Material and Methods section 2.9. FRAP analysis of H1 TKO/GFP-H1d H1 TKO/GFP-H1d^{K46R} ESCs revealed that GFP-H1d^{K46R} proteins have a slower recovery rate as compared with GFP-H1d (Figure 41). Calculation of

the half time of recovery (t1/2) indicates that the t1/2 of GFP-H1d, 51.29 seconds, is significantly shorter than that of GFP-H1d^{K46R}, 63.05 seconds. Taken together, the results from FRAP analysis revealed that H1d^{K46R} has lower mobility and reduced dynamics compared with WT H1d. The reduction in dynamic mobility of H1d may contribute to the inability of H1d^{K46R} in the restoration of neurite outgrowth in the reconstituted H1 TKO/GFP-H1d^{K46R} ESCs.

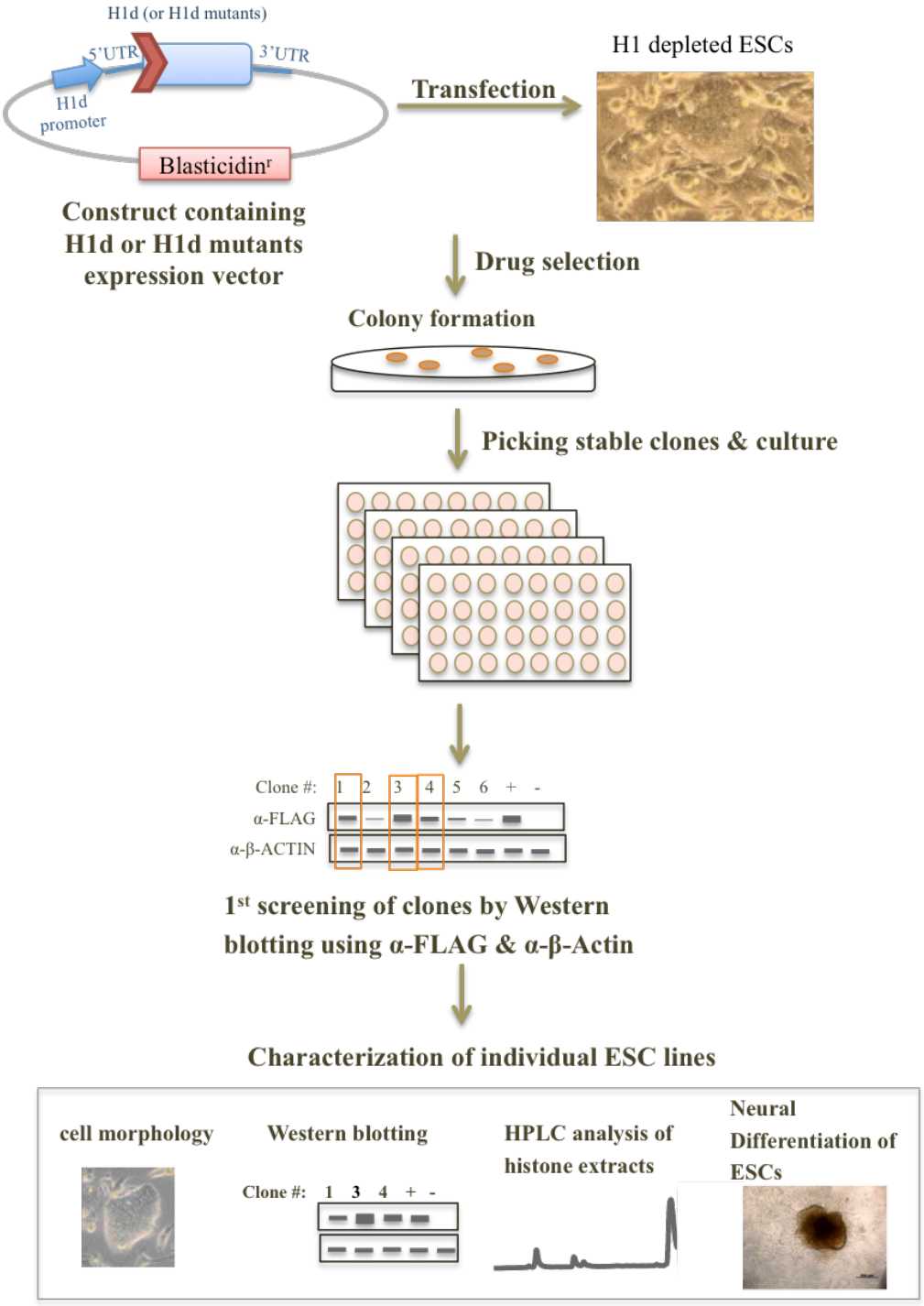

Figure 3. Experimental approach of generation and characterization of reconstituted H1 ESC lines.
H1 depleted ESCs were reconstituted with exogenous H1s, H1 domains, and H1 mutants.

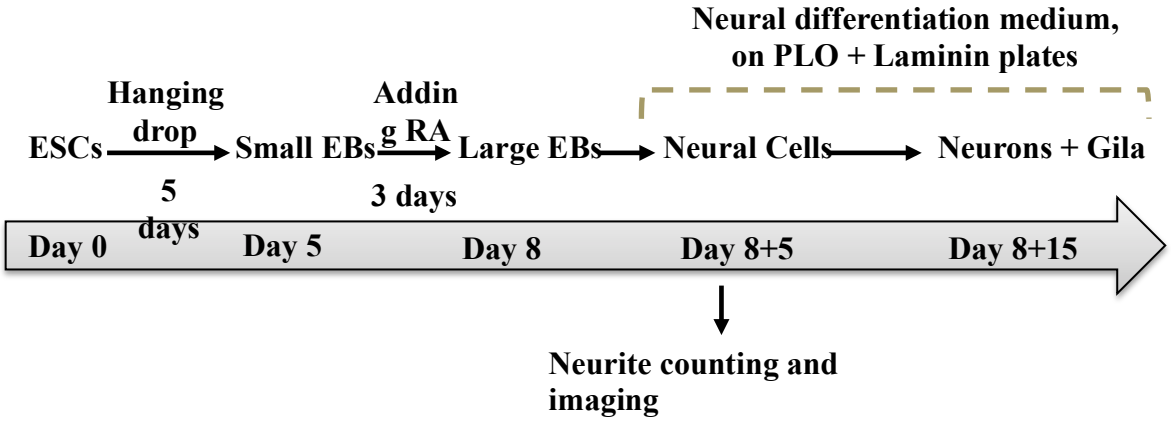

Figure 4. Optimized *in vitro* neural differentiation scheme of ESCs.
Modified from Zhang et al., 2012 and Pan et al., in preparation.

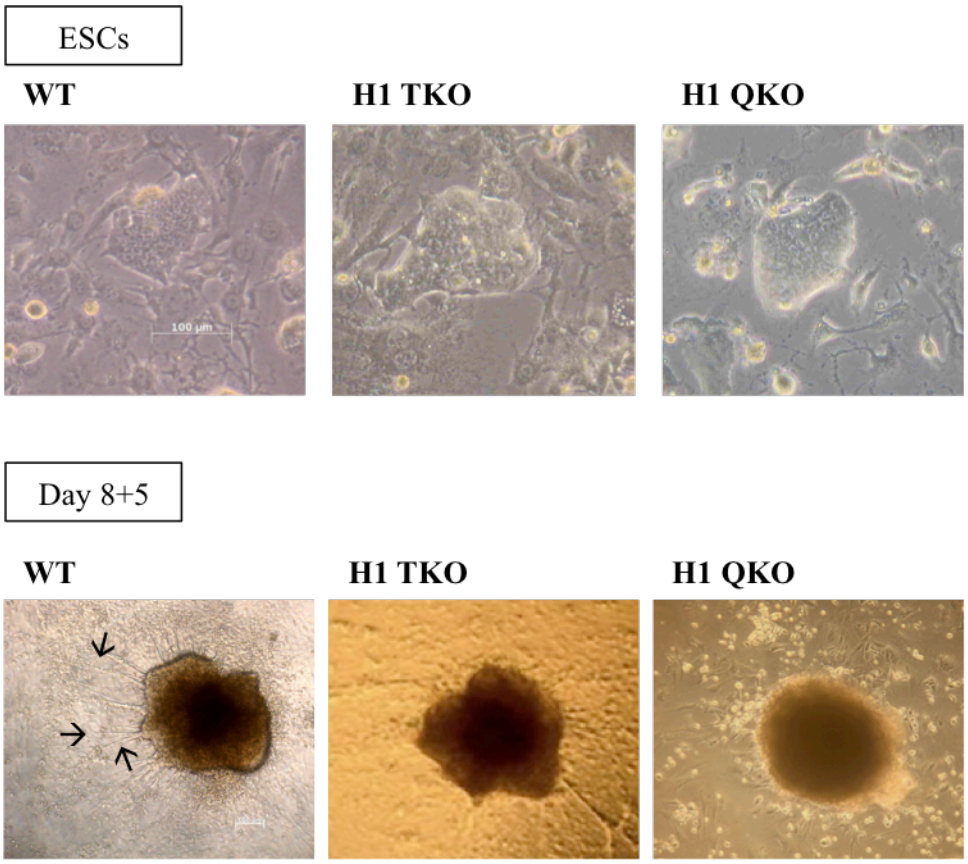

Figure 5. Morphology of WT, H1 TKO and H1 QKO ESCs and day 8+5 EBs during neural differentiation.
Phase contrast images of ESCs and day 8+5 differentiating EBs of WT, H1 TKO, and H1 QKO are shown. Arrows indicate representative neurite outgrowth. Scale bar, 100 µm.

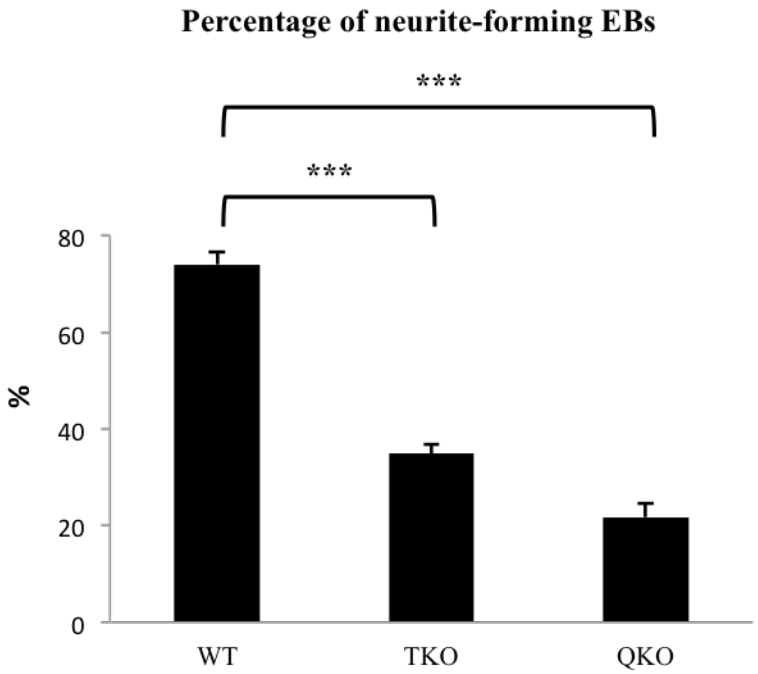

Figure 6. H1 QKO ESCs are deficient in neural differentiation of ESCs.
Percentage of neurite-forming EBs among total EBs analyzed for each genotype is presented. Each EB was observed and analyzed for neurite outgrowth. Over 100 EBs were analyzed for each genotype per experiment. Numbers were averaged from at least 4 experiments; WT, n=13; TKO, n=5; QKO, n=9. All data are presented as means ± S.E.M. ***: $p<0.001$. Y axis: Percentage of neurite-forming EBs.

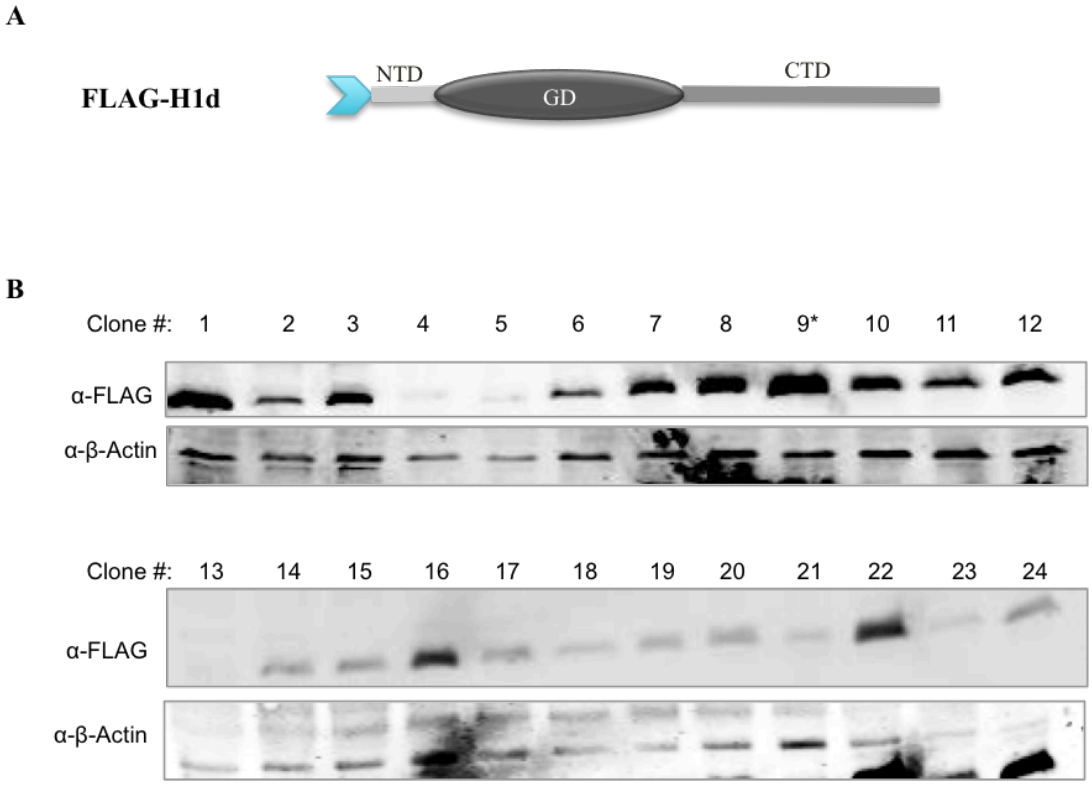

Figure 7. Generation of H1 QKO/H1d ESC cell lines.

A) A schematic diagram of the FLAG tagged H1d. NTD: N-terminal domain. GD: globular domain. CTD: C-terminal domain. The light blue arrowhead represents a flag tag which is fused to the N-terminus of H1d.

B) Western blotting analysis of expression levels of FLAG-H1d in H1 QKO/H1d ESCs. H1 QKO ESCs were transfected with vectors expressing FLAG-H1d. Representative immunoblots of twenty-four H1QKO/H1d ESC clones using anti-FLAG and anti-β-Actin antibodies are shown. The clone indicated with asterisks, demonstrating high expression levels of H1d, was one of the ESC lines selected for further characterization.

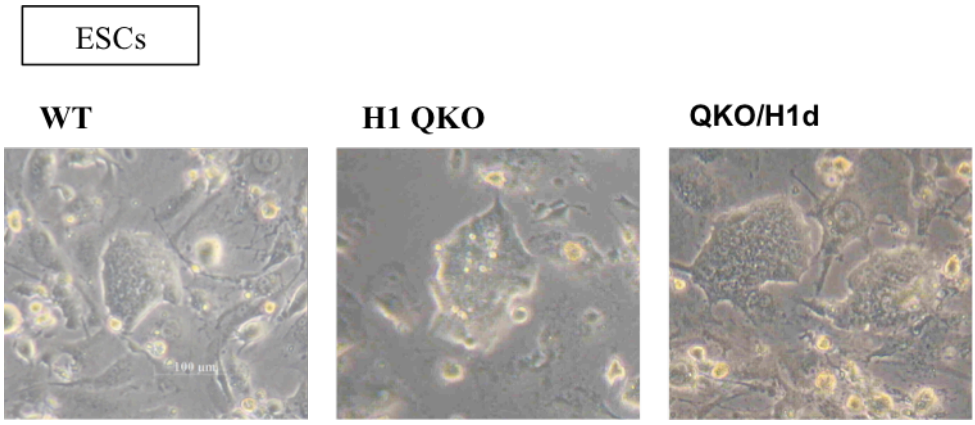

Figure 8. H1 QKO/H1d ESCs exhibit normal ESC colony morphology.
Phase contrast images of WT, H1 QKO, and H1 QKO/H1d ESCs are shown. Scale bar, 100 μm.

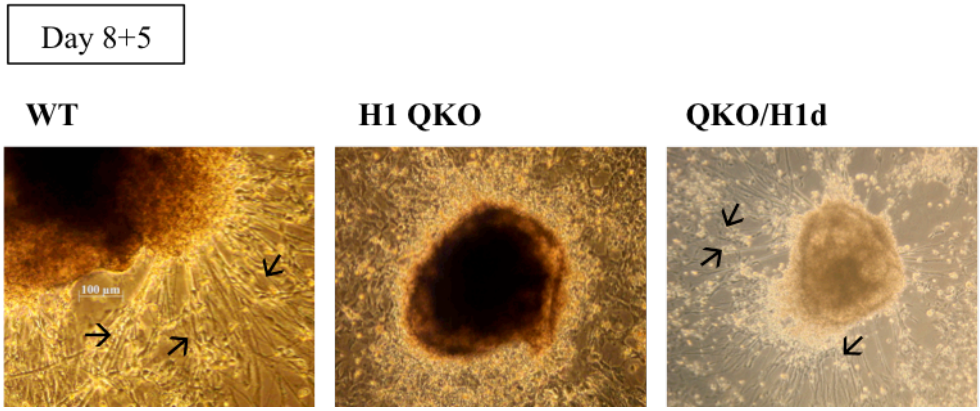

Figure 9. Neurite outgrowth defects during neural differentiation of H1 QKO/H1d ESCs.
Phase contrast images of day 8+5 EBs during neural differentiation of WT, H1 QKO, and H1 QKO/H1d ESCs are shown. Arrows indicate representative neurite outgrowth. Scale bar, 100 μm.

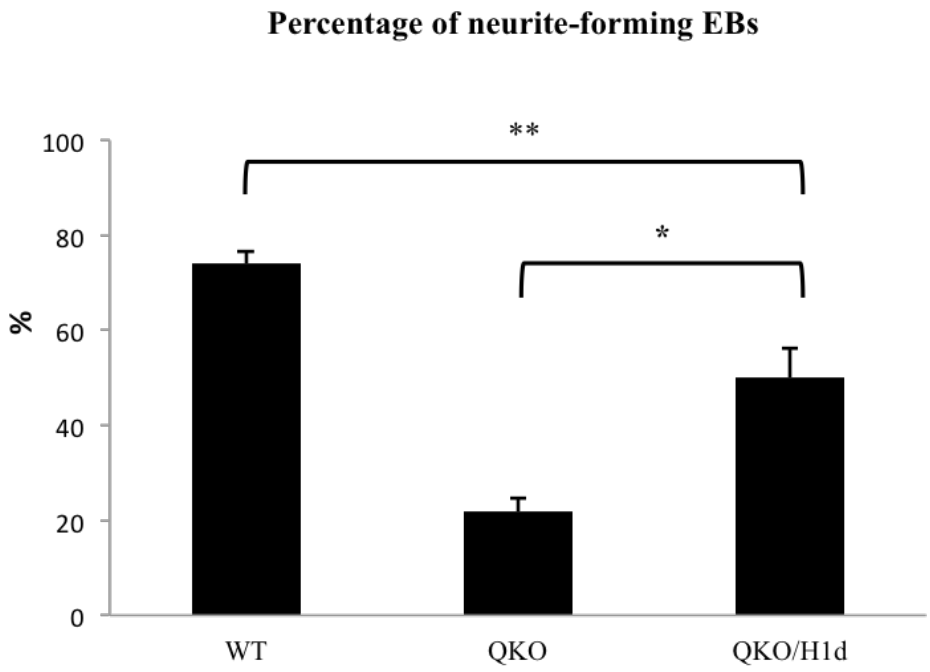

Figure 10. Overexpressing H1d in H1 QKO ESCs partially rescues neurite outgrowth defects of H1 QKO EBs.
Percentage of neurite-forming EBs among total EBs analyzed for each genotype is presented. Each EB was observed and analyzed for neurite outgrowth. Over 100 EBs were analyzed for each genotype per experiment. Numbers were averaged from at least 4 experiments; WT, n=13; QKO, n=9; QKO/H1d n=4. All data are presented as means ± S.E.M. *: p-value < 0.05; ** :p-value <0.01.

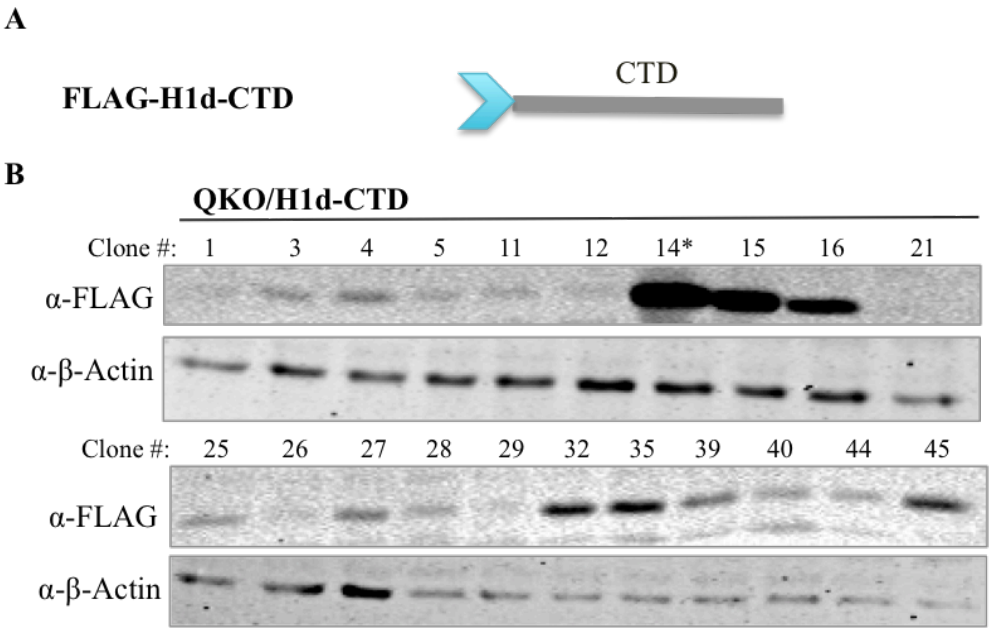

Figure 11. Generation of H1 QKO/H1d-CTD ESC lines.

A) A schematic diagram of the FLAG tagged H1d-CTD. CTD: C-terminal domain. The light blue arrowhead represents a flag tag which is fused to the N-terminus of H1d-CTD.

B) Western blotting analysis of expression levels of FLAG tagged H1d-CTD in H1 QKO/H1d-CTD ESC lines. H1 QKO ESCs were transfected with vectors expressing FLAG-H1d-CTD. Forty-eight stable ESC clones were picked and screened by Western blotting using an anti-FLAG antibody. Representative immunoblots of FLAG-H1d-CTD expressing cell clones are shown. Immunoblots with anti-β-Actin antibody were included as loading controls. The clone indicated with asterisks, demonstrating high expression levels of H1d-CTD, was one of the ESC lines selected for further analysis.

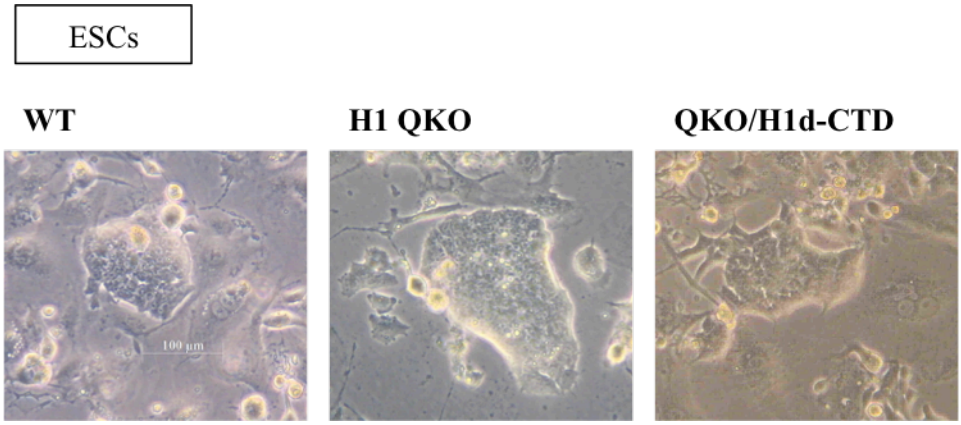

Figure 12. H1 QKO/H1d-CTD ESCs exhibit normal ESC colony morphology. Phase contrast images of WT, H1 QKO, and H1 QKO/H1d-CTD ESCs are shown. Scale bar, 100 µm.

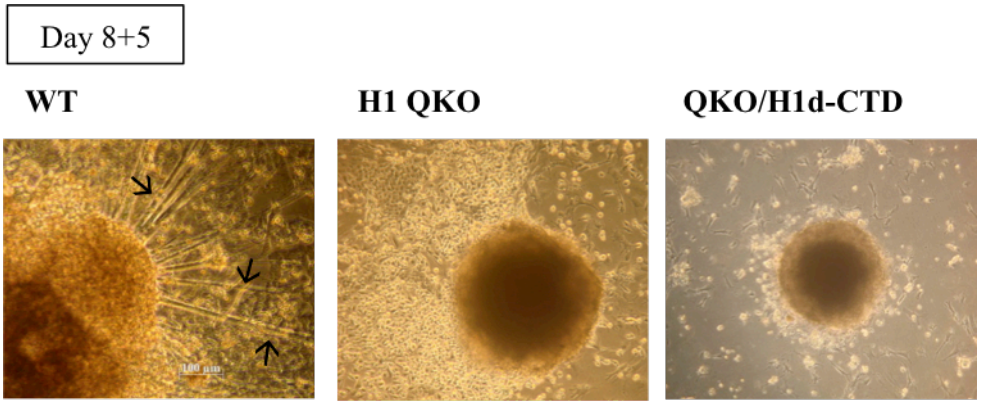

Figure 13. Neurite outgrowth of H1 QKO/H1d-CTD EBs.
Phase contrast images of day 8+5 EBs during neural differentiation of WT, H1 QKO, and H1 QKO/H1d-CTD ESCs are shown. Arrows indicate representative neurite outgrowth. Scale bar, 100 μm.

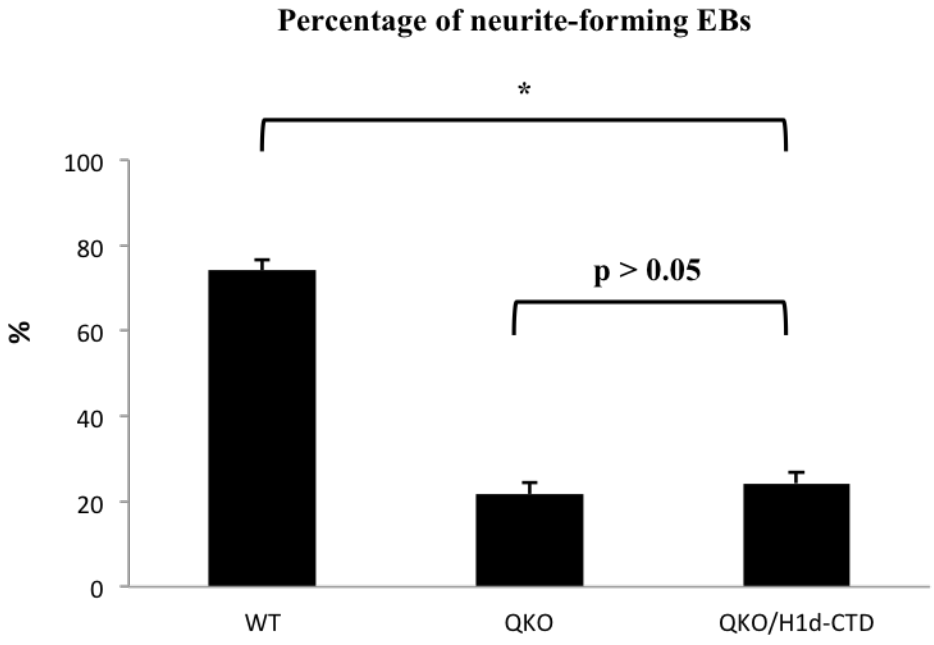

Figure 14. Overexpressing H1d-CTD in H1 QKO ESCs does not restore neurite outgrowth.
Percentage of neurite-forming EBs among total EBs analyzed for each genotype is presented. Each EB was observed and analyzed for neurite outgrowth. Over 100 EBs were analyzed for each genotype per experiment. Numbers were averaged from at least 4 experiments; WT, n=13; QKO, n=9; QKO/H1d-CTD, n=9. All data are presented as means ± S.E.M. *: p-value< 0.05.

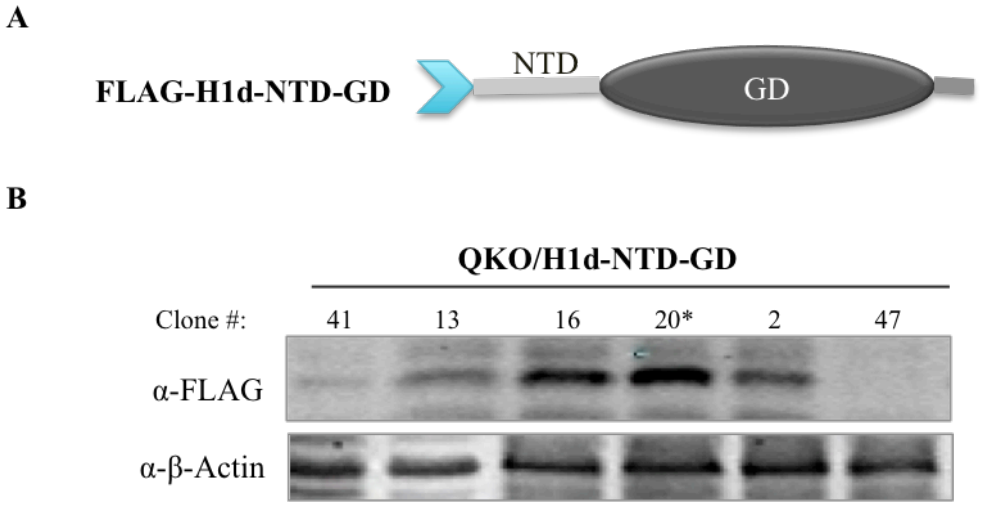

Figure 15. Generation of H1 QKO/H1d-NTD-GD ESC lines.

A) A schematic diagram of the FLAG tagged H1d-NTD-GD. NTD: N-terminal domain. GD: globular domain. The light blue arrowhead indicates a flag tag which is fused at N-terminal of H1d-NTD-GD.

B) Western blotting analysis of expression levels of FLAG tagged H1d-NTD-GD in H1 QKO/H1d-NTD-GD ESC lines. H1 QKO ESCs were transfected with vectors expressing FLAG-H1d-NTD-GD. Forty-eight stable ESC clones were picked for each transfection and screened using an anti-FLAG antibody. Representative immunoblots of FLAG-H1d-NTD-GD expressing cell clones are shown. Immunoblots with anti-β-Actin antibody were included as loading controls. The clone indicated with asterisks was one of the ESC lines selected for further analysis.

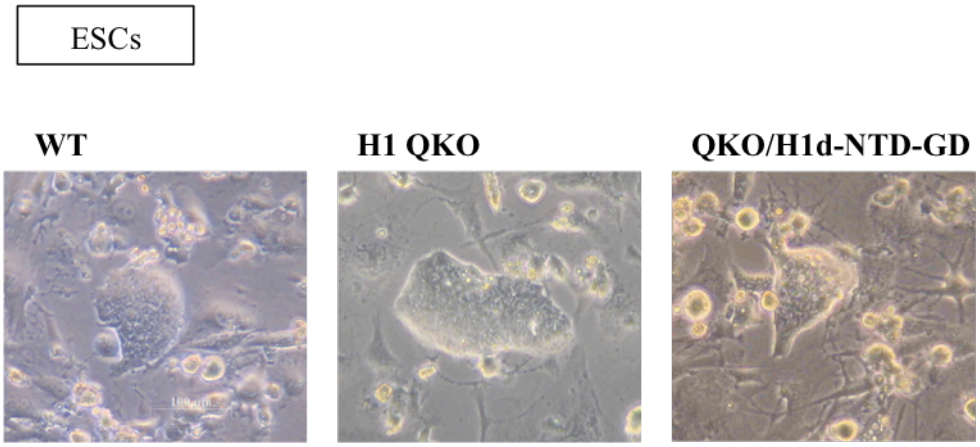

Figure 16. H1 QKO/H1d-NTD-GD ESCs exhibit normal ESC colony morphology.
Phase contrast images of WT, H1 QKO, and H1 QKO/H1d-NTD-GD ESCs are shown. Scale bar, 100 μm.

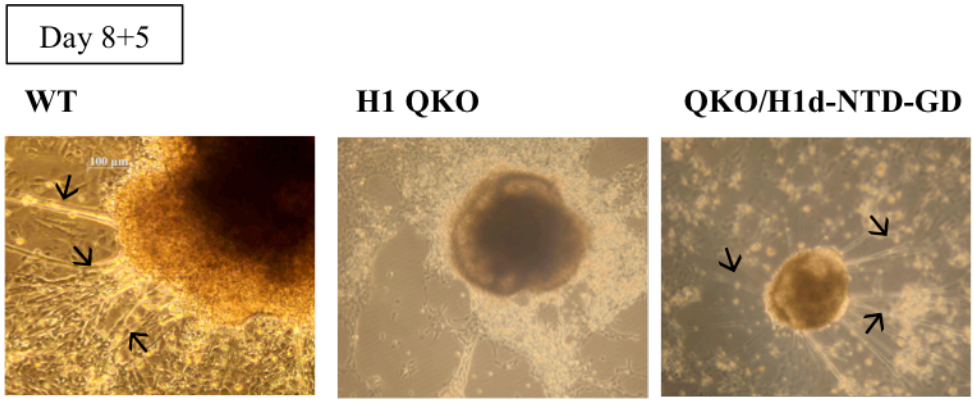

Figure 17. Neurite outgrowth of H1 QKO/H1d-NTD-GD EBs.
Phase contrast images of day 8+5 EBs during neural differentiation of WT, H1 QKO, and H1QKO/H1d-NTD-GD ESCs are shown. Arrows indicate neurite outgrowth. Scale bar, 100 μm.

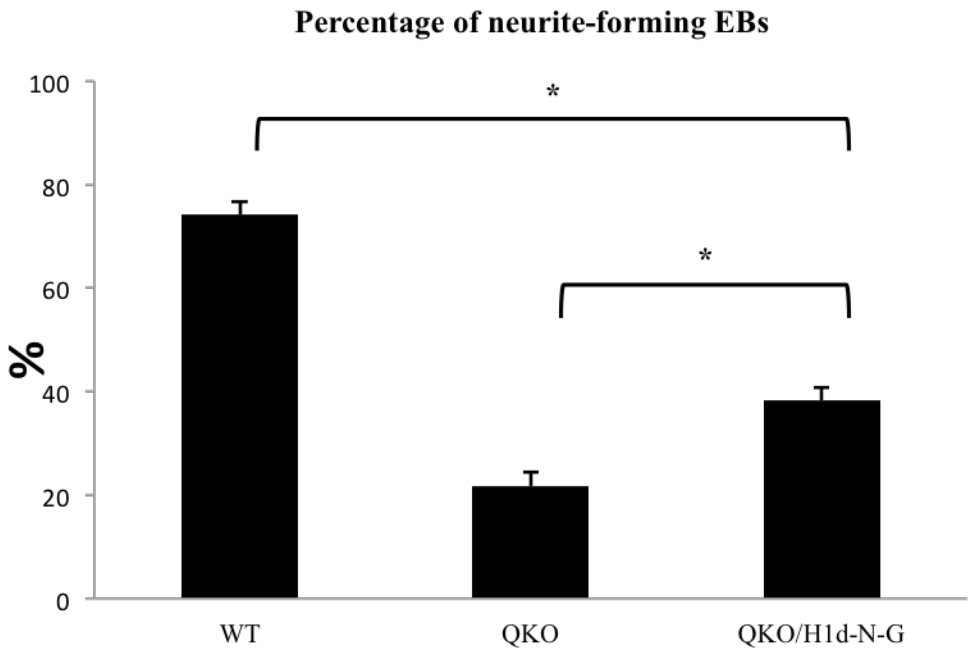

Figure 18. Overexpressing H1d-NTD-GD in H1 QKO ESCs partially rescues neuronal differentiation defects of H1 QKO ESCs.
Percentage of neurite-forming EBs among total EBs analyzed for each genotype is presented. Each EB was observed and analyzed for neurite outgrowth. Over 100 EBs were analyzed for each genotype per experiment. Numbers were averaged from at least 4 experiments; WT, n=13; QKO, n=9; QKO/H1d-N-G, n=6. All data are presented as means ± S.E.M. *: p-value <0.05.

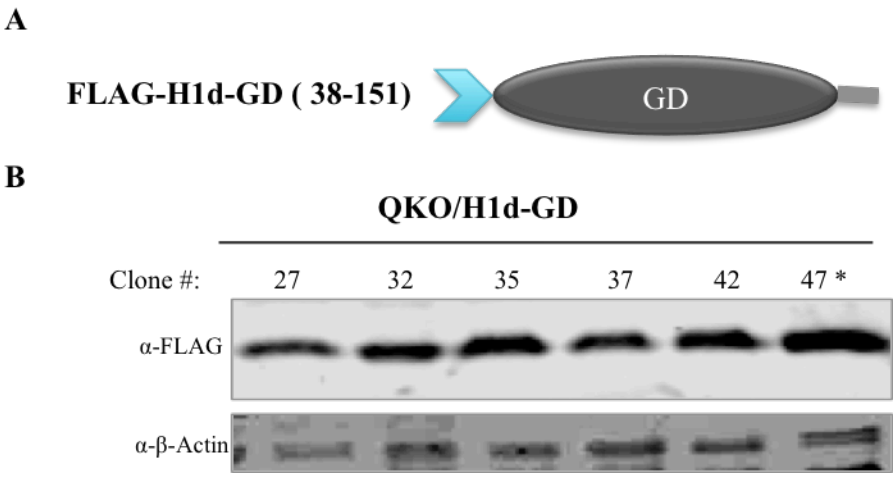

Figure 19. Generation of H1 QKO/H1d-GD ESC lines.

A) A schematic diagram of the FLAG tagged H1d-GD. GD: globular domain. The light blue arrowhead represents a flag tag which is fused to the N-terminus of H1d-GD .

B) Western blotting analysis of expression levels of FLAG tagged H1d-GD in H1 QKO/H1d-GD ESCs. H1 QKO ESCs were transfected with vectors expressing FLAG-H1d-GD . Forty-eight stable ESC clones were picked for each transfection and screened using an anti-FLAG antibody. Representative immunoblots of FLAG-H1d-GD expressing cell clones are shown. Immunoblots with anti-β-Actin antibody were included as loading controls. The clone indicated with asterisks was one of the ESC lines used for further analysis.

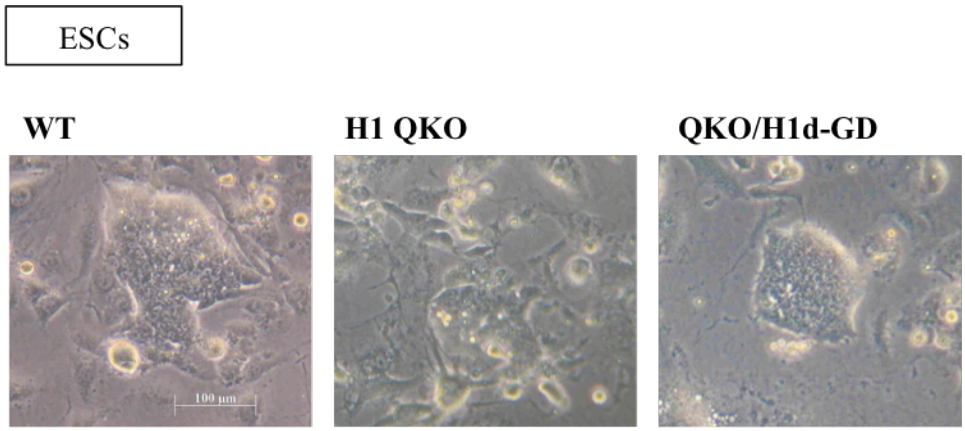

Figure 20. H1 QKO/H1d-GD ESCs exhibit normal ESC colony morphology. Phase contrast images of WT, H1 QKO, and H1 QKO/H1d-GD ESCs are shown. Scale bar, 100 μm.

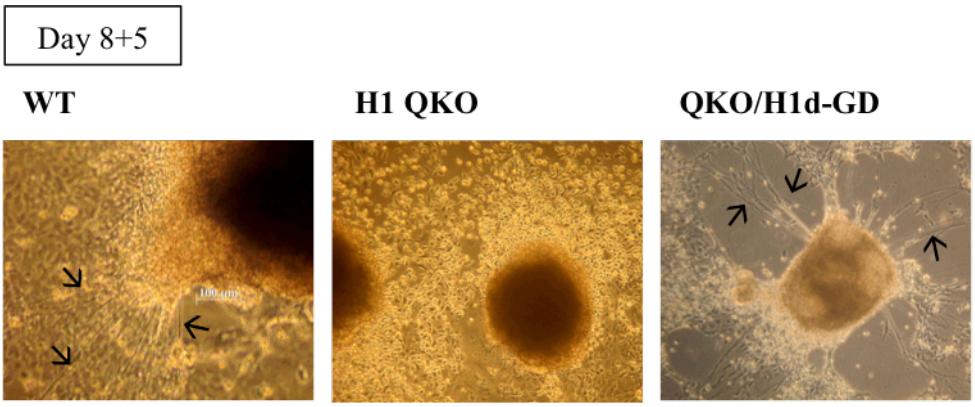

Figure 21. Neurite outgrowth of H1 QKO/H1d-GD EBs.
Phase contrast images of day 8+5 EBs during neural differentiation of WT, H1 QKO, and H1 QKO/H1d-GD ESCs are shown. Arrows indicate neurite outgrowth. Scale bar, 100 μm.

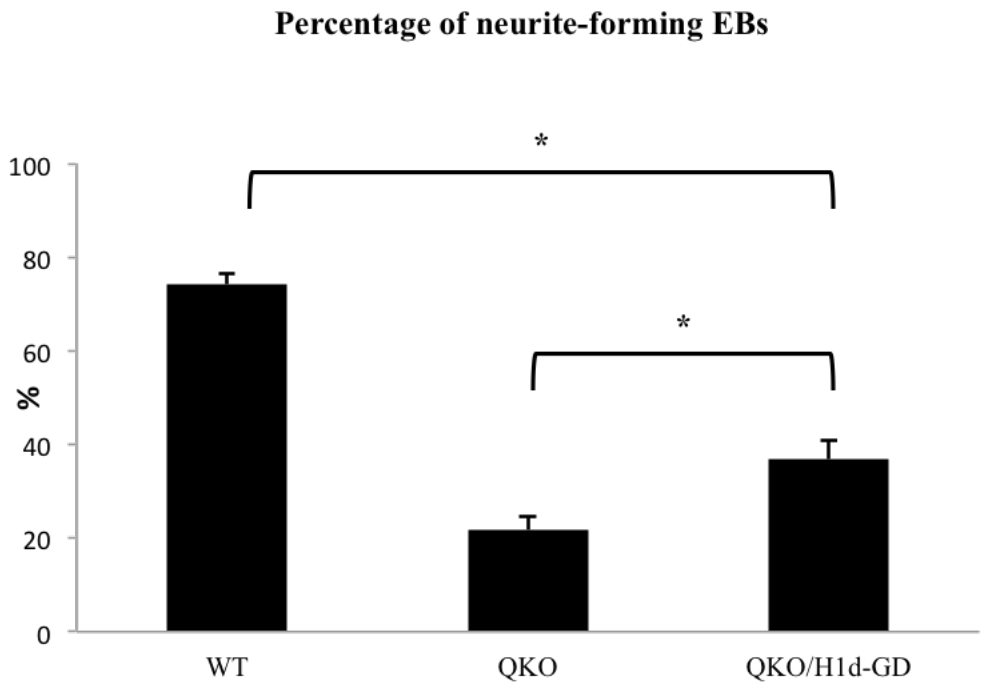

Figure 22. H1d-GD Overexpression partially rescues neurite outgrowth defects during neural differentiation of H1 QKO ESCs.
Percentage of neurite-forming EBs among total EBs analyzed for each genotype is presented. Each EB was observed and analyzed for neurite outgrowth. Over 100 EBs were analyzed for each genotype per experiment. Numbers were averaged from at least 4 experiments; WT, n=13; QKO, n=9; QKO/H1d-GD, n=7. All data are presented as means ± S.E.M. *: p value <0.05.

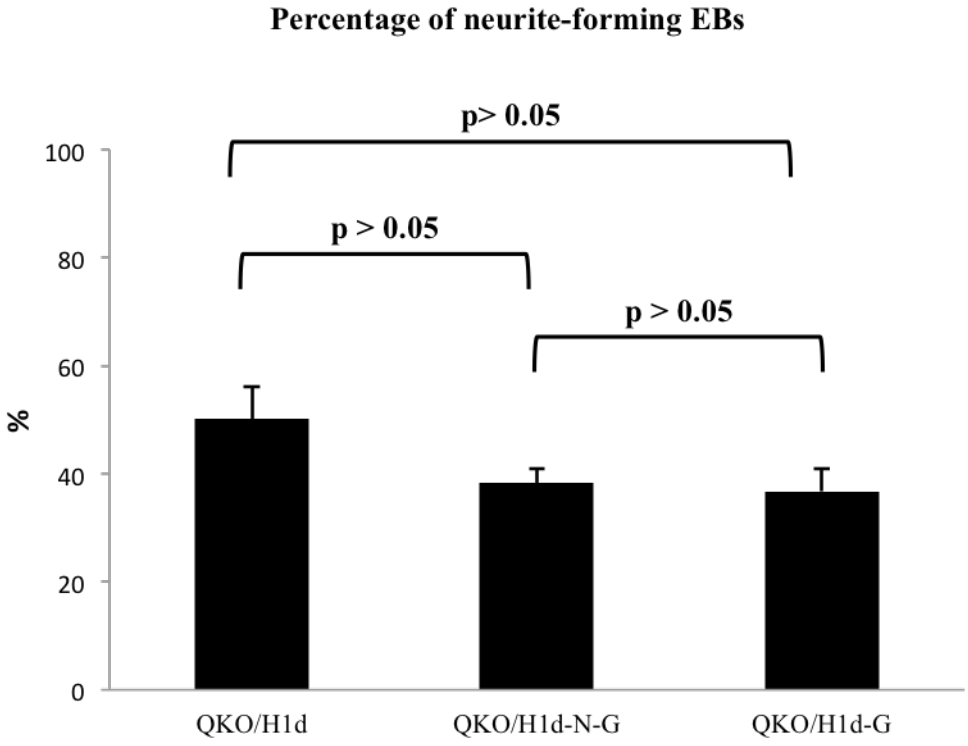

Figure 23. Comparison of neurite outgrowth efficiency of H1 QKO/H1d, QKO/H1d-NTD-GD and QKO/H1d-GD EBs.
Percentage of neurite-forming EBs among total EBs analyzed for each genotype is presented. Each EB was observed and analyzed for neurite outgrowth. Over 100 EBs were analyzed for each genotype per experiment. Numbers were averaged from at least 4 experiments; QKO/H1d, n=4; QKO/H1d-N-G, n=6; QKO/H1d-GD, n=7. All data are presented as means ± S.E.M.

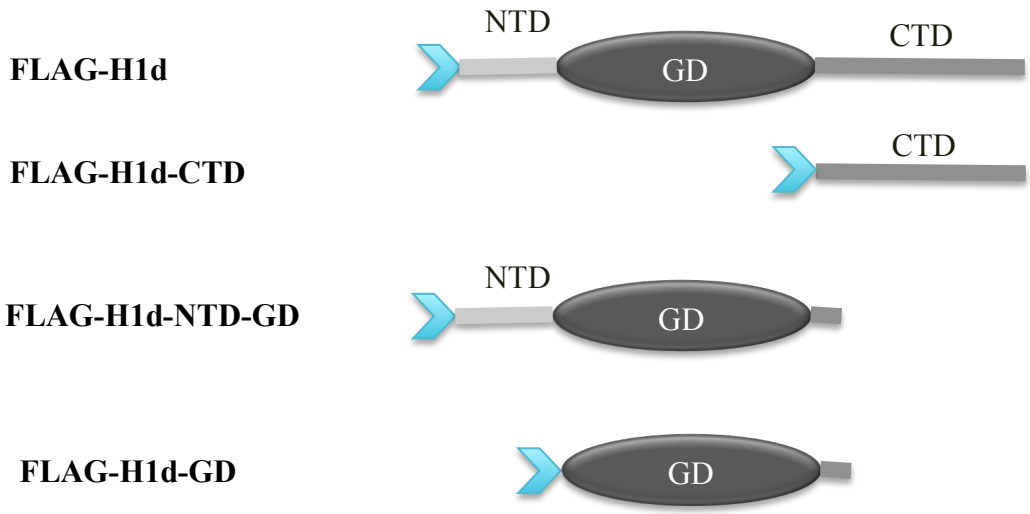

Figure 24. A schematic diagram of FLAGH1d and FLAGH1d-domains.
The light blue arrowhead represents a flag tag which is fused to the N-terminus of H1d and H1d-domains.

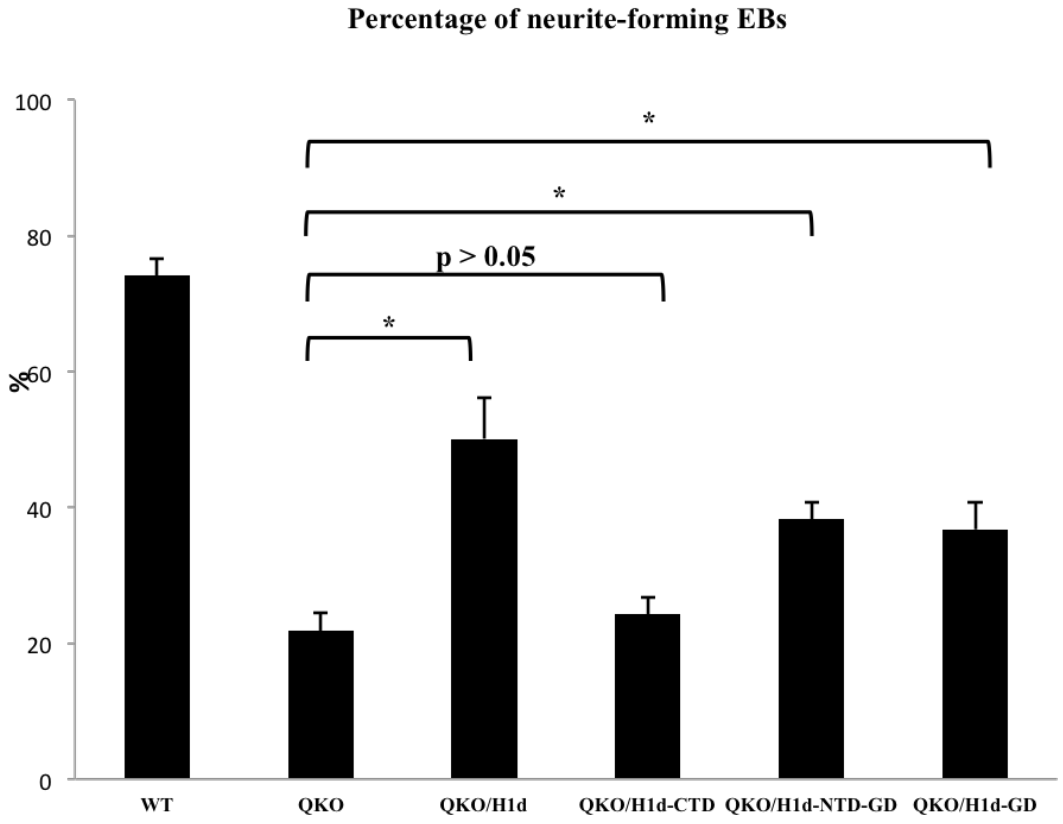

Figure 25. Summary of neurite outgrowth efficiency of ESC lines of WT, H1 QKO, H1 QKO/H1d and QKO/H1d-domains.
Percentage of neurite-forming EBs among total EBs analyzed for each genotype is presented. Each EB was observed and analyzed for neurite outgrowth. Over 100 EBs were analyzed for each genotype per experiment. Numbers were averaged from at least 4 experiments. All data are presented as means ± S.E.M. *: p-value <0.05.

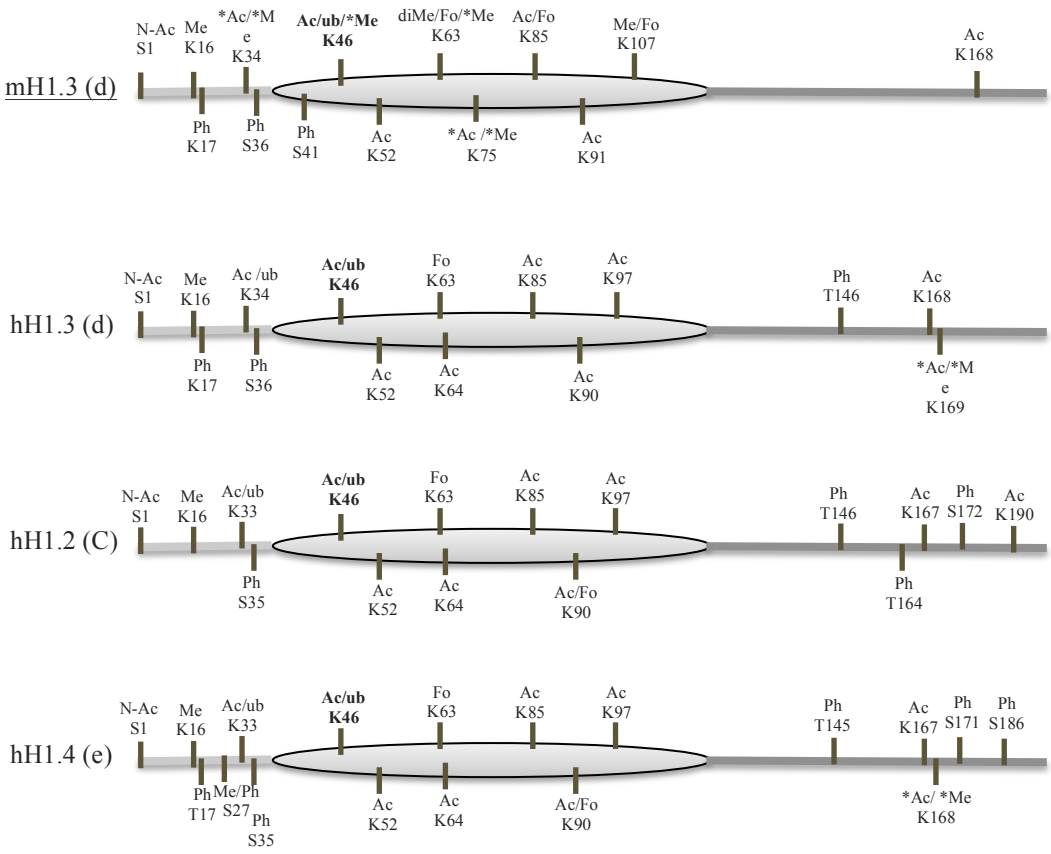

Figure 26. Comparisons of histone posttranslational modification marks on mouse H1.3 (H1d) and human H1.2 (H1c), H1.3 (H1d) & H1.4 (H1e).
Acetylation (Ac), methylation (Me), phosphorylation (Ph), ubiquitylation (Ub) and formylation (Fo) in histone H1 variants are shown. Tissue-specific modifications are marked by asterisks. The data are compiled from Kowalski and Palyga (2016), Kamieniarz et al. (2012), Weiss et al. (2010), and Wiśniewski et al. (2007).

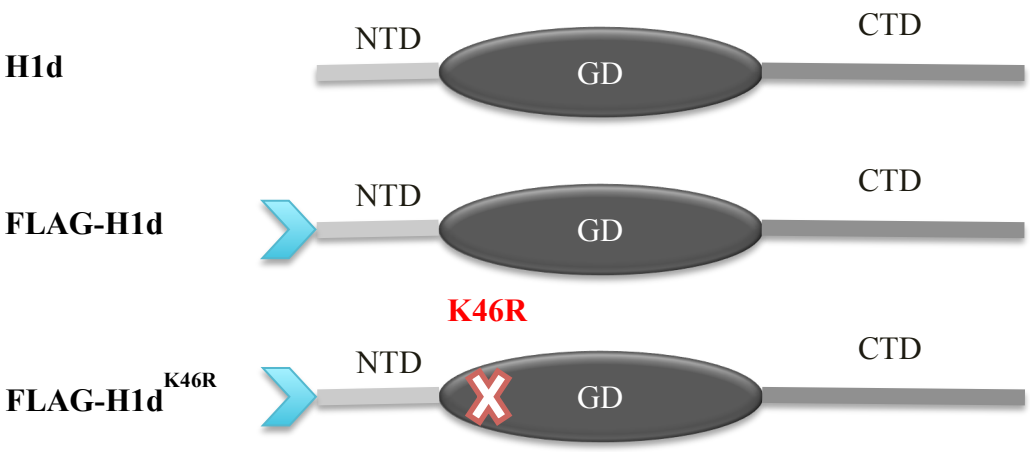

Figure 27. A schematic diagram of mouse H1d, FLAGH1d, FLAG^{K46R} mutant.

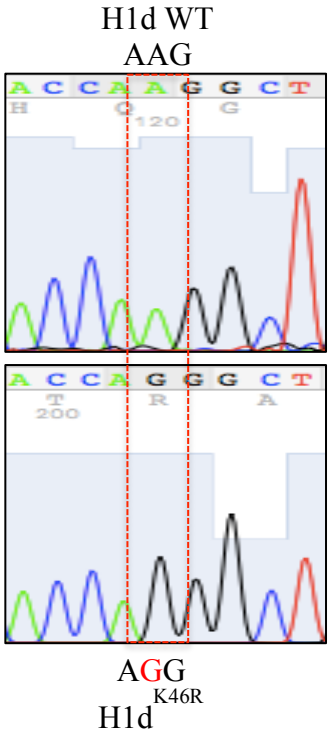

Figure 28. Generation of H1d^{K46R} mutant.
DNA sequencing validation shows that A in 140 is replaced by G, which changes AAG, coding for Lysine (K) at position 46 of the H1d WT protein, to AGG, coding for Arginine (R) at position 46 of the H1d^{K46R} mutant protein. The sequence of full length of H1d was verified by sequencing and the sequence around the mutation is shown.

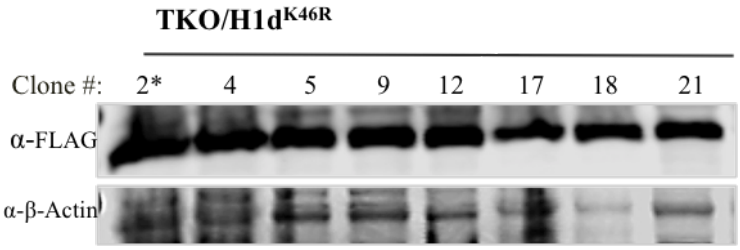

Figure 29. Generation of H1 TKO/H1d^{K46R} ESC lines.
Western blotting analysis of expression levels of FLAG tagged H1d^{K46R} in the H1 TKO/FLAGH1d^{K46R} ESCs. H1 TKO ESCs were transfected with a vector expressing FLAG-H1d^{K46R}. Twenty-four stable ESC clones were picked for each transfection and screened using an anti-FLAG antibody. Representative immunoblots of FLAG-H1d^{K46R} expressing cell clones are shown. Immunoblots with anti-β-Actin antibody were included as loading controls. The clone indicated with asterisks, demonstrating high expression levels of H1d^{K46R}, was one of the ESC lines used in subsequent analysis.

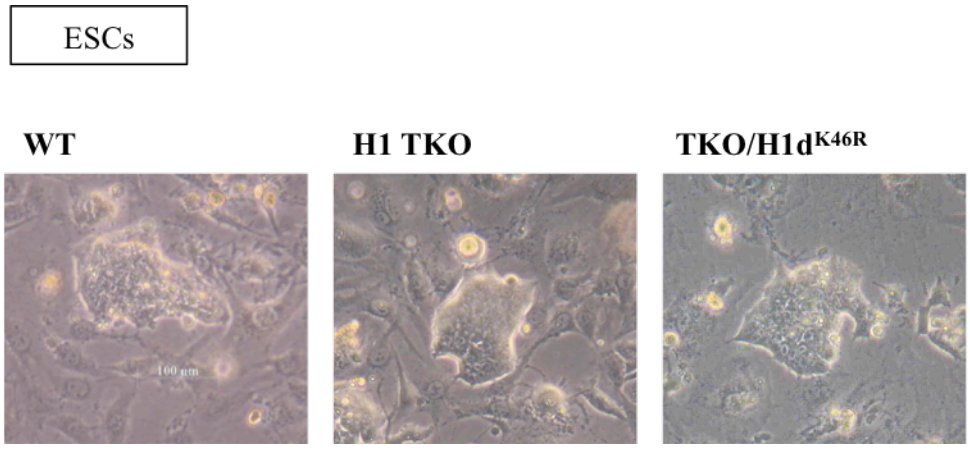

Figure 30. H1 TKO/ H1d^{K46R} ESCs exhibit normal ESC colony morphology. Phase contrast images of WT, H1 TKO and H1 TKO/H1d^{K46R} ESCs are shown. Scale bar, 100 μm.

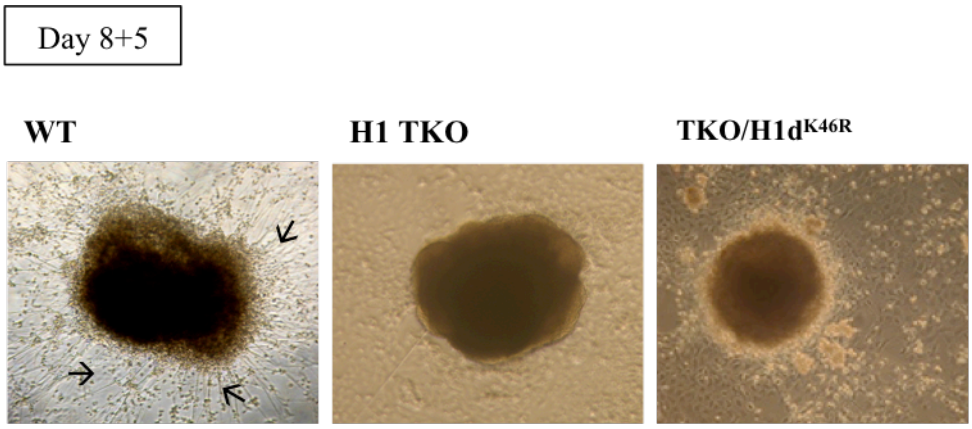

Figure 31. Neurite outgrowth defects during neural differentiation of H1 TKO/H1d^{K46R} ESCs.
Phase contrast images of day 8+5 EBs during neural differentiation of WT, H1 TKO, and H1 TKO/H1d^{K46R} ESCs are shown. Arrows indicate neurite outgrowth. Scale bar, 100 μm.

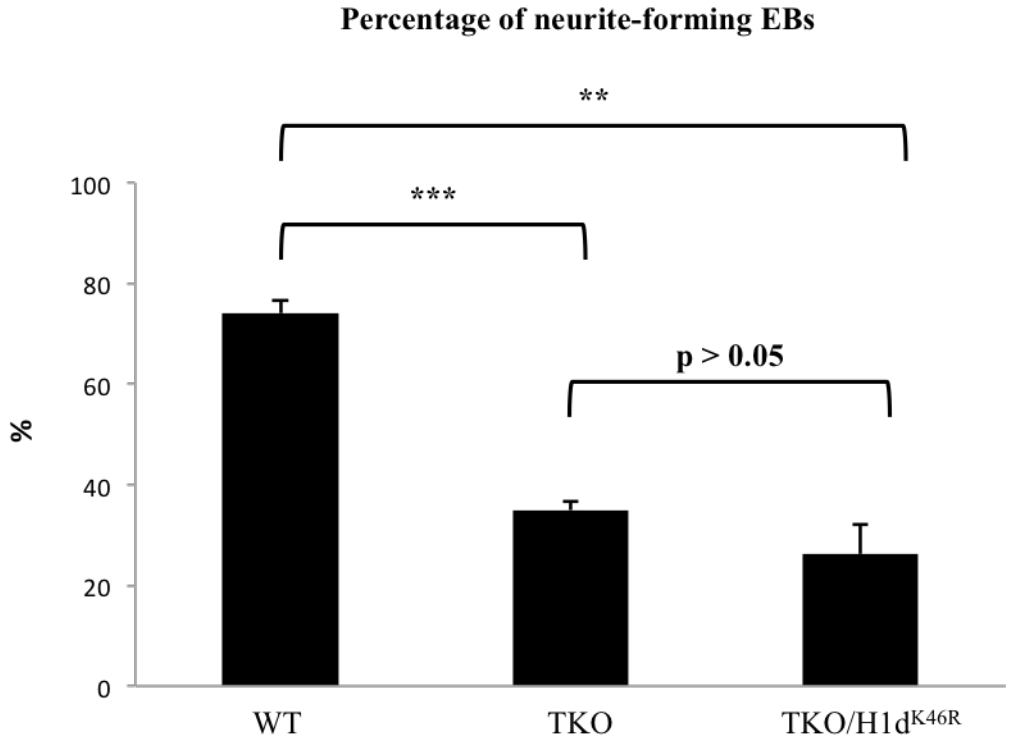

Figure 32. Overexpressing H1d^{K46R} in H1 TKO ESCs does not rescue neurite outgrowth defects of H1 TKO EBs.

Percentage of neurite-forming EBs among total EBs analyzed for each genotype is presented. Each EB was observed and analyzed for neurite outgrowth. Over 100 EBs were analyzed for each genotype per experiment. Numbers were averaged from at least 3 experiments; WT, n=13; TKO, n=5; TKO/H1d^{K46R}, n=3. All data are presented as means ± S.E.M. **; $p<0.01$; ***: p-value < 0.001

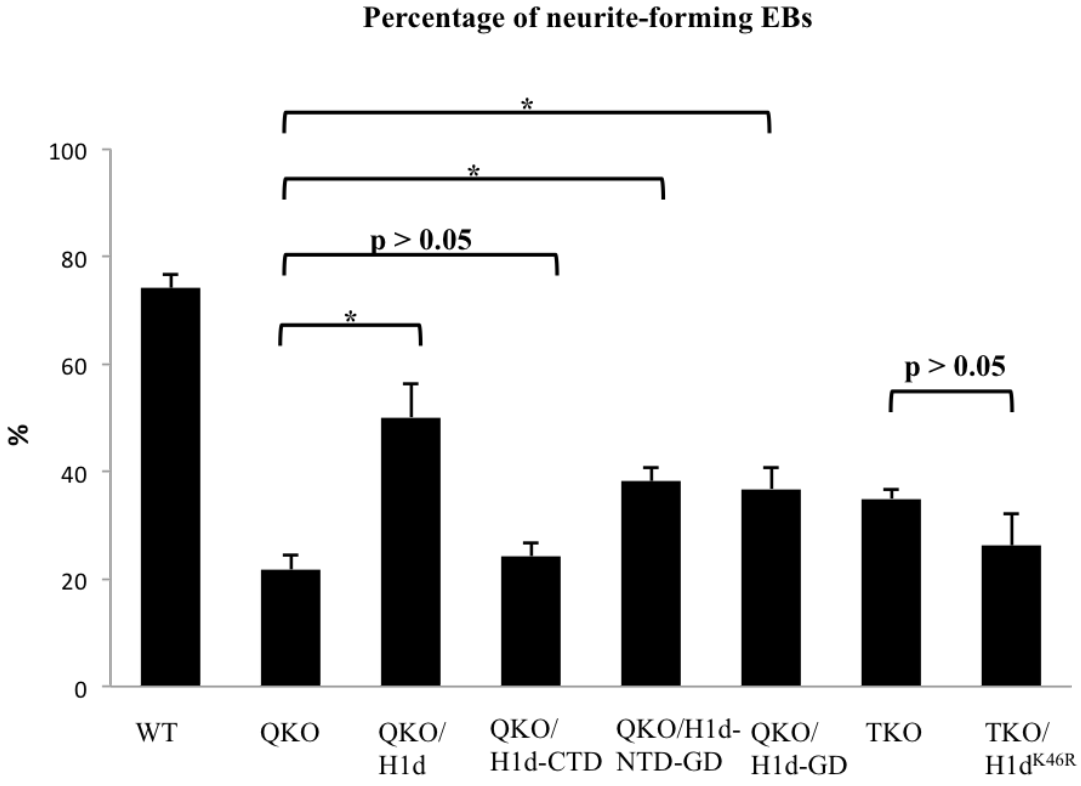

Figure 33. Summary of neurite outgrowth including all mutants.
Percentage of neurite-forming EBs among total EBs analyzed for each genotype is presented. Each EB was observed and analyzed for neurite outgrowth. Over 100 EBs were analyzed for each genotype per experiment. Numbers were averaged from at least 4 experiments. All data are presented as means ± S.E.M. * $P<0.05$.

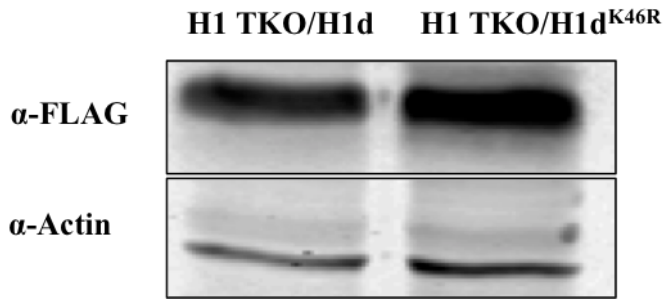

Figure 34. Expression of FLAG-H1d and FLAG-H1d^{K46R} in H1 TKO/H1d and H1 TKO/H1d^{K46R} ESCs.

CHAPTER 4

CONCLUSIONS AND DISCUSSION

H1 Linker histones are key chromatin structural proteins that facilitate the folding of higher order chromatin structure. Previous studies have demonstrated that H1 is essential for mammalian development and important for ESC differentiation (Fan et al., 2003; Zhang et al., 2012). In this thesis, we took a functional reconstitution approach and utilized H1 depleted ESCs defective in neural differentiation to identify the regions and site of H1 proteins that are critical for the role of H1 in mediating ESC differentiation.

By generation and characterization of H1 QKO/H1d stable ESC lines, we have identified H1d being effective in restoration of neurite outgrowth defects of H1 QKO EBs. Further dissection of H1d into a series of domains allowed us to pinpoint the GD as the key domain responsible for the role of H1d in mediating neurite outgrowth.

Furthermore, we investigate the potential role of H1 modifications in ESC differentiation. Based on our finding of the key role of GD in ESC differentiation, combined with compilation of all identified PTMs of H1 in the literature as well as sequence conservation analysis, we were able to focus our analysis on K46, a conserved hotspot for PTMs within H1d globular domain. Indeed, mutation of lysine to arginine at site 46 (K46R) disrupts the function of H1d in mediating neurite outgrowth during neural differentiation, even though K46R does not appear to change

the biochemical properties and hydrophobicity of H1d. FRAP analysis indicates K46R reduces H1d mobility and dynamics in ESCs.

Taken together, these studies have identified GD as a key domain in mediating the role of H1d in mediating the neurite outgrowth during neural differentiation of ESCs and demonstrated the necessity of PTMs on H1d K46 in ESC differentiation. Our results also suggest that PTMs on K46 may facilitate the mobility of H1d, contributing to its role in ESC differentiation.

In this thesis, we have established an H1 functional reconstitution cellular system with quantifiable phenotypic traits and have effectively tested the function of various H1 variants, H1 domains and specific site in ESC differentiation, particularly in the neurite outgrowth of differentiating EBs. Because H1c/H1d/H1e triple knockout and H1c/H1d/H1e/$H1^0$ quadruple knockout in ESCs do not affect ESC proliferation, H1 TKO and H1 QKO ESCs have normal ESC self-renewal, providing an excellent opportunity for development of the H1 reconstitution cellular systems. On the other hand, H1 QKO and H1 TKO ESCs are severely impaired in ESC differentiation, allowing us to dissect the role of H1 in ESC differentiation by induction of differentiation with a well-defined neural differentiation protocol. We have taken advantage of these cellular systems in this thesis and demonstrated their utility and effectiveness in dissecting the role of H1 domains and specific site in ESC differentiation. This approach and the cell lines generated here should be very useful resources and provide a foundation for further investigation of regulatory mechanisms of H1 in stem cell differentiation.

Using H1 QKO ESCs, we show that expressing full length H1d increases the

neurite outgrowth rate of EBs from 21.8% to 50.1%. Given that WT ESCs had 74.1% of EBs with robust neurite outgrowth, it is intriguing to note that overexpressing H1d does not lead to a complete restoration of the neurite outgrowth defects exhibited by H1 QKO ESCs. It remains to be addressed whether the full restoration is dependent on a higher level of expression of the exogenous H1d or requires complementation from two different H1 variants.

Through sequential deletion of H1d domain(s) and characterization of the functional reconstituted ESCs with H1 deletion mutants, we have identified that the globular domain serves as an essential component in mediating ESC differentiation. H1 QKO/H1d-NTD-GD and H1 QKO/H1d-GD EBs had similar neurite outgrowth rate with 38.2% and 36.8%, respectively. In contrast, overexpressing the C-terminal domain of H1d in H1 QKO ESCs had no obvious effects on neurite outgrowth capacity. CTD accounts for more than half of the H1 sequence and has been shown to be critical for high affinity binding of H1 to chromatin. Thus it is surprising that the neurite outgrowth rate of H1 QKO/H1-GD EBs is not significantly lower than that of H1 QKO/H1d. We speculate that the globular domain of H1 plays a key role in regulating specific genes necessary for mediating the neurite outgrowth during neural differentiation of ESCs. Further studies of gene expression profiles and chromatin compaction status of H1 QKO/H1-GD EBs and H1 QKO/H1-GD EBs are likely to offer new insights to the underlying regulatory mechanisms.

Linker histone H1 family functions as the major architectural proteins mediating higher order chromatin condensation (Happel and Doenecke, 2009; Lyubitelev et al., 2016). The globular domain of linker histone H1 is the most

conserved domain in H1 and is critical for H1 binding to nucleosomes and chromatin (Allan et al., 1980; Brown et al., 2006; Cui and Zhurkin, 2009; Fan and Roberts, 2006; George et al., 2010; Ramakrishnan et al., 1993; Syed et al., 2010; Zhou et al., 1998). The N-terminal domain of H1 is not required for chromatin folding (Allan et al., 1986; Hendzel et al., 2004; Vila et al., 2001; Vyas and Brown, 2012). The C-terminal domain is likely to participated in competitive interaction both with chromatin fiber and many other proteins (Lu et al., 2009). The H1 C-terminal domain assists proper H1 binding to the nucleosomes and linker DNA, and it is necessary for high affinity binding of H1. Both NTD and CTD adopt specific secondary structure when bound to DNA (Lu and Hansen, 2003; Roque et al., 2005).

A working model was proposed to explain the binding dynamics of H1 to chromatin in facilitating chromatin condensation (Catez et al., 2006). Initially, the C-terminal domain of H1 non-specifically binds to the linker DNA mainly through the charge interactions. The globular domain binds to the nucleosomal dyad axis through two binding sites, which comprise several positive charge residues. Proper placement of the globular domain induces conformational changes of the N- and C-terminal domains and further mediates the structure changes for chromatin folding (Brown et al., 2006). The finding that GD is a key domain in mediating ESC differentiation indicates a role of GD in cellular fate regulation besides its curial structural role in proper binding to the nucleosome and chromatin folding.

Having identified the globular domain as the main component mediating the role of H1 in ESC differentiation, we further investigated whether specific PTMs in GD are responsible for this role. We focused on Lys^{46}, a highly conserved, hot-spot

site for H1 modifications, which is the only conserved site in GD of H1 variants subjected to as many as three types of post-translational modifications, including ubiquitination, acetylation and methylation (Wisniewski et al., 2007). We find that H1 TKO/H1d^{K46R} EBs and H1 TKO EBs had comparable neurite outgrowth. While the K to R mutation at K46 of H1d would abolish the potential post-translational modifications at this site, this mutation does not affect the biochemical properties and hydrophobicity of H1d as shown by HPLC analysis of histones extracted from the chromatin of H1 TKO/H1d^{K46R} ESCs. These results suggest that the histone modifications on Lys^{46} of H1d may be crucial for proper differentiation of ESCs.

ESC genome contains hyperdynamic chromatin and exhibits hyperactive global transcription. It is postulated that when ESCs enter the differentiation states, the chromatin would turn from a relatively "open" state into a relative "close" state and significant portion of genome would undergo gene silencing (Ahmed et al., 2010; Efroni et al., 2008; Gaspar-Maia et al., 2011; Meshorer et al., 2006). Recent studies have reinforced that an open chromatin structure is a distinct property for pluripotency (Fussner et al., 2010; Gaspar-Maia et al., 2011).

The FRAP analysis indicates that GFP-H1d^{K46R} has reduced mobility and decreased dynamics compared with H1d, suggesting that the modifications on Lysine 46 site may increase the mobility of H1d *in vivo* and that the regulation of H1d dynamics may be necessary or contribute to the role of H1 in mediating ESC differentiation. Indeed, H1 acetylation, one of the three possible modifications on K46, reduces the basic charges of H1 protein, which leads to reduced H1 binding affinity to nucleosomal DNA and increased H1 mobility. Consistently, most of the

sites within H1 GD subject to modification by acetylation have been found to be associated with DNA binding (Wisniewski et al., 2007). Thus H1 acetylation may be important for dynamic regulation of H1 association with chromatin. While ubiquitination does not change charges on protein, it is rather bulky and may interfere H1 binding to chromatin. For example, K63-ubiquitinated H1s were found to have reduced association with chromatin than unmodified H1s (Thorslund et al., 2015). K46 is located in the first alpha helix in the H1 globular domain. Ubiquitination and tissue specific methylation on H1d K46 have been detected by Mass Spectrometry but have not been investigated further.

Additionally, PTMs on H1d K46 may be required for regulating genes necessary for ESC differentiation. H1 acetylation in general has been linked to activation (Happel and Doenecke, 2009), and evidence suggests that H1 ubiquitination plays an important role in gene activation. $TAF_{II}250$, a component of the general transcription factor TFIID, ubiquitinates H1 in *Drosophila* embryo, suggesting that H1 ubiquitination may participate in transcriptional regulation of a subset of genes (Pham and Sauer, 2000). Gene expression profiling of H1 TKO/H1d^{K46R}, H1 TKO as well as H1 TKO/H1d cells would offer new leads of target genes regulated by PTMs on H1d K46. It would be important to further investigate the underlying mechanisms by which the modifications on K46 regulate ESC differentiation.

REFERENCES

Ahmed, K., Dehghani, H., Rugg-Gunn, P., Fussner, E., Rossant, J., and Bazett-Jones, D.P. (2010). Global chromatin architecture reflects pluripotency and lineage commitment in the early mouse embryo. PLoS One *5*, e10531.

Allan, J., Hartman, P.G., Crane-Robinson, C., and Aviles, F.X. (1980). The structure of histone H1 and its location in chromatin. Nature *288*, 675-679.

Allan, J., Mitchell, T., Harborne, N., Bohm, L., and Crane-Robinson, C. (1986). Roles of H1 domains in determining higher order chromatin structure and H1 location. Journal of molecular biology *187*, 591-601.

Allard, P., Yang, Q., Marzluff, W.F., and Clarke, H.J. (2005). The stem-loop binding protein regulates translation of histone mRNA during mammalian oogenesis. Dev Biol *286*, 195-206.

Balhorn, R., Balhorn, M., and Chalkley, R. (1972). Lysine-rach histone phosphorylation and hyperplasia in the developing rat. Dev Biol *29*, 199-203.

Baxevanis, A.D., and Landsman, D. (1998). Histone Sequence Database: new histone fold family members. Nucleic Acids Res *26*, 372-375.

Bednar, J., Garcia-Saez, I., Boopathi, R., Cutter, A.R., Papai, G., Reymer, A., Syed, S.H., Lone, I.N., Tonchev, O., Crucifix, C., *et al.* (2017). Structure and Dynamics of a 197 bp Nucleosome in Complex with Linker Histone H1. Mol Cell *66*, 729.

Bharath, M.M., Ramesh, S., Chandra, N.R., and Rao, M.R. (2002). Identification of a 34 amino acid stretch within the C-terminus of histone H1 as the DNA-condensing domain by site-directed mutagenesis. Biochemistry *41*, 7617-7627.

Bhattacharjee, R.N., Banks, G.C., Trotter, K.W., Lee, H.L., and Archer, T.K. (2001). Histone H1 phosphorylation by Cdk2 selectively modulates mouse mammary tumor virus transcription through chromatin remodeling. Mol Cell Biol *21*, 5417-5425.

Boggs, B.A., Allis, C.D., and Chinault, A.C. (2000). Immunofluorescent studies of human chromosomes with antibodies against phosphorylated H1 histone. Chromosoma *108*, 485-490.

Bohm, L., and Mitchell, T.C. (1985). Sequence conservation in the N-terminal domain of histone H1. FEBS Lett *193*, 1-4.

Bonet-Costa, C., Vilaseca, M., Diema, C., Vujatovic, O., Vaquero, A., Omenaca, N., Castejon, L., Bernues, J., Giralt, E., and Azorin, F. (2012). Combined bottom-up and top-down mass spectrometry analyses of the pattern of post-translational modifications of Drosophila melanogaster linker histone H1. J Proteomics *75*, 4124-4138.

Bradbury, E.M., Inglis, R.J., and Matthews, H.R. (1974). Control of cell division by very lysine rich histone (F1) phosphorylation. Nature *247*, 257-261.

Bradbury, E.M., Inglis, R.J., Matthews, H.R., and Sarner, N. (1973). Phosphorylation of very-lysine-rich histone in Physarum polycephalum. Correlation with chromosome condensation. Eur J Biochem *33*, 131-139.

Brown, D.T. (2001). Histone variants: are they functionally heterogeneous? Genome Biol *2*, REVIEWS0006.

Brown, D.T., Izard, T., and Misteli, T. (2006). Mapping the interaction surface of linker histone H1(0) with the nucleosome of native chromatin in vivo. Nat Struct Mol Biol *13*, 250-255.

Cao, K., Lailler, N., Zhang, Y., Kumar, A., Uppal, K., Liu, Z., Lee, E.K., Wu, H., Medrzycki, M., Pan, C.*, et al.* (2013). High-resolution mapping of h1 linker histone variants in embryonic stem cells. PLoS genetics *9*, e1003417.

Catez, F., Ueda, T., and Bustin, M. (2006). Determinants of histone H1 mobility and chromatin binding in living cells. Nat Struct Mol Biol *13*, 305-310.

Chadee, D.N., Taylor, W.R., Hurta, R.A., Allis, C.D., Wright, J.A., and Davie, J.R. (1995). Increased phosphorylation of histone H1 in mouse fibroblasts transformed

with oncogenes or constitutively active mitogen-activated protein kinase kinase. J Biol Chem *270*, 20098-20105.

Cui, F., and Zhurkin, V.B. (2009). Distinctive sequence patterns in metazoan and yeast nucleosomes: implications for linker histone binding to AT-rich and methylated DNA. Nucleic Acids Res *37*, 2818-2829.

Cutter, A.R., and Hayes, J.J. (2017). Linker histones: novel insights into structure-specific recognition of the nucleosome. Biochem Cell Biol *95*, 171-178.

Daujat, S., Zeissler, U., Waldmann, T., Happel, N., and Schneider, R. (2005). HP1 binds specifically to Lys26-methylated histone H1.4, whereas simultaneous Ser27 phosphorylation blocks HP1 binding. J Biol Chem *280*, 38090-38095.

Efroni, S., Duttagupta, R., Cheng, J., Dehghani, H., Hoeppner, D.J., Dash, C., Bazett-Jones, D.P., Le Grice, S., McKay, R.D., Buetow, K.H.*, et al.* (2008). Global transcription in pluripotent embryonic stem cells. Cell Stem Cell *2*, 437-447.

Fan, L., and Roberts, V.A. (2006). Complex of linker histone H5 with the nucleosome and its implications for chromatin packing. Proc Natl Acad Sci U S A *103*, 8384-8389.

Fan, Y., Nikitina, T., Morin-Kensicki, E.M., Zhao, J., Magnuson, T.R., Woodcock, C.L., and Skoultchi, A.I. (2003). H1 linker histones are essential for mouse development and affect nucleosome spacing in vivo. Mol Cell Biol *23*, 4559-4572.

Fan, Y., Nikitina, T., Zhao, J., Fleury, T.J., Bhattacharyya, R., Bouhassira, E.E., Stein, A., Woodcock, C.L., and Skoultchi, A.I. (2005). Histone H1 depletion in mammals alters global chromatin structure but causes specific changes in gene regulation. Cell *123*, 1199-1212.

Fan, Y., Sirotkin, A., Russell, R.G., Ayala, J., and Skoultchi, A.I. (2001). Individual somatic H1 subtypes are dispensable for mouse development even in mice lacking the H1(0) replacement subtype. Mol Cell Biol *21*, 7933-7943.

Fan, Y., and Skoultchi, A.I. (2004). Genetic analysis of H1 linker histone subtypes and their functions in mice. Methods Enzymol *377*, 85-107.

Fang, H., Clark, D.J., and Hayes, J.J. (2012). DNA and nucleosomes direct distinct folding of a linker histone H1 C-terminal domain. Nucleic Acids Res *40*, 1475-1484.

Fischle, W., Franz, H., Jacobs, S.A., Allis, C.D., and Khorasanizadeh, S. (2008). Specificity of the chromodomain Y chromosome family of chromodomains for lysine-methylated ARK(S/T) motifs. J Biol Chem *283*, 19626-19635.

Fussner, E., Ahmed, K., Dehghani, H., Strauss, M., and Bazett-Jones, D.P. (2010). Changes in chromatin fiber density as a marker for pluripotency. Cold Spring Harb Symp Quant Biol *75*, 245-249.

Gaspar-Maia, A., Alajem, A., Meshorer, E., and Ramalho-Santos, M. (2011). Open chromatin in pluripotency and reprogramming. Nat Rev Mol Cell Biol *12*, 36-47.

George, E.M., Izard, T., Anderson, S.D., and Brown, D.T. (2010). Nucleosome interaction surface of linker histone H1c is distinct from that of H1(0). J Biol Chem *285*, 20891-20896.

Gorgoni, B., Andrews, S., Schaller, A., Schumperli, D., Gray, N.K., and Muller, B. (2005). The stem-loop binding protein stimulates histone translation at an early step in the initiation pathway. RNA *11*, 1030-1042.

Gurley, L.R., Valdez, J.G., and Buchanan, J.S. (1995). Characterization of the mitotic specific phosphorylation site of histone H1. Absence of a consensus sequence for the p34cdc2/cyclin B kinase. J Biol Chem *270*, 27653-27660.

Halmer, L., and Gruss, C. (1996). Effects of cell cycle dependent histone H1 phosphorylation on chromatin structure and chromatin replication. Nucleic Acids Res *24*, 1420-1427.

Hansen, J.C., Lu, X., Ross, E.D., and Woody, R.W. (2006). Intrinsic protein disorder, amino acid composition, and histone terminal domains. J Biol Chem *281*, 1853-1856.

Happel, N., and Doenecke, D. (2009). Histone H1 and its isoforms: contribution to chromatin structure and function. Gene *431*, 1-12.

Happel, N., Schulze, E., and Doenecke, D. (2005). Characterisation of human histone H1x. Biol Chem *386*, 541-551.

Harshman, S.W., Chen, M.M., Branson, O.E., Jacob, N.K., Johnson, A.J., Byrd, J.C., and Freitas, M.A. (2013a). Isolation and analysis of linker histones across cellular compartments. J Proteomics *91*, 595-604.

Harshman, S.W., Young, N.L., Parthun, M.R., and Freitas, M.A. (2013b). H1 histones: current perspectives and challenges. Nucleic Acids Res *41*, 9593-9609.

Hendzel, M.J., Lever, M.A., Crawford, E., and Th'ng, J.P. (2004). The C-terminal domain is the primary determinant of histone H1 binding to chromatin in vivo. J Biol Chem *279*, 20028-20034.

Hergeth, S.P., and Schneider, R. (2015). The H1 linker histones: multifunctional proteins beyond the nucleosomal core particle. EMBO Rep *16*, 1439-1453.

Jenuwein, T., and Allis, C.D. (2001). Translating the histone code. Science *293*, 1074-1080.

Jiang, T., Zhou, X., Taghizadeh, K., Dong, M., and Dedon, P.C. (2007). N-formylation of lysine in histone proteins as a secondary modification arising from oxidative DNA damage. Proc Natl Acad Sci U S A *104*, 60-65.

Kalashnikova, A.A., Winkler, D.D., McBryant, S.J., Henderson, R.K., Herman, J.A., DeLuca, J.G., Luger, K., Prenni, J.E., and Hansen, J.C. (2013). Linker histone H1.0 interacts with an extensive network of proteins found in the nucleolus. Nucleic Acids Res *41*, 4026-4035.

Kamieniarz, K., Izzo, A., Dundr, M., Tropberger, P., Ozretic, L., Kirfel, J., Scheer, E., Tropel, P., Wisniewski, J.R., Tora, L.*, et al.* (2012). A dual role of linker histone H1.4 Lys 34 acetylation in transcriptional activation. Genes Dev *26*, 797-802.

Koop, R., Di Croce, L., and Beato, M. (2003). Histone H1 enhances synergistic activation of the MMTV promoter in chromatin. EMBO J *22*, 588-599.

Kouzarides, T. (2007). Chromatin modifications and their function. Cell *128*, 693-705.

Kowalski, A., and Palyga, J. (2012). Linker histone subtypes and their allelic variants. Cell Biol Int *36*, 981-996.

Kowalski, A., and Palyga, J. (2016). Modulation of chromatin function through linker histone H1 variants. Biol Cell *108*, 339-356.

Krishnan, S., Smits, A.H., Vermeulen, M., and Reinberg, D. (2017). Phospho-H1 Decorates the Inter-chromatid Axis and Is Evicted along with Shugoshin by SET during Mitosis. Mol Cell.

Kuzmichev, A., Jenuwein, T., Tempst, P., and Reinberg, D. (2004). Different EZH2-containing complexes target methylation of histone H1 or nucleosomal histone H3. Mol Cell *14*, 183-193.

Kuzmichev, A., Margueron, R., Vaquero, A., Preissner, T.S., Scher, M., Kirmizis, A., Ouyang, X., Brockdorff, N., Abate-Shen, C., Farnham, P.*, et al.* (2005). Composition and histone substrates of polycomb repressive group complexes change during cellular differentiation. Proc Natl Acad Sci U S A *102*, 1859-1864.

Langan, T.A., Gautier, J., Lohka, M., Hollingsworth, R., Moreno, S., Nurse, P., Maller, J., and Sclafani, R.A. (1989). Mammalian growth-associated H1 histone kinase: a homolog of cdc2+/CDC28 protein kinases controlling mitotic entry in yeast and frog cells. Mol Cell Biol *9*, 3860-3868.

Lever, M.A., Th'ng, J.P., Sun, X., and Hendzel, M.J. (2000). Rapid exchange of histone H1.1 on chromatin in living human cells. Nature *408*, 873-876.

Ling, J., Morley, S.J., Pain, V.M., Marzluff, W.F., and Gallie, D.R. (2002). The histone 3'-terminal stem-loop-binding protein enhances translation through a functional and physical interaction with eukaryotic initiation factor 4G (eIF4G) and eIF3. Mol Cell Biol *22*, 7853-7867.

Lippincott-Schwartz, J., Snapp, E., and Kenworthy, A. (2001). Studying protein dynamics in living cells. Nat Rev Mol Cell Biol *2*, 444-456.

Lu, M.J., Mpoke, S.S., Dadd, C.A., and Allis, C.D. (1995). Phosphorylated and dephosphorylated linker histone H1 reside in distinct chromatin domains in Tetrahymena macronuclei. Mol Biol Cell *6*, 1077-1087.

Lu, X., Hamkalo, B., Parseghian, M.H., and Hansen, J.C. (2009). Chromatin condensing functions of the linker histone C-terminal domain are mediated by specific amino acid composition and intrinsic protein disorder. Biochemistry *48*, 164-172.

Lu, X., and Hansen, J.C. (2003). Revisiting the structure and functions of the linker histone C-terminal tail domain. Biochem Cell Biol *81*, 173-176.

Lu, X., and Hansen, J.C. (2004). Identification of specific functional subdomains within the linker histone H10 C-terminal domain. J Biol Chem *279*, 8701-8707.

Lyubitelev, A.V., Nikitin, D.V., Shaytan, A.K., Studitsky, V.M., and Kirpichnikov, M.P. (2016). Structure and Functions of Linker Histones. Biochemistry (Mosc) *81*, 213-223.

Marzluff, W.F., Gongidi, P., Woods, K.R., Jin, J., and Maltais, L.J. (2002). The human and mouse replication-dependent histone genes. Genomics *80*, 487-498.

Medrzycki, M., Zhang, Y., Cao, K., and Fan, Y. (2012). Expression analysis of mammalian linker-histone subtypes. J Vis Exp.

Meergans, T., Albig, W., and Doenecke, D. (1997). Varied expression patterns of human H1 histone genes in different cell lines. DNA Cell Biol *16*, 1041-1049.

Meshorer, E., Yellajoshula, D., George, E., Scambler, P.J., Brown, D.T., and Misteli, T. (2006). Hyperdynamic plasticity of chromatin proteins in pluripotent embryonic stem cells. Dev Cell *10*, 105-116.

Misteli, T., Gunjan, A., Hock, R., Bustin, M., and Brown, D.T. (2000). Dynamic binding of histone H1 to chromatin in living cells. Nature *408*, 877-881.

Oberg, C., and Belikov, S. (2012). The N-terminal domain determines the affinity and specificity of H1 binding to chromatin. Biochem Biophys Res Commun *420*, 321-324.

Pan, C., and Fan, Y. (2016). Role of H1 linker histones in mammalian development and stem cell differentiation. Biochim Biophys Acta *1859*, 496-509.

Phair, R.D., Gorski, S.A., and Misteli, T. (2004). Measurement of dynamic protein binding to chromatin in vivo, using photobleaching microscopy. Methods Enzymol *375*, 393-414.

Pham, A.D., and Sauer, F. (2000). Ubiquitin-activating/conjugating activity of TAFII250, a mediator of activation of gene expression in Drosophila. Science *289*, 2357-2360.

Rabini, S., Franke, K., Saftig, P., Bode, C., Doenecke, D., and Drabent, B. (2000). Spermatogenesis in mice is not affected by histone H1.1 deficiency. Exp Cell Res *255*, 114-124.

Ramakrishnan, V., Finch, J.T., Graziano, V., Lee, P.L., and Sweet, R.M. (1993). Crystal structure of globular domain of histone H5 and its implications for nucleosome binding. Nature *362*, 219-223.

Reits, E.A., and Neefjes, J.J. (2001). From fixed to FRAP: measuring protein mobility and activity in living cells. Nat Cell Biol *3*, E145-147.

Roque, A., Iloro, I., Ponte, I., Arrondo, J.L., and Suau, P. (2005). DNA-induced secondary structure of the carboxyl-terminal domain of histone H1. J Biol Chem *280*, 32141-32147.

Roque, A., Ponte, I., and Suau, P. (2016). Interplay between histone H1 structure and function. Biochim Biophys Acta *1859*, 444-454.

Sarg, B., Lopez, R., Lindner, H., Ponte, I., Suau, P., and Roque, A. (2015). Identification of novel post-translational modifications in linker histones from chicken erythrocytes. J Proteomics *113*, 162-177.

Sirotkin, A.M., Edelmann, W., Cheng, G., Klein-Szanto, A., Kucherlapati, R., and Skoultchi, A.I. (1995). Mice develop normally without the H1(0) linker histone. Proc Natl Acad Sci U S A *92*, 6434-6438.

Sprague, B.L., and McNally, J.G. (2005). FRAP analysis of binding: proper and fitting. Trends Cell Biol *15*, 84-91.

Strahl, B.D., and Allis, C.D. (2000). The language of covalent histone modifications. Nature *403*, 41-45.

Syed, S.H., Goutte-Gattat, D., Becker, N., Meyer, S., Shukla, M.S., Hayes, J.J., Everaers, R., Angelov, D., Bednar, J., and Dimitrov, S. (2010). Single-base resolution

mapping of H1-nucleosome interactions and 3D organization of the nucleosome. Proc Natl Acad Sci U S A *107*, 9620-9625.

Talasz, H., Sarg, B., and Lindner, H.H. (2009). Site-specifically phosphorylated forms of H1.5 and H1.2 localized at distinct regions of the nucleus are related to different processes during the cell cycle. Chromosoma *118*, 693-709.

Thorslund, T., Ripplinger, A., Hoffmann, S., Wild, T., Uckelmann, M., Villumsen, B., Narita, T., Sixma, T.K., Choudhary, C., Bekker-Jensen, S.*, et al.* (2015). Histone H1 couples initiation and amplification of ubiquitin signalling after DNA damage. Nature *527*, 389-393.

Van Holde, K.E. (1989). Chromatin (New York: Springer-Verlag).

Vicent, G.P., Koop, R., and Beato, M. (2002). Complex role of histone H1 in transactivation of MMTV promoter chromatin by progesterone receptor. J Steroid Biochem Mol Biol *83*, 15-23.

Vila, R., Ponte, I., Collado, M., Arrondo, J.L., Jimenez, M.A., Rico, M., and Suau, P. (2001). DNA-induced alpha-helical structure in the NH2-terminal domain of histone H1. J Biol Chem *276*, 46429-46435.

Vyas, P., and Brown, D.T. (2012). N- and C-terminal domains determine differential nucleosomal binding geometry and affinity of linker histone isotypes H1(0) and H1c. J Biol Chem *287*, 11778-11787.

Wassarman, P.M., and Wolffe, A. (1999). Chromatin. In Methods in enzymology v 304 (San Diego: Academic Press,), pp. 1 online resource (xxxiv, 815 p.).

Weiss, T., Hergeth, S., Zeissler, U., Izzo, A., Tropberger, P., Zee, B.M., Dundr, M., Garcia, B.A., Daujat, S., and Schneider, R. (2010). Histone H1 variant-specific lysine methylation by G9a/KMT1C and Glp1/KMT1D. Epigenetics Chromatin *3*, 7.

Whitfield, M.L., Zheng, L.X., Baldwin, A., Ohta, T., Hurt, M.M., and Marzluff, W.F. (2000). Stem-loop binding protein, the protein that binds the 3' end of histone mRNA, is cell cycle regulated by both translational and posttranslational mechanisms. Mol Cell Biol *20*, 4188-4198.

Wisniewski, J.R., Zougman, A., Kruger, S., and Mann, M. (2007). Mass spectrometric mapping of linker histone H1 variants reveals multiple acetylations, methylations, and phosphorylation as well as differences between cell culture and tissue. Mol Cell Proteomics *6*, 72-87.

Wolffe, A.P. (1997). Histone H1. Int J Biochem Cell Biol *29*, 1463-1466.

Yamamoto, T., and Horikoshi, M. (1996). Cloning of the cDNA encoding a novel subtype of histone H1. Gene *173*, 281-285.

Yang, S.M., Kim, B.J., Norwood Toro, L., and Skoultchi, A.I. (2013). H1 linker histone promotes epigenetic silencing by regulating both DNA methylation and histone H3 methylation. Proc Natl Acad Sci U S A *110*, 1708-1713.

Zhang, Y., Cooke, M., Panjwani, S., Cao, K., Krauth, B., Ho, P.Y., Medrzycki, M., Berhe, D.T., Pan, C., McDevitt, T.C.*, et al.* (2012). Histone h1 depletion impairs embryonic stem cell differentiation. PLoS genetics *8*, e1002691.

Zheng, Y., John, S., Pesavento, J.J., Schultz-Norton, J.R., Schiltz, R.L., Baek, S., Nardulli, A.M., Hager, G.L., Kelleher, N.L., and Mizzen, C.A. (2010). Histone H1 phosphorylation is associated with transcription by RNA polymerases I and II. J Cell Biol *189*, 407-415.

Zhou, B.R., Feng, H., Kato, H., Dai, L., Yang, Y., Zhou, Y., and Bai, Y. (2013). Structural insights into the histone H1-nucleosome complex. Proc Natl Acad Sci U S A *110*, 19390-19395.

Zhou, Y.B., Gerchman, S.E., Ramakrishnan, V., Travers, A., and Muyldermans, S. (1998). Position and orientation of the globular domain of linker histone H5 on the nucleosome. Nature *395*, 402-405.

Zlatanova, J., and Doenecke, D. (1994). Histone H1 zero: a major player in cell differentiation? FASEB J *8*, 1260-1268.

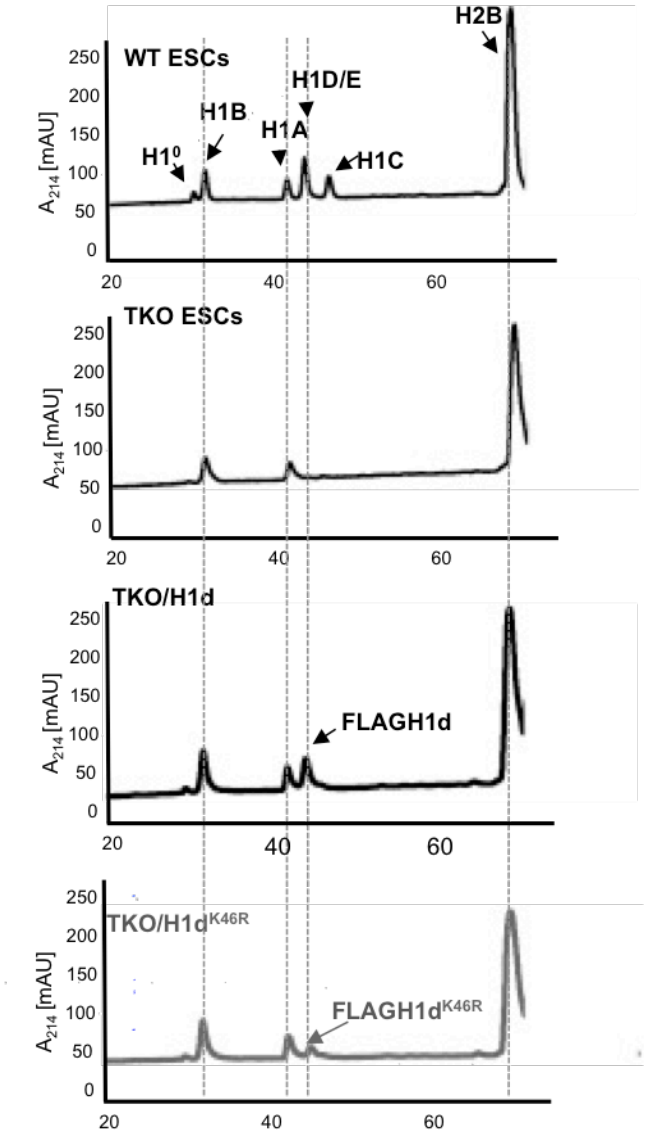

Figure 35. K46R mutation does not affect H1d biochemical properties.
HPLC analysis of histones extracted from chromatin of H1 WT, H1 TKO, H1 TKO/H1d and H1 TKO/H1d^{K46R} ESCs. X axis: elution time; Y axis: absorbency at A_{214}; mAU, milli-absorbency units. H1 variants and H2B are indicated by arrowheads.

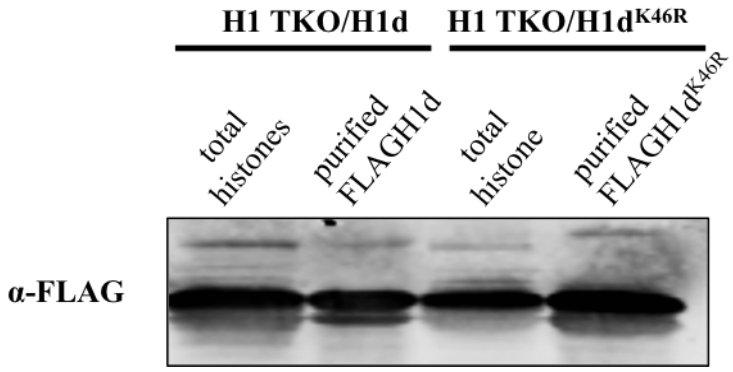

Figure 36. Purification of FLAG-H1D and FLAG-H1D^{K46R} proteins from H1 TKO/H1d and H1 TKO/H1dd^{K46R} ESCs.

Purified FLAG-H1D and FLAG-H1D^{K46R} proteins were obtained from the elutes of HPLC fractions with similar hydrophobicity as that of H1d. Western blotting of total histones and purified proteins using anti-FLAG indicates the presence of the transfected FLAG-H1d and FLAG-H1d^{K46R} exogenous proteins in respective ESCs.

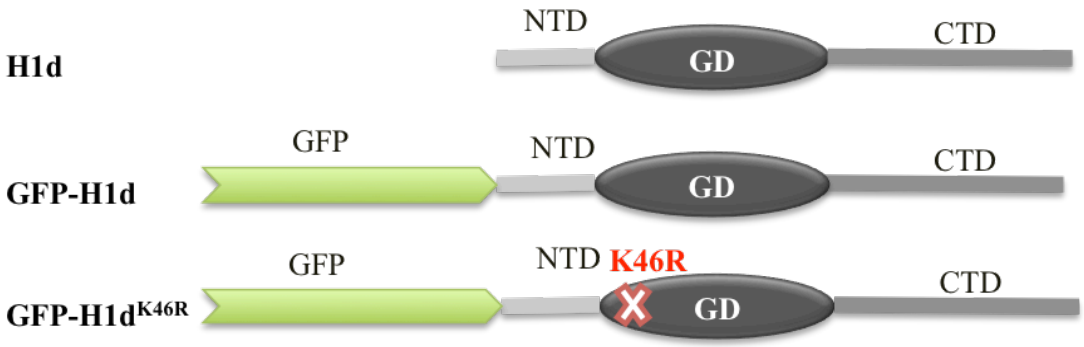

Figure 37. A schematic diagram of the GFP tagged H1d WT and H1d K46R mutant.
The light green arrowhead indicates GFP which is fused to the N-terminus of H1d and H1d^{K46R}.

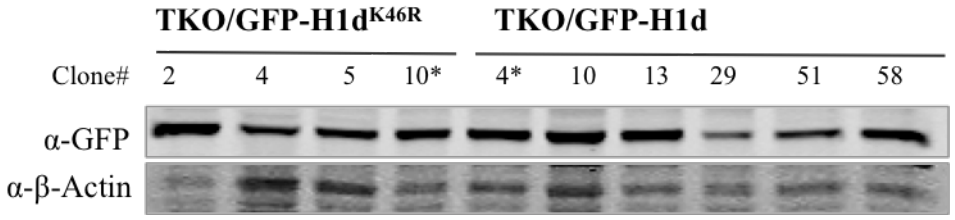

Figure 38. Generation of H1 TKO/GFP-H1d and H1 TKO/GFP-H1d^{K46R} ESC lines.

H1 TKO ESCs were transfected with vectors expressing GFP-H1d and GFP-H1d^{K46R}, and sixty and twenty-four stable ESC clones were picked for respective transfections. Expression of GFP-H1D and GFP-H1D^{K46R} was analyzed by Western blotting using an anti-GFP antibody. Representative immunoblots of GFP-H1d and GFP-H1d^{K46R} expressing ESC clones are shown. Immunoblots with anti-β-Actin antibody are included as loading controls. Clones indicated with asterisks, demonstrating high expression levels of H1D or H1D^{K46R} proteins, were used in subsequent analysis.

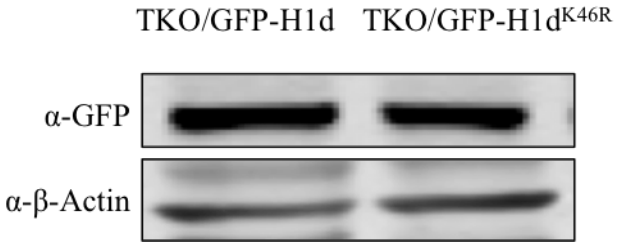

Figure 39. Expression of GFP-H1D and GFP-H1D^{K46R} in H1 TKO/GFP-H1d and H1 TKO/GFP-H1d^{K46R} ESC lines.
Western blotting analysis with anti-GFP and anti-β-Actin are shown. Immunoblotting with anti-β-actin antibody was included as loading controls.

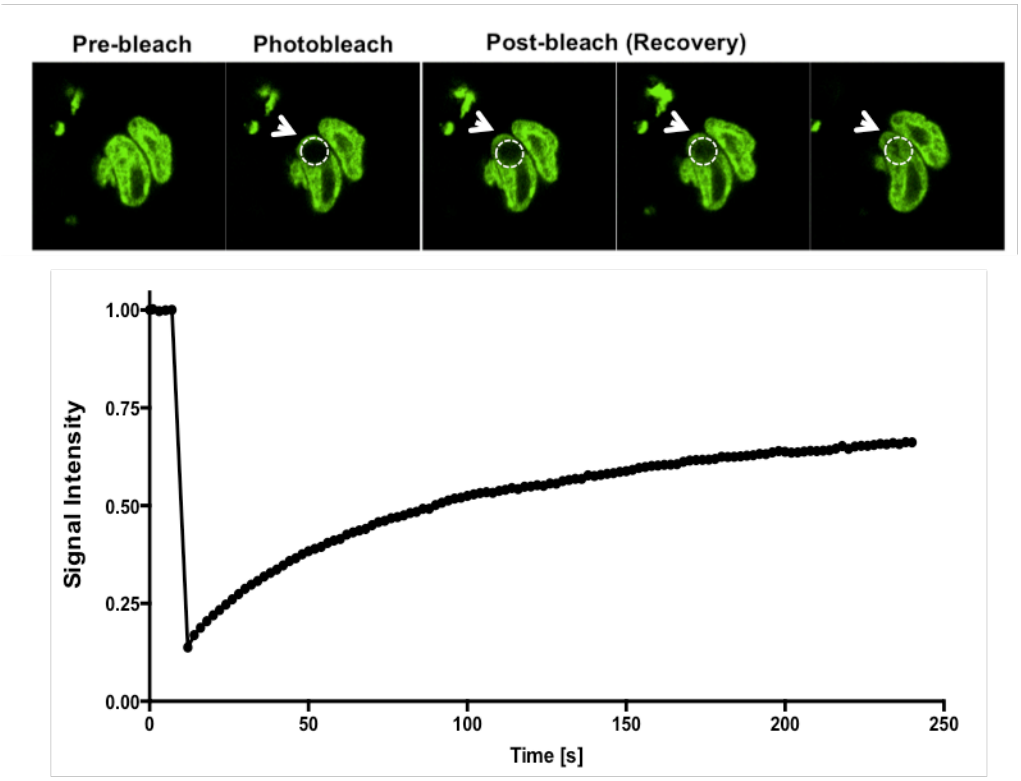

Figure 40. Illustration of Fluorescence Recovery After Photobleaching (FRAP) analysis.
Top: cell images captured during FRAP assay illustrating the FRAP technique. Bottom: a plot illustrating green fluorescence intensity changes in a region of interest before and after photobleaching.

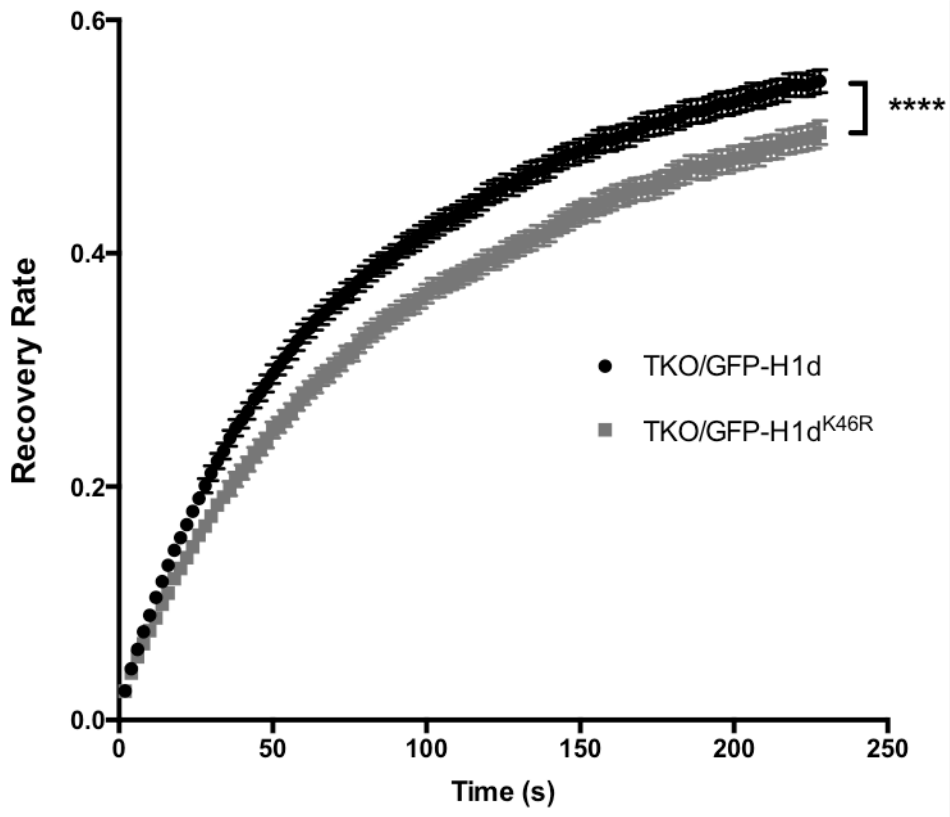

Figure 41. K46R mutation in H1d reduces H1d mobility.

FRAP analysis of H1 TKO/GFP-H1D and H1 TKO/GFP-H1D^{K46R}. FRAP analysis was performed as described in Material and Methods section 2.9. Data were collected from at least 5 independent experiments ($n \geq 5$). Thirty cells for each ESC line were analyzed for each experiment. Values are shown in means ± S.D. ****P< 0.0001.

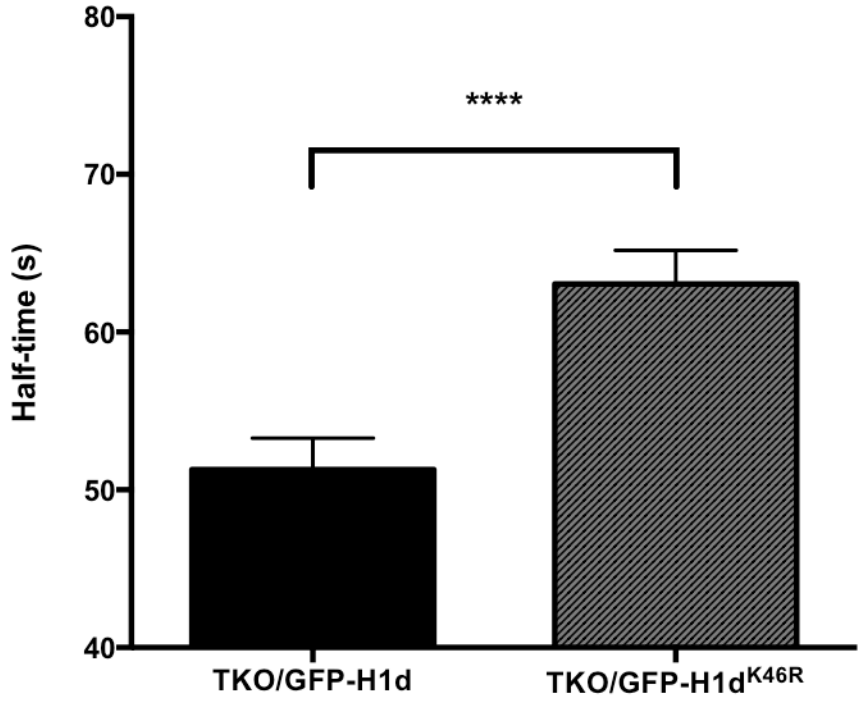

Figure 42. Half-time of maximum recovery (t1/2) of FRAP analysis of H1 TKO/GFP-H1d and H1 TKO/GFP-H1d^{K46R} ESCs.
Data were collected from at least 5 independent experiments ($n \geq 5$). Values are shown in means ± S.D., $n \geq 5$. **** $P < 0.0001$.

CHAPTER 4

CONCLUSIONS AND DISCUSSION

H1 Linker histones are key chromatin structural proteins that facilitate the folding of higher order chromatin structure. Previous studies have demonstrated that H1 is essential for mammalian development and important for ESC differentiation (Fan et al., 2003; Zhang et al., 2012). In this thesis, we took a functional reconstitution approach and utilized H1 depleted ESCs defective in neural differentiation to identify the regions and site of H1 proteins that are critical for the role of H1 in mediating ESC differentiation.

By generation and characterization of H1 QKO/H1d stable ESC lines, we have identified H1d being effective in restoration of neurite outgrowth defects of H1 QKO EBs. Further dissection of H1d into a series of domains allowed us to pinpoint the GD as the key domain responsible for the role of H1d in mediating neurite outgrowth.

Furthermore, we investigate the potential role of H1 modifications in ESC differentiation. Based on our finding of the key role of GD in ESC differentiation, combined with compilation of all identified PTMs of H1 in the literature as well as sequence conservation analysis, we were able to focus our analysis on K46, a conserved hotspot for PTMs within H1d globular domain. Indeed, mutation of lysine to arginine at site 46 (K46R) disrupts the function of H1d in mediating neurite outgrowth during neural differentiation, even though K46R does not appear to change

the biochemical properties and hydrophobicity of H1d. FRAP analysis indicates K46R reduces H1d mobility and dynamics in ESCs.

Taken together, these studies have identified GD as a key domain in mediating the role of H1d in mediating the neurite outgrowth during neural differentiation of ESCs and demonstrated the necessity of PTMs on H1d K46 in ESC differentiation. Our results also suggest that PTMs on K46 may facilitate the mobility of H1d, contributing to its role in ESC differentiation.

In this thesis, we have established an H1 functional reconstitution cellular system with quantifiable phenotypic traits and have effectively tested the function of various H1 variants, H1 domains and specific site in ESC differentiation, particularly in the neurite outgrowth of differentiating EBs. Because H1c/H1d/H1e triple knockout and H1c/H1d/H1e/$H1^0$ quadruple knockout in ESCs do not affect ESC proliferation, H1 TKO and H1 QKO ESCs have normal ESC self-renewal, providing an excellent opportunity for development of the H1 reconstitution cellular systems. On the other hand, H1 QKO and H1 TKO ESCs are severely impaired in ESC differentiation, allowing us to dissect the role of H1 in ESC differentiation by induction of differentiation with a well-defined neural differentiation protocol. We have taken advantage of these cellular systems in this thesis and demonstrated their utility and effectiveness in dissecting the role of H1 domains and specific site in ESC differentiation. This approach and the cell lines generated here should be very useful resources and provide a foundation for further investigation of regulatory mechanisms of H1 in stem cell differentiation.

Using H1 QKO ESCs, we show that expressing full length H1d increases the

neurite outgrowth rate of EBs from 21.8% to 50.1%. Given that WT ESCs had 74.1% of EBs with robust neurite outgrowth, it is intriguing to note that overexpressing H1d does not lead to a complete restoration of the neurite outgrowth defects exhibited by H1 QKO ESCs. It remains to be addressed whether the full restoration is dependent on a higher level of expression of the exogenous H1d or requires complementation from two different H1 variants.

Through sequential deletion of H1d domain(s) and characterization of the functional reconstituted ESCs with H1 deletion mutants, we have identified that the globular domain serves as an essential component in mediating ESC differentiation. H1 QKO/H1d-NTD-GD and H1 QKO/H1d-GD EBs had similar neurite outgrowth rate with 38.2% and 36.8%, respectively. In contrast, overexpressing the C-terminal domain of H1d in H1 QKO ESCs had no obvious effects on neurite outgrowth capacity. CTD accounts for more than half of the H1 sequence and has been shown to be critical for high affinity binding of H1 to chromatin. Thus it is surprising that the neurite outgrowth rate of H1 QKO/H1-GD EBs is not significantly lower than that of H1 QKO/H1d. We speculate that the globular domain of H1 plays a key role in regulating specific genes necessary for mediating the neurite outgrowth during neural differentiation of ESCs. Further studies of gene expression profiles and chromatin compaction status of H1 QKO/H1-GD EBs and H1 QKO/H1-GD EBs are likely to offer new insights to the underlying regulatory mechanisms.

Linker histone H1 family functions as the major architectural proteins mediating higher order chromatin condensation (Happel and Doenecke, 2009; Lyubitelev et al., 2016). The globular domain of linker histone H1 is the most

conserved domain in H1 and is critical for H1 binding to nucleosomes and chromatin (Allan et al., 1980; Brown et al., 2006; Cui and Zhurkin, 2009; Fan and Roberts, 2006; George et al., 2010; Ramakrishnan et al., 1993; Syed et al., 2010; Zhou et al., 1998). The N-terminal domain of H1 is not required for chromatin folding (Allan et al., 1986; Hendzel et al., 2004; Vila et al., 2001; Vyas and Brown, 2012). The C-terminal domain is likely to participated in competitive interaction both with chromatin fiber and many other proteins (Lu et al., 2009). The H1 C-terminal domain assists proper H1 binding to the nucleosomes and linker DNA, and it is necessary for high affinity binding of H1. Both NTD and CTD adopt specific secondary structure when bound to DNA (Lu and Hansen, 2003; Roque et al., 2005).

A working model was proposed to explain the binding dynamics of H1 to chromatin in facilitating chromatin condensation (Catez et al., 2006). Initially, the C-terminal domain of H1 non-specifically binds to the linker DNA mainly through the charge interactions. The globular domain binds to the nucleosomal dyad axis through two binding sites, which comprise several positive charge residues. Proper placement of the globular domain induces conformational changes of the N- and C-terminal domains and further mediates the structure changes for chromatin folding (Brown et al., 2006). The finding that GD is a key domain in mediating ESC differentiation indicates a role of GD in cellular fate regulation besides its curial structural role in proper binding to the nucleosome and chromatin folding.

Having identified the globular domain as the main component mediating the role of H1 in ESC differentiation, we further investigated whether specific PTMs in GD are responsible for this role. We focused on Lys^{46}, a highly conserved, hot-spot

site for H1 modifications, which is the only conserved site in GD of H1 variants subjected to as many as three types of post-translational modifications, including ubiquitination, acetylation and methylation (Wisniewski et al., 2007). We find that H1 TKO/H1d^{K46R} EBs and H1 TKO EBs had comparable neurite outgrowth. While the K to R mutation at K46 of H1d would abolish the potential post-translational modifications at this site, this mutation does not affect the biochemical properties and hydrophobicity of H1d as shown by HPLC analysis of histones extracted from the chromatin of H1 TKO/H1d^{K46R} ESCs. These results suggest that the histone modifications on Lys^{46} of H1d may be crucial for proper differentiation of ESCs.

ESC genome contains hyperdynamic chromatin and exhibits hyperactive global transcription. It is postulated that when ESCs enter the differentiation states, the chromatin would turn from a relatively "open" state into a relative "close" state and significant portion of genome would undergo gene silencing (Ahmed et al., 2010; Efroni et al., 2008; Gaspar-Maia et al., 2011; Meshorer et al., 2006). Recent studies have reinforced that an open chromatin structure is a distinct property for pluripotency (Fussner et al., 2010; Gaspar-Maia et al., 2011).

The FRAP analysis indicates that GFP-H1d^{K46R} has reduced mobility and decreased dynamics compared with H1d, suggesting that the modifications on Lysine 46 site may increase the mobility of H1d *in vivo* and that the regulation of H1d dynamics may be necessary or contribute to the role of H1 in mediating ESC differentiation. Indeed, H1 acetylation, one of the three possible modifications on K46, reduces the basic charges of H1 protein, which leads to reduced H1 binding affinity to nucleosomal DNA and increased H1 mobility. Consistently, most of the

sites within H1 GD subject to modification by acetylation have been found to be associated with DNA binding (Wisniewski et al., 2007). Thus H1 acetylation may be important for dynamic regulation of H1 association with chromatin. While ubiquitination does not change charges on protein, it is rather bulky and may interfere H1 binding to chromatin. For example, K63-ubiquitinated H1s were found to have reduced association with chromatin than unmodified H1s (Thorslund et al., 2015). K46 is located in the first alpha helix in the H1 globular domain. Ubiquitination and tissue specific methylation on H1d K46 have been detected by Mass Spectrometry but have not been investigated further.

Additionally, PTMs on H1d K46 may be required for regulating genes necessary for ESC differentiation. H1 acetylation in general has been linked to activation (Happel and Doenecke, 2009), and evidence suggests that H1 ubiquitination plays an important role in gene activation. $TAF_{II}250$, a component of the general transcription factor TFIID, ubiquitinates H1 in *Drosophila* embryo, suggesting that H1 ubiquitination may participate in transcriptional regulation of a subset of genes (Pham and Sauer, 2000). Gene expression profiling of H1 TKO/H1d^{K46R}, H1 TKO as well as H1 TKO/H1d cells would offer new leads of target genes regulated by PTMs on H1d K46. It would be important to further investigate the underlying mechanisms by which the modifications on K46 regulate ESC differentiation.

REFERENCES

Ahmed, K., Dehghani, H., Rugg-Gunn, P., Fussner, E., Rossant, J., and Bazett-Jones, D.P. (2010). Global chromatin architecture reflects pluripotency and lineage commitment in the early mouse embryo. PLoS One *5*, e10531.

Allan, J., Hartman, P.G., Crane-Robinson, C., and Aviles, F.X. (1980). The structure of histone H1 and its location in chromatin. Nature *288*, 675-679.

Allan, J., Mitchell, T., Harborne, N., Bohm, L., and Crane-Robinson, C. (1986). Roles of H1 domains in determining higher order chromatin structure and H1 location. Journal of molecular biology *187*, 591-601.

Allard, P., Yang, Q., Marzluff, W.F., and Clarke, H.J. (2005). The stem-loop binding protein regulates translation of histone mRNA during mammalian oogenesis. Dev Biol *286*, 195-206.

Balhorn, R., Balhorn, M., and Chalkley, R. (1972). Lysine-rach histone phosphorylation and hyperplasia in the developing rat. Dev Biol *29*, 199-203.

Baxevanis, A.D., and Landsman, D. (1998). Histone Sequence Database: new histone fold family members. Nucleic Acids Res *26*, 372-375.

Bednar, J., Garcia-Saez, I., Boopathi, R., Cutter, A.R., Papai, G., Reymer, A., Syed, S.H., Lone, I.N., Tonchev, O., Crucifix, C., *et al.* (2017). Structure and Dynamics of a 197 bp Nucleosome in Complex with Linker Histone H1. Mol Cell *66*, 729.

Bharath, M.M., Ramesh, S., Chandra, N.R., and Rao, M.R. (2002). Identification of a 34 amino acid stretch within the C-terminus of histone H1 as the DNA-condensing domain by site-directed mutagenesis. Biochemistry *41*, 7617-7627.

Bhattacharjee, R.N., Banks, G.C., Trotter, K.W., Lee, H.L., and Archer, T.K. (2001). Histone H1 phosphorylation by Cdk2 selectively modulates mouse mammary tumor virus transcription through chromatin remodeling. Mol Cell Biol *21*, 5417-5425.

Boggs, B.A., Allis, C.D., and Chinault, A.C. (2000). Immunofluorescent studies of human chromosomes with antibodies against phosphorylated H1 histone. Chromosoma *108*, 485-490.

Bohm, L., and Mitchell, T.C. (1985). Sequence conservation in the N-terminal domain of histone H1. FEBS Lett *193*, 1-4.

Bonet-Costa, C., Vilaseca, M., Diema, C., Vujatovic, O., Vaquero, A., Omenaca, N., Castejon, L., Bernues, J., Giralt, E., and Azorin, F. (2012). Combined bottom-up and top-down mass spectrometry analyses of the pattern of post-translational modifications of Drosophila melanogaster linker histone H1. J Proteomics *75*, 4124-4138.

Bradbury, E.M., Inglis, R.J., and Matthews, H.R. (1974). Control of cell division by very lysine rich histone (F1) phosphorylation. Nature *247*, 257-261.

Bradbury, E.M., Inglis, R.J., Matthews, H.R., and Sarner, N. (1973). Phosphorylation of very-lysine-rich histone in Physarum polycephalum. Correlation with chromosome condensation. Eur J Biochem *33*, 131-139.

Brown, D.T. (2001). Histone variants: are they functionally heterogeneous? Genome Biol *2*, REVIEWS0006.

Brown, D.T., Izard, T., and Misteli, T. (2006). Mapping the interaction surface of linker histone H1(0) with the nucleosome of native chromatin in vivo. Nat Struct Mol Biol *13*, 250-255.

Cao, K., Lailler, N., Zhang, Y., Kumar, A., Uppal, K., Liu, Z., Lee, E.K., Wu, H., Medrzycki, M., Pan, C.*, et al.* (2013). High-resolution mapping of h1 linker histone variants in embryonic stem cells. PLoS genetics *9*, e1003417.

Catez, F., Ueda, T., and Bustin, M. (2006). Determinants of histone H1 mobility and chromatin binding in living cells. Nat Struct Mol Biol *13*, 305-310.

Chadee, D.N., Taylor, W.R., Hurta, R.A., Allis, C.D., Wright, J.A., and Davie, J.R. (1995). Increased phosphorylation of histone H1 in mouse fibroblasts transformed

with oncogenes or constitutively active mitogen-activated protein kinase kinase. J Biol Chem *270*, 20098-20105.

Cui, F., and Zhurkin, V.B. (2009). Distinctive sequence patterns in metazoan and yeast nucleosomes: implications for linker histone binding to AT-rich and methylated DNA. Nucleic Acids Res *37*, 2818-2829.

Cutter, A.R., and Hayes, J.J. (2017). Linker histones: novel insights into structure-specific recognition of the nucleosome. Biochem Cell Biol *95*, 171-178.

Daujat, S., Zeissler, U., Waldmann, T., Happel, N., and Schneider, R. (2005). HP1 binds specifically to Lys26-methylated histone H1.4, whereas simultaneous Ser27 phosphorylation blocks HP1 binding. J Biol Chem *280*, 38090-38095.

Efroni, S., Duttagupta, R., Cheng, J., Dehghani, H., Hoeppner, D.J., Dash, C., Bazett-Jones, D.P., Le Grice, S., McKay, R.D., Buetow, K.H.*, et al.* (2008). Global transcription in pluripotent embryonic stem cells. Cell Stem Cell *2*, 437-447.

Fan, L., and Roberts, V.A. (2006). Complex of linker histone H5 with the nucleosome and its implications for chromatin packing. Proc Natl Acad Sci U S A *103*, 8384-8389.

Fan, Y., Nikitina, T., Morin-Kensicki, E.M., Zhao, J., Magnuson, T.R., Woodcock, C.L., and Skoultchi, A.I. (2003). H1 linker histones are essential for mouse development and affect nucleosome spacing in vivo. Mol Cell Biol *23*, 4559-4572.

Fan, Y., Nikitina, T., Zhao, J., Fleury, T.J., Bhattacharyya, R., Bouhassira, E.E., Stein, A., Woodcock, C.L., and Skoultchi, A.I. (2005). Histone H1 depletion in mammals alters global chromatin structure but causes specific changes in gene regulation. Cell *123*, 1199-1212.

Fan, Y., Sirotkin, A., Russell, R.G., Ayala, J., and Skoultchi, A.I. (2001). Individual somatic H1 subtypes are dispensable for mouse development even in mice lacking the H1(0) replacement subtype. Mol Cell Biol *21*, 7933-7943.

Fan, Y., and Skoultchi, A.I. (2004). Genetic analysis of H1 linker histone subtypes and their functions in mice. Methods Enzymol *377*, 85-107.

Fang, H., Clark, D.J., and Hayes, J.J. (2012). DNA and nucleosomes direct distinct folding of a linker histone H1 C-terminal domain. Nucleic Acids Res *40*, 1475-1484.

Fischle, W., Franz, H., Jacobs, S.A., Allis, C.D., and Khorasanizadeh, S. (2008). Specificity of the chromodomain Y chromosome family of chromodomains for lysine-methylated ARK(S/T) motifs. J Biol Chem *283*, 19626-19635.

Fussner, E., Ahmed, K., Dehghani, H., Strauss, M., and Bazett-Jones, D.P. (2010). Changes in chromatin fiber density as a marker for pluripotency. Cold Spring Harb Symp Quant Biol *75*, 245-249.

Gaspar-Maia, A., Alajem, A., Meshorer, E., and Ramalho-Santos, M. (2011). Open chromatin in pluripotency and reprogramming. Nat Rev Mol Cell Biol *12*, 36-47.

George, E.M., Izard, T., Anderson, S.D., and Brown, D.T. (2010). Nucleosome interaction surface of linker histone H1c is distinct from that of H1(0). J Biol Chem *285*, 20891-20896.

Gorgoni, B., Andrews, S., Schaller, A., Schumperli, D., Gray, N.K., and Muller, B. (2005). The stem-loop binding protein stimulates histone translation at an early step in the initiation pathway. RNA *11*, 1030-1042.

Gurley, L.R., Valdez, J.G., and Buchanan, J.S. (1995). Characterization of the mitotic specific phosphorylation site of histone H1. Absence of a consensus sequence for the p34cdc2/cyclin B kinase. J Biol Chem *270*, 27653-27660.

Halmer, L., and Gruss, C. (1996). Effects of cell cycle dependent histone H1 phosphorylation on chromatin structure and chromatin replication. Nucleic Acids Res *24*, 1420-1427.

Hansen, J.C., Lu, X., Ross, E.D., and Woody, R.W. (2006). Intrinsic protein disorder, amino acid composition, and histone terminal domains. J Biol Chem *281*, 1853-1856.

Happel, N., and Doenecke, D. (2009). Histone H1 and its isoforms: contribution to chromatin structure and function. Gene *431*, 1-12.

Happel, N., Schulze, E., and Doenecke, D. (2005). Characterisation of human histone H1x. Biol Chem *386*, 541-551.

Harshman, S.W., Chen, M.M., Branson, O.E., Jacob, N.K., Johnson, A.J., Byrd, J.C., and Freitas, M.A. (2013a). Isolation and analysis of linker histones across cellular compartments. J Proteomics *91*, 595-604.

Harshman, S.W., Young, N.L., Parthun, M.R., and Freitas, M.A. (2013b). H1 histones: current perspectives and challenges. Nucleic Acids Res *41*, 9593-9609.

Hendzel, M.J., Lever, M.A., Crawford, E., and Th'ng, J.P. (2004). The C-terminal domain is the primary determinant of histone H1 binding to chromatin in vivo. J Biol Chem *279*, 20028-20034.

Hergeth, S.P., and Schneider, R. (2015). The H1 linker histones: multifunctional proteins beyond the nucleosomal core particle. EMBO Rep *16*, 1439-1453.

Jenuwein, T., and Allis, C.D. (2001). Translating the histone code. Science *293*, 1074-1080.

Jiang, T., Zhou, X., Taghizadeh, K., Dong, M., and Dedon, P.C. (2007). N-formylation of lysine in histone proteins as a secondary modification arising from oxidative DNA damage. Proc Natl Acad Sci U S A *104*, 60-65.

Kalashnikova, A.A., Winkler, D.D., McBryant, S.J., Henderson, R.K., Herman, J.A., DeLuca, J.G., Luger, K., Prenni, J.E., and Hansen, J.C. (2013). Linker histone H1.0 interacts with an extensive network of proteins found in the nucleolus. Nucleic Acids Res *41*, 4026-4035.

Kamieniarz, K., Izzo, A., Dundr, M., Tropberger, P., Ozretic, L., Kirfel, J., Scheer, E., Tropel, P., Wisniewski, J.R., Tora, L.*, et al.* (2012). A dual role of linker histone H1.4 Lys 34 acetylation in transcriptional activation. Genes Dev *26*, 797-802.

Koop, R., Di Croce, L., and Beato, M. (2003). Histone H1 enhances synergistic activation of the MMTV promoter in chromatin. EMBO J *22*, 588-599.

Kouzarides, T. (2007). Chromatin modifications and their function. Cell *128*, 693-705.

Kowalski, A., and Palyga, J. (2012). Linker histone subtypes and their allelic variants. Cell Biol Int *36*, 981-996.

Kowalski, A., and Palyga, J. (2016). Modulation of chromatin function through linker histone H1 variants. Biol Cell *108*, 339-356.

Krishnan, S., Smits, A.H., Vermeulen, M., and Reinberg, D. (2017). Phospho-H1 Decorates the Inter-chromatid Axis and Is Evicted along with Shugoshin by SET during Mitosis. Mol Cell.

Kuzmichev, A., Jenuwein, T., Tempst, P., and Reinberg, D. (2004). Different EZH2-containing complexes target methylation of histone H1 or nucleosomal histone H3. Mol Cell *14*, 183-193.

Kuzmichev, A., Margueron, R., Vaquero, A., Preissner, T.S., Scher, M., Kirmizis, A., Ouyang, X., Brockdorff, N., Abate-Shen, C., Farnham, P.*, et al.* (2005). Composition and histone substrates of polycomb repressive group complexes change during cellular differentiation. Proc Natl Acad Sci U S A *102*, 1859-1864.

Langan, T.A., Gautier, J., Lohka, M., Hollingsworth, R., Moreno, S., Nurse, P., Maller, J., and Sclafani, R.A. (1989). Mammalian growth-associated H1 histone kinase: a homolog of cdc2+/CDC28 protein kinases controlling mitotic entry in yeast and frog cells. Mol Cell Biol *9*, 3860-3868.

Lever, M.A., Th'ng, J.P., Sun, X., and Hendzel, M.J. (2000). Rapid exchange of histone H1.1 on chromatin in living human cells. Nature *408*, 873-876.

Ling, J., Morley, S.J., Pain, V.M., Marzluff, W.F., and Gallie, D.R. (2002). The histone 3'-terminal stem-loop-binding protein enhances translation through a functional and physical interaction with eukaryotic initiation factor 4G (eIF4G) and eIF3. Mol Cell Biol *22*, 7853-7867.

Lippincott-Schwartz, J., Snapp, E., and Kenworthy, A. (2001). Studying protein dynamics in living cells. Nat Rev Mol Cell Biol *2*, 444-456.

Lu, M.J., Mpoke, S.S., Dadd, C.A., and Allis, C.D. (1995). Phosphorylated and dephosphorylated linker histone H1 reside in distinct chromatin domains in Tetrahymena macronuclei. Mol Biol Cell *6*, 1077-1087.

Lu, X., Hamkalo, B., Parseghian, M.H., and Hansen, J.C. (2009). Chromatin condensing functions of the linker histone C-terminal domain are mediated by specific amino acid composition and intrinsic protein disorder. Biochemistry *48*, 164-172.

Lu, X., and Hansen, J.C. (2003). Revisiting the structure and functions of the linker histone C-terminal tail domain. Biochem Cell Biol *81*, 173-176.

Lu, X., and Hansen, J.C. (2004). Identification of specific functional subdomains within the linker histone H10 C-terminal domain. J Biol Chem *279*, 8701-8707.

Lyubitelev, A.V., Nikitin, D.V., Shaytan, A.K., Studitsky, V.M., and Kirpichnikov, M.P. (2016). Structure and Functions of Linker Histones. Biochemistry (Mosc) *81*, 213-223.

Marzluff, W.F., Gongidi, P., Woods, K.R., Jin, J., and Maltais, L.J. (2002). The human and mouse replication-dependent histone genes. Genomics *80*, 487-498.

Medrzycki, M., Zhang, Y., Cao, K., and Fan, Y. (2012). Expression analysis of mammalian linker-histone subtypes. J Vis Exp.

Meergans, T., Albig, W., and Doenecke, D. (1997). Varied expression patterns of human H1 histone genes in different cell lines. DNA Cell Biol *16*, 1041-1049.

Meshorer, E., Yellajoshula, D., George, E., Scambler, P.J., Brown, D.T., and Misteli, T. (2006). Hyperdynamic plasticity of chromatin proteins in pluripotent embryonic stem cells. Dev Cell *10*, 105-116.

Misteli, T., Gunjan, A., Hock, R., Bustin, M., and Brown, D.T. (2000). Dynamic binding of histone H1 to chromatin in living cells. Nature *408*, 877-881.

Oberg, C., and Belikov, S. (2012). The N-terminal domain determines the affinity and specificity of H1 binding to chromatin. Biochem Biophys Res Commun *420*, 321-324.

Pan, C., and Fan, Y. (2016). Role of H1 linker histones in mammalian development and stem cell differentiation. Biochim Biophys Acta *1859*, 496-509.

Phair, R.D., Gorski, S.A., and Misteli, T. (2004). Measurement of dynamic protein binding to chromatin in vivo, using photobleaching microscopy. Methods Enzymol *375*, 393-414.

Pham, A.D., and Sauer, F. (2000). Ubiquitin-activating/conjugating activity of TAFII250, a mediator of activation of gene expression in Drosophila. Science *289*, 2357-2360.

Rabini, S., Franke, K., Saftig, P., Bode, C., Doenecke, D., and Drabent, B. (2000). Spermatogenesis in mice is not affected by histone H1.1 deficiency. Exp Cell Res *255*, 114-124.

Ramakrishnan, V., Finch, J.T., Graziano, V., Lee, P.L., and Sweet, R.M. (1993). Crystal structure of globular domain of histone H5 and its implications for nucleosome binding. Nature *362*, 219-223.

Reits, E.A., and Neefjes, J.J. (2001). From fixed to FRAP: measuring protein mobility and activity in living cells. Nat Cell Biol *3*, E145-147.

Roque, A., Iloro, I., Ponte, I., Arrondo, J.L., and Suau, P. (2005). DNA-induced secondary structure of the carboxyl-terminal domain of histone H1. J Biol Chem *280*, 32141-32147.

Roque, A., Ponte, I., and Suau, P. (2016). Interplay between histone H1 structure and function. Biochim Biophys Acta *1859*, 444-454.

Sarg, B., Lopez, R., Lindner, H., Ponte, I., Suau, P., and Roque, A. (2015). Identification of novel post-translational modifications in linker histones from chicken erythrocytes. J Proteomics *113*, 162-177.

Sirotkin, A.M., Edelmann, W., Cheng, G., Klein-Szanto, A., Kucherlapati, R., and Skoultchi, A.I. (1995). Mice develop normally without the H1(0) linker histone. Proc Natl Acad Sci U S A *92*, 6434-6438.

Sprague, B.L., and McNally, J.G. (2005). FRAP analysis of binding: proper and fitting. Trends Cell Biol *15*, 84-91.

Strahl, B.D., and Allis, C.D. (2000). The language of covalent histone modifications. Nature *403*, 41-45.

Syed, S.H., Goutte-Gattat, D., Becker, N., Meyer, S., Shukla, M.S., Hayes, J.J., Everaers, R., Angelov, D., Bednar, J., and Dimitrov, S. (2010). Single-base resolution

mapping of H1-nucleosome interactions and 3D organization of the nucleosome. Proc Natl Acad Sci U S A *107*, 9620-9625.

Talasz, H., Sarg, B., and Lindner, H.H. (2009). Site-specifically phosphorylated forms of H1.5 and H1.2 localized at distinct regions of the nucleus are related to different processes during the cell cycle. Chromosoma *118*, 693-709.

Thorslund, T., Ripplinger, A., Hoffmann, S., Wild, T., Uckelmann, M., Villumsen, B., Narita, T., Sixma, T.K., Choudhary, C., Bekker-Jensen, S.*, et al.* (2015). Histone H1 couples initiation and amplification of ubiquitin signalling after DNA damage. Nature *527*, 389-393.

Van Holde, K.E. (1989). Chromatin (New York: Springer-Verlag).

Vicent, G.P., Koop, R., and Beato, M. (2002). Complex role of histone H1 in transactivation of MMTV promoter chromatin by progesterone receptor. J Steroid Biochem Mol Biol *83*, 15-23.

Vila, R., Ponte, I., Collado, M., Arrondo, J.L., Jimenez, M.A., Rico, M., and Suau, P. (2001). DNA-induced alpha-helical structure in the NH2-terminal domain of histone H1. J Biol Chem *276*, 46429-46435.

Vyas, P., and Brown, D.T. (2012). N- and C-terminal domains determine differential nucleosomal binding geometry and affinity of linker histone isotypes H1(0) and H1c. J Biol Chem *287*, 11778-11787.

Wassarman, P.M., and Wolffe, A. (1999). Chromatin. In Methods in enzymology v 304 (San Diego: Academic Press,), pp. 1 online resource (xxxiv, 815 p.).

Weiss, T., Hergeth, S., Zeissler, U., Izzo, A., Tropberger, P., Zee, B.M., Dundr, M., Garcia, B.A., Daujat, S., and Schneider, R. (2010). Histone H1 variant-specific lysine methylation by G9a/KMT1C and Glp1/KMT1D. Epigenetics Chromatin *3*, 7.

Whitfield, M.L., Zheng, L.X., Baldwin, A., Ohta, T., Hurt, M.M., and Marzluff, W.F. (2000). Stem-loop binding protein, the protein that binds the 3' end of histone mRNA, is cell cycle regulated by both translational and posttranslational mechanisms. Mol Cell Biol *20*, 4188-4198.

Wisniewski, J.R., Zougman, A., Kruger, S., and Mann, M. (2007). Mass spectrometric mapping of linker histone H1 variants reveals multiple acetylations, methylations, and phosphorylation as well as differences between cell culture and tissue. Mol Cell Proteomics *6*, 72-87.

Wolffe, A.P. (1997). Histone H1. Int J Biochem Cell Biol *29*, 1463-1466.

Yamamoto, T., and Horikoshi, M. (1996). Cloning of the cDNA encoding a novel subtype of histone H1. Gene *173*, 281-285.

Yang, S.M., Kim, B.J., Norwood Toro, L., and Skoultchi, A.I. (2013). H1 linker histone promotes epigenetic silencing by regulating both DNA methylation and histone H3 methylation. Proc Natl Acad Sci U S A *110*, 1708-1713.

Zhang, Y., Cooke, M., Panjwani, S., Cao, K., Krauth, B., Ho, P.Y., Medrzycki, M., Berhe, D.T., Pan, C., McDevitt, T.C.*, et al.* (2012). Histone h1 depletion impairs embryonic stem cell differentiation. PLoS genetics *8*, e1002691.

Zheng, Y., John, S., Pesavento, J.J., Schultz-Norton, J.R., Schiltz, R.L., Baek, S., Nardulli, A.M., Hager, G.L., Kelleher, N.L., and Mizzen, C.A. (2010). Histone H1 phosphorylation is associated with transcription by RNA polymerases I and II. J Cell Biol *189*, 407-415.

Zhou, B.R., Feng, H., Kato, H., Dai, L., Yang, Y., Zhou, Y., and Bai, Y. (2013). Structural insights into the histone H1-nucleosome complex. Proc Natl Acad Sci U S A *110*, 19390-19395.

Zhou, Y.B., Gerchman, S.E., Ramakrishnan, V., Travers, A., and Muyldermans, S. (1998). Position and orientation of the globular domain of linker histone H5 on the nucleosome. Nature *395*, 402-405.

Zlatanova, J., and Doenecke, D. (1994). Histone H1 zero: a major player in cell differentiation? FASEB J *8*, 1260-1268.